Linking gas, particulate, and toxic endpoints to air emissions in the Community Regional Atmospheric Chemistry Multiphase Mechanism (CRACMM)

Havala O. T. Pye[1], Bryan K. Place[2], Benjamin N. Murphy[1], Karl M. Seltzer[2,3], Emma L. D'Ambro[1], Christine Allen[4], Ivan R. Piletic[1], Sara Farrell[2], Rebecca H. Schwantes[5], Matthew M. Coggon[5], Emily Saunders[7], Lu Xu[5,6], Golam Sarwar[1], William T. Hutzell[1], Kristen M. Foley[1], George Pouliot[1], Jesse Bash[1], and William R. Stockwell[8]

[1]Office of Research and Development, US Environmental Protection Agency, Research Triangle Park, North Carolina, USA
[2]Oak Ridge Institute for Science and Engineering (ORISE) Postdoctoral Program at the Office of Research and Development, US Environmental Protection Agency, Research Triangle Park, North Carolina, USA
[3]Office of Air and Radiation, US Environmental Protection Agency, Research Triangle Park, North Carolina, USA
[4]General Dynamics Information Technology, Research Triangle Park, North Carolina, USA
[5]NOAA Chemical Science Laboratory (CSL), Boulder, Colorado, USA
[6]Cooperative Institute for Research in Environmental Science (CIRES), University of Colorado, Boulder, Colorado, USA
[7]Office of Chemical Safety and Pollution Prevention, US Environmental Protection Agency, Washington D.C, USA
[8]University of Texas at El Paso, El Paso, Texas, USA

Correspondence to: Havala O. T. Pye (pye.havala@epa.gov)

Abstract. Chemical mechanisms describe the atmospheric transformations of organic and inorganic species and connect air emissions to secondary species such as ozone, fine particles, and hazardous air pollutants (HAPs) like formaldehyde. Recent advances in our understanding of several chemical systems and shifts in the drivers of atmospheric chemistry warrant updates to mechanisms used in chemical transport models such as the Community Multiscale Air Quality (CMAQ) modeling system. This work builds on the Regional Atmospheric Chemistry Mechanism version 2 (RACM2) and develops the Community Regional Atmospheric Chemistry Multiphase Mechanism (CRACMM) version 1.0, which demonstrates a fully coupled representation of chemistry leading to ozone and secondary organic aerosol (SOA) with consideration of HAPs. CRACMM v1.0 includes 178 gas-phase species, 51 particulate species, and 508 reactions spanning gas-phase and heterogeneous pathways. To support estimation of health risks associated with HAPs, nine species in CRACMM cover 50% of the total cancer and 60% of the total noncancer emission-weighted toxicity estimated for primary HAPs from anthropogenic and biomass burning sources in the U.S., with the coverage of toxicity higher (>80%) when secondary formaldehyde and acrolein are considered. In addition, new mechanism species were added based on the importance of their emissions for ozone, organic aerosol, or atmospheric burden of total reactive organic carbon (ROC): sesquiterpenes, furans, propylene glycol, alkane-like low to intermediate volatility organic compounds (9 species), low to intermediate volatility oxygenated species (16 species), intermediate volatility aromatic hydrocarbons (2 species), and slowly reacting organic carbon. Intermediate and lower volatility organic compounds were estimated to increase the coverage of anthropogenic and biomass burning ROC emissions by 40%

compared to current operational mechanisms. Autoxidation, a gas-phase reaction particularly effective in producing SOA, was added for C_{10} and larger alkanes, aromatic hydrocarbons, sesquiterpenes, and monoterpene systems including second generation aldehydes. Integrating the radical and SOA chemistry put additional constraints on both systems and enabled the implementation of previously unconsidered SOA pathways from phenolic and furanone compounds, which were predicted to account for ~30% of total aromatic hydrocarbon SOA under typical atmospheric conditions. CRACMM organic aerosol species were found to span the atmospherically relevant range of carbon number, number of oxygens per carbon, and oxidation state with a slight high bias in number of hydrogens per carbon. In total, eleven new emitted species were implemented as precursors to SOA compared to current CMAQv5.3.3 representations resulting in a bottom-up prediction of SOA, which is required for accurate source attribution and design of control strategies. CRACMMv1.0 is available in CMAQv5.4.

1 Introduction

Reactive organic carbon (ROC) (Safieddine et al., 2017) includes all atmospheric organic species excluding methane and is abundant throughout the troposphere. Particulate forms of ROC are found in fine particles ($PM_{2.5}$) and gaseous ROC is a major precursor to ozone (O_3) and secondary organic aerosol (SOA) (Heald and Kroll, 2020). Recent work indicates that preferentially controlling emissions of ROC could yield significant health benefits by mitigating the mortality associated with ambient air pollution in the U.S. (Pye et al., 2022). These predicted benefits come primarily from reductions in SOA which is strongly associated with cardiorespiratory mortality (Pye et al., 2021; Pond et al., 2022). ROC also includes hazardous air pollutants (HAPs) such as benzene and formaldehyde that result in cancer and noncancer risks to health (Scheffe et al., 2016).

Atmospheric chemical mechanisms connect ROC emissions to endpoints like SOA, O_3, and secondary HAPs and are used to inform air quality management strategies to mitigate the impacts of air pollution. Chemical mechanisms were traditionally designed for estimating ambient O_3 although not necessarily the lower levels of O_3 observed today (Kaduwela et al., 2015) or sources of growing importance around the globe such as volatile chemical products (VCPs, also referred to as solvents) (Coggon et al., 2021; Karl et al., 2018; McDonald et al., 2018; Zheng et al., 2018) and biomass burning (Jaffe and Wigder, 2012) that are changing the composition of emissions towards increasingly oxygenated ROC (Venecek et al., 2018). While mechanisms may predict O_3 reasonably well on broad spatial and temporal scales (Simon et al., 2012; Xing et al., 2015; Young et al., 2018), regional biases in predicted O_3 can exceed 10 ppb (Young et al., 2018; Solazzo et al., 2017) or 20% (Appel et al., 2012; Appel et al., 2021). Global model estimates of chemical production and loss of ozone also vary by a factor of ~2 (Young et al., 2018), and emerging chemical pathways missing from standard models, such as particulate nitrate photolysis, can increase free tropospheric ozone by 5 ppb (Shah et al., 2023) indicating a continued need for model development for ozone prediction. Furthermore, even when mechanisms are relatively similar in their O_3 predictions, they can differ substantially in terms of predicted intermediates like the hydroxyl radical (HO) and nitrate radical (NO_3) as well as products like formaldehyde and SOA (Knote et al., 2015). Model representations of organic aerosol are particularly diverse and span a factor of 10 in their

estimates of global SOA source strength (Tsigaridis et al., 2014). Given parts of 22 different states are in marginal attainment to extreme nonattainment for the current U.S. 8-hour (2012) O_3 standard (as of August 2022) (U.S. Environmental Protection Agency, 2022d) as well as recent work demonstrating health effects below the current fine particle standards (Makar et al., 2017), increasingly accurate representations of emissions and how they connect to chemistry will be needed to inform air quality management strategies going forward. In addition, future implementation of global air quality guidelines, such as those from the World Health Organization, may need to account for the speciation of ambient aerosol since different species have different anthropogenic contributions (Pai et al., 2022).

In most chemical transport models used for air quality prediction, SOA algorithms are disconnected from the gas-phase radical chemistry leading to O_3 formation (Pye et al., 2010; Ahmadov et al., 2012; Koo et al., 2014; Tilmes et al., 2015) leading to duplication of mass in the O_3 and SOA representations. Gas-phase chemical mechanisms also typically exclude non-traditional species with saturation concentrations, C_i^*, in the low volatility organic compound (LVOC, $10^{-2.5} \leq C_i^* < 10^{-0.5}$ μg m^{-3}) and semivolatile organic compound (SVOC, $10^{-0.5} \leq C_i^* < 10^{2.5}$ μg m^{-3}) range. In addition, some gas-phase mechanisms also exclude intermediate volatility organic compounds (IVOCs, $10^{2.5} \leq C_i^* < 10^{6.5}$ μg m^{-3}) (Shah et al., 2020) which are potent SOA precursors but are somewhat less important for O_3 formation than volatile organic compounds (VOCs, $C_i^* \geq 10^{6.5}$ μg m^{-3}). Recent studies have noted that the magnitude of VCP emissions exerts significant impact on model-predicted O_3 but predicted SOA mass is relatively insensitive to VCP emissions due to a lack of suitable SOA precursors in standard mechanisms (Qin et al., 2021; Pennington et al., 2021; Zhu et al., 2019). This conclusion is consistent with ROC budget analysis for Pasadena, California by Heald et al. (2020) that suggests SOA formation requires consideration of precursors beyond traditional, non-oxygenated volatile hydrocarbons represented in most current SOA treatments.

Due to the challenges in representing SOA chemistry in mechanisms, some chemical transport models have opted to use empirical representations of anthropogenic SOA. These parameterizations are not tied to the behavior of specific parent hydrocarbon compounds or emissions sources and fall into two classes: multigenerational and simplified. Multigenerational anthropogenic SOA treatments (Robinson et al., 2007) generally leverage the volatility basis set (VBS) framework and add IVOC and SVOC emissions thought to be missed by current measurement techniques (Koo et al., 2014; Ahmadov et al., 2012). Species throughout the $C_i^* < 10^{6.5}$ μg m^{-3} volatility range are chemically processed over multiple HO reactions leading to production of lower volatility species and SOA mass. Simplified representations use CO (Hodzic and Jimenez, 2011; Kim et al., 2015), primary organic aerosol (Murphy et al., 2017), or C_4H_{10} (Dunne et al., 2020) as a surrogate for anthropogenic activity and precursor emissions that oxidize in one step to SOA. Since the SOA predicted from traditional anthropogenic hydrocarbon precursors has typically been small compared to observed SOA in urban locations (Woody et al., 2016), these schemes can be implemented in parallel to, or as a replacement for, explicit SOA precursor schemes based on traditional VOC precursors. The simplified surrogate approaches are fit to ambient data and thus have the advantage of reproducing observed levels of SOA (Qin et al., 2021; Nault et al., 2018; Murphy et al., 2017). For applications like calculation of present-day aerosol optical depth

or $PM_{2.5}$ mass (e.g., Pye et al. (2021)), empirical representations of anthropogenic SOA may be sufficient. However, the policy applications of empirical approaches are limited because they add emissions external to the regulatory reporting and model platform framework, do not allow for the separation of individual anthropogenic source contributions, and do not consider the representativeness of the emitted proxy in the context of changing emissions or chemical regime, all of which are needed for design of regulatory control strategies.

In this work, the first version of the Community Regional Atmospheric Chemistry Multiphase Mechanism (CRACMM) is developed and presented. CRACMM v1.0 builds off the history of the Regional Atmospheric Chemistry Mechanism (RACM) development (Stockwell et al., 1997). RACM version 2 (Goliff et al., 2013) was chosen as a framework since it is implemented in regional models such as the Community Multiscale Air Quality (CMAQ) modeling system (Sarwar et al., 2013), provides competitive computational speed with mechanisms used in regulatory applications (Sarwar et al., 2013), retains the carbon backbone of emitted species, represents individual peroxy radicals, and relies minimally on aggregated species for radical cycling (operators). Because of these features, RACM2 facilitates comparison with observations, provides transparency in emissions mapping, and is relatively easy to modify and expand.

The purpose of the CRACMM version 1.0 effort described here is to demonstrate a coupled representation of NO_X-ROC-O_3 chemistry including SOA and consideration of HAPs. In addition, this work includes development of rules for mapping emitted ROC to mechanism species and updates to rate constants leading to a publicly available mechanism upon which further developments can be built. CRACMM is expected to become the default option in CMAQ in the future (U.S. Environmental Protection Agency, 2021c). While the mechanism is presented in the context of U.S. conditions, it is informed by conditions outside the U.S. (e.g., the work of Zhao et al. (2016) for China) and is meant to be generally relevant for tropospheric chemistry. CRACMM is available in the public release of CMAQv5.4 (U.S. EPA Office of Research and Development, 2022) and is distributed as a stand-alone mechanism (U.S. Environmental Protection Agency, 2022b). In this work, the aggregation of individual organic species to mechanism species (Sect. 2), the chemistry (Sect. 3), and representation of HAPs (Sect. 4) are described for atmospheric ROC. The manuscript continues with a characterization of ROC in terms of oxidation state and van Krevelen space as well as estimated implications for O_3 and fine particle mass (Sect. 5). The manuscript concludes with a discussion of the importance of mechanism development with recommendations for future work (Sect. 6).

2 ROC Emissions

Various aspects of the development of CRACMM are related to the identity of ROC emissions. The methods behind characterizing emitted ROC and how it maps to mechanism species are described in the following section.

2.1 Individual emitted species

To inform the aggregation of individual species to mechanism species as well as estimate the contributions of mechanism species to endpoints like O_3 and SOA, an emission inventory of individual ROC species was created for 2017 U.S. conditions. Total ROC emissions from wildland fires, oil and gas extraction, vehicles, volatile chemical products (solvents), residential wood combustion, and other non-biogenic sectors were obtained following the EPA's Air QUAlity TimE Series (EQUATES) methods (Foley et al., 2022) based on the U.S. National Emissions Inventory (NEI). The HAPs naphthalene, benzene, acetaldehyde, formaldehyde, and methanol (NBAFM) were included as specific species when available in the NEI. In the case of mobile emissions estimated with the MOVES model (U.S. Environmental Protection Agency, 2020) and solvents estimated with the Volatile Chemical Products in python (VCPy) model (Seltzer et al., 2021), total ROC and individual HAPs (e.g., ethyl benzene, acrolein, styrene, and others in addition to NBAFM) were estimated consistently. For the remaining sectors, HAP species were estimated as a fraction of total ROC based on speciation profiles for different sources. In addition to the base EQUATES emissions, L/S/IVOC emissions missing from the mobile-sector inventoried ROC mass, estimated at 4.6% of non-methane organic gases (NMOG) for gasoline vehicles and 55% of NMOG from diesel vehicles, were added using the volatility distribution from the work of Lu et al. (2020). An additional 20% of NMOG from wood burning sources (wildland, prescribed, and residential) was estimated to be an IVOC (assigned a C_i^* of 10^4 μg m^{-3}) following the estimates of Jathar et al. (2014). L/S/IVOC emissions inventoried as part of primary $PM_{2.5}$ were estimated using published volatility profiles for vehicles (Lu et al., 2020) and wood burning (May et al., 2013; Woody et al., 2016). Other sources of POA were assumed to behave as a species with C_i^* of 10^{-2} μg m^{-3}.

The identity of the individual species within inventoried ROC as well as the L/S/IVOCs (Jathar et al., 2014; Lu et al., 2020) were characterized using the EPA SPECIATE Database (Simon et al., 2010) version 5.2 (pre-release version, see data availability). To provide chemical structure information and facilitate automated property estimation, compounds in the SPECIATE database were assigned a unique Distributed Structure-Searchable Toxicity Database Substance Identifier (DTXSID) (Grulke et al., 2019) using U.S. EPA's CompTox Chemicals Dashboard (the Dashboard, U.S. Environmental Protection Agency (2021d)) (Williams et al., 2017). DTXSIDs allowed for each emitted species to be associated with structural identifiers like Simplified Molecular Input Line Entry System (SMILES) and IUPAC (International Union of Pure and Applied Chemistry) International Chemical Identifier (InChI) representations. In about two-thirds of cases, the emitted SPECIATE species could be exactly matched to a representative compound with a DTXSID in the Dashboard. In the other cases, an isomer or generally representative compound with similar functionality (e.g., presence of aromaticity or other functional groups) and carbon number (e.g., undecane for "isomers of undecane") was manually selected. For the small number of cases in which the SPECIATE species was indicated as "unknown," "unidentified", or similarly undefined, n-decane was assigned as the representative compound. If the unidentified compound was also indicated as exempt from the regulatory definition of VOC (Code of Federal Regulations, 1986) (e.g., "Aggregated exempt compounds", "other, lumped, exempts, individually <2% of

category"), acetone was used as the representative compound. The representative compound's preferred name from the Dashboard, DTXSID identifier, and a degree of assignment confidence score (1: species not well defined, 2: species manually mapped, 3: species automatically matched in Dashboard but some properties inconsistent, 4: exact match in Dashboard) were added to SPECIATEv5.2 (U.S. Environmental Protection Agency, 2022e). A logical (true/false) field in the SPECIATE database was also used to identify individual compounds classified as HAPs (see Sect. 4).

By mapping each emitted species, *i*, to a unique structural identifier, properties of the emissions could be estimated in a traceable manner. The batch feature of the Dashboard (Lowe and Williams, 2021) was used to obtain molecular weights, SMILES strings, and molecular formulas as well as perform OPEn structure–activity/property Relationship App (OPERA) (Mansouri et al., 2018) calculations for the Henry's Law coefficient, rate constant for atmospheric reaction with HO (k_{OH}), and vapor pressure of each ROC species. Vapor pressures $\left(P_i^{vap}\right)$ and molecular weights (M_i) were used to calculate pure-species saturation concentrations (Donahue et al., 2006) at a temperature (T) of 298 K ($C_i^* = P_i^{vap} M_i/(RT)$, where R is the gas constant and C_i^* is reported in μg m^{-3}).

While actual mechanism calculations are required to estimate the contribution of any species to O_3 and SOA in a specific location, two simple structure activity relationships (SARs) were created for screening level analysis of organic aerosol (OA) and O_3 formation potentials of individual ROC species. In the case of OA potential, several sources, largely following high-NO_X conditions outlined in the work of Seltzer et al. (2021), were aggregated to estimate the SOA yield of individual species. In this work, exponential or quadratic polynomial fits depending on what was most applicable were applied to data on the yield of SOA vs $\log_{10}(C_i^*)$ by chemical class for oxygenated hydrocarbons, polycyclic aromatic hydrocarbons (PAHs), substituted aromatics, and alkenes, and to the yield of SOA vs. number of carbons for normal, branched, and cyclic alkanes. Most systems showed a good correlation between predicted and expected SOA yield with coefficient of determination (r^2) of 0.67 in the case of oxygenated hydrocarbons and greater for the other species types. Explicit yield assignments were made based on published data in the case of sesquiterpenes, monoterpenes, benzene, toluene, and xylene (Pye et al., 2010; Ng et al., 2007). Published single-ring aromatic yields were scaled up by the vapor wall loss factor (Zhang et al., 2014). An OA concentration of 10 μg m^{-3} and equal low-NO_X vs high-NO_X behavior, typical of northern hemisphere July conditions (Porter et al., 2021), were assumed for these explicit yield assignments. While this OA concentration is on the high end of the atmospherically relevant range, it is on the low end of concentrations probed in laboratory studies (Porter et al., 2021) thus providing a bridge between observations and ambient conditions.

A second simple SAR was created to estimate the role of individual ROC species in O_3 formation as indicated by maximum incremental reactivity (MIR). Input data for regression fits were obtained from the SAPRC database (Carter, 2019) which contains MIR data for over 1000 compounds. In the case of ill-defined compounds in the SAPRC database, representative

compound structures with DTXSIDs were assigned. Compounds were filtered into various chemical classes (halocarbons, oxygenated, aromatic, alkenes, etc.). Within a given class, the MIR was fit as a function of number of carbons per molecule, HO rate constant (from OPERA), number of oxygens, number of double bonds, number of ring structures, number of double bonded oxygen, and/or number of branches depending on the chemical class. The overall r^2 between SAPRC-estimated and simple-SAR predicted MIRs (Fig. S8) was 0.72. The MIRs are most appropriate for comparing species under a given set of conditions as changes in chemical (or meteorological) regime, such as those in the U.S. between 1988 and 2010, have been found to decrease species MIRs by about 20% on average (Venecek et al., 2018). The SARs were used to estimate average SOA yields and MIR for all ROC species in the SPECIATE database.

2.2 Mechanism species

CRACMM species were designed to leverage the original RACM2 chemistry while also considering the properties of present-day emitted species, including properties indicative of SOA formation potential, with a goal of maintaining a reasonable mechanism size (by species count) for computational efficiency. New explicit species were added for multiple reasons. First, certain species are known to contribute significantly to cancer and noncancer health risk (Scheffe et al., 2016). Second, recent advances in measurement techniques, particularly for VOCs, have increased the number of measured species available, which motivates adding these newly measured species explicitly into models for direct comparison. Third, some individual species are emitted in significant quantities and explicit representation facilitates better conservation of mass and representation of product distributions. New lumped species were also added when existing RACM2 species did not provide a good fit in terms of molecular properties, SOA yields, or O_3 formation potential for emissions.

A python mapper (see Code Availability) was developed to automate mapping of individual, emitted ROC species to mechanism species. Once initial rules were created with the intent of following RACM2, properties of the mechanism species were visualized, and mapping rules were manually adjusted to better preserve mass (minimize the spread in number of carbon per molecule, molecular weight, and molar oxygen to carbon ratio within the model species), estimate SOA (minimized spread in saturation concentration, SOA yield, and Henry's law coefficient within the model species), and predict O_3 (minimize spread in HO rate constant and O_3 formation potential within each model species). A decision tree summarizing the final mapper is provided schematically in Supplement Fig. S1-S4. The mapper uses as input the SMILES string for the ROC species, HO rate constant, and pure component C_i^*. Both k_{OH} and C_i^* can be estimated from a SMILES string prior to mapper input using OPERA algorithms (Mansouri et al., 2018) available for any organic species through the EPA Chemical Transformation Simulator (U.S. Environmental Protection Agency, 2022f). This emission mapping follows a hierarchy of rules in which explicit species are mapped first followed by lumped biogenic VOCs (α-pinene and other monoterpenes with one double bond, API; limonene and other monoterpenes with two or more double bonds, LIM; and sesquiterpenes, SESQ). Other lumped species and mapping rules were created to consider volatility, functional groups (parsed in python using the work of RDKit (2022)), and k_{OH}. For L/SVOCs, mechanism assignment was based purely on volatility except in the case of PAHs (more than one aromatic ring)

which were grouped with naphthalenes (NAPH, Sect. 3.5). For IVOCs, assignments considered volatility and presence of specific functional groups (aromatic, oxygenated, alkane). For VOCs, mapping considered only functional groups and k_{OH}.

Figures 1-3 (and Supplementary Fig. S5-S6) show the final U.S. 2017 emission-weighted distributions of compound properties for all emitted ROC species in CRACMMv1.0. Looking across multiple properties illustrates the hierarchy of emission mapping rules. For example, three classes of alkane-like species (discussed in Sect. 3.1) were inherited from RACM2: HC3, HC5, and HC10 (formerly HC8). In carbon-number space (Fig. 1), these species overlap in their coverage of individual compounds with all three classes including species with 2 to 8 carbons per molecule. Their saturation concentration distributions (Fig. 2) also show overlap. The $\log_{10}(k_{OH})$ (Fig. 3) highlights that HC3, HC5, and HC10 are defined by distinct and mutually exclusive ranges of the HO rate constant. Indeed, the HO rate constant is the classifying property for the HC3, HC5, and HC10 species and is implemented after volatility, functional group identity, and other features of the species have been considered. As another example, SLOWROC is multimodal in number of carbons per molecule (n_C) and C_i^* (Fig. 1-2) which could necessitate separation into more species. However, SLOWROC reacts so slowly (Fig. 3) that additional speciation is not warranted. The systems in Fig. 1-3 indicated by color coding will be further discussed in the next section.

3 ROC Chemistry

Multiple data sources were used to build the chemistry of CRACMM. As CRACMM will be a community mechanism in which different chemical systems are developed by different investigators, individual systems are expected to evolve at different rates and will be informed by different sources of data. Development of CRACMM v1.0 leveraged existing chemical mechanisms including the Generator for Explicit Chemistry and Kinetics of Organics in the Atmosphere (GECKO-A, Aumont et al. (2005)), Master Chemical Mechanism (MCM, Jenkin et al. (1997)), SAPRC-18 Mechanism Generation System (Carter, 2020b), and RACM2, as well as literature. ROC systems not previously represented in RACM2 (such as furans and L/S/IVOCs), precursors to SOA, and systems with new kinetic data (Sect. 3.10) were targeted for development in this initial CRACMM version. Future work will continue to expand this initial representation by extending it to new chemical systems and/or updating these parameterizations with new data.

CRACMM v1.0 includes 178 gas-phase species (ROC species in Appendix A) and 508 reactions spanning gas-phase and heterogeneous pathways (Appendix B). In the CMAQv5.4 modal aerosol implementation, CRACMM includes 51 different chemical species in the particulate phase (81 model species across Aitken, accumulation, and coarse modes). These 51 particulate species in CRACMM include inorganic aerosol species such as sulfate, nitrate, ammonium, calcium, and other trace metals as in previous versions of CMAQ. To fully describe the state of atmospheric aerosol in CMAQ, CRACMM interacts with ISORROPIA II (Fountoukis and Nenes, 2007) and other algorithms describing nucleation and condensation. CRACMM specifically builds on the implementation of RACM2 chemistry coupled with aerosol chemistry of AERO6 (411 reactions) in

the CMAQ v5.3.3 model which differs slightly from the original RACM2 implementation (Goliff et al., 2013) (363 reactions) due to SOA pathways, parameterized effects of halogens on ozone (Sarwar et al., 2015), and other minor updates (see the work of Sarwar et al. (2013) and Code Availability section for the CMAQ implementation of RACM2).

In contrast to almost all SOA representations in current chemical transport models, SOA systems in CRACMM are integrated with the gas-phase radical chemistry. Specifically, all condensible or soluble precursors to SOA are formed directly as gas-phase products with the ability to condense (systems in Sect. 3.1-3.7) or react heterogeneously (Sect. 3.8) and form SOA. Formation of SOA thus removes mass from the gas phase, sequestering RO_2, NO, and/or hydrogen oxide (HO_X) radicals with implications for ozone and species modulated by oxidant abundance such as sulfate.

All CRACMM species (both primary and secondary) have a representative structure (ROC species in Appendix A) based on the most abundantly emitted species or likely oxidation product. Representative structures were used to obtain properties such as the molecular weight, rate coefficient, solubility, and/or volatility of species except in 2 cases (SLOWROC in Sect. 3.1, ROCIOXY in Sect. 3.3). These representative structures can enable future prediction of other properties such as aerosol viscosity and propensity to phase separate as well as deviations from ideal partitioning. They can also be used to synthesize CRACMM chemistry as demonstrated in Sect. 5. The species and chemistry of the major ROC systems updated compared to RACM2, reactions for two additional new HAPs, as well as rate constant updates (including many for inorganic reactions) are described in this section. Table 1 summarizes the SOA pathways.

3.1 Alkane-like ROC

CRACMM includes 14 classes of alkane-like species ranging from low-volatility compounds to ethane (Fig. 1-3 red series). Methane reaction with HO is from RACM2 and assumes a fixed background concentration (1.85 ppm for the late 2010s, Dlugokencky (2022)). After remapping all ROC species, the RACM2 alkane class HC8 (alkanes and other species with $k_{OH} > 6.8\times10^{-12}$ cm^3 $molec^{-1}$ s^{-1}) was renamed to HC10 based on the n_C (Fig. 1) and is consistent with a $C_i^* \sim 10^7$ µg m^{-3} (Fig. 2). Nine new alkane-like mechanism species with high OA formation potential span the L/S/IVOC range and are grouped by $log_{10}(C_i^*)$ into ROCN2ALK, ROCN1ALK, ROCP0ALK, ROCP1ALK, ROCP2ALK, ROCP3ALK, ROCP4ALK, ROCP5ALK, and ROCP6ALK, where the numbers indicate the negative (N) or positive (P) $log_{10}(C_i^*[\mu g\ m^{-3}])$ value (Fig. 2). When the species reside in the gas-phase as a vapor, it is prepended with a "V" (as in Appendix B) and when in the particulate aerosol phase, an "A." For example, VROCN2ALK is an alkane-like vapor species with C_i^* of 10^{-2} µg m^{-3}, and AROCN2ALK is a particulate species of the same volatility.

The 9 new alkane-like model species roughly correspond to carbon numbers of 30, 29, 28, 27, 24, 21, 18, 14, and 12 (Fig. 1) and are not represented in traditional atmospheric chemical mechanisms due to low ozone formation potential per unit mass (Fig. S5). For example, ~C_8 is the largest alkane category in RACM2 and SAPRC18, and n-dodecane (C_{12}) is the largest alkane

in MCM (Jenkin et al., 1997). Conceptually, for deposition and other processes, the gas-phase paraffinic species in Carbon Bond (CB6r3) is equivalent to a C_4 species. Regardless of the chemical mechanism, regional modeling emission infrastructure previously used by CMAQ did not classify species with ~20 or more carbons (Pye and Pouliot, 2012), and S/IVOC emissions were not propagated to model-ready species for CMAQ mechanisms (Shah et al., 2020). The CRACMM species with $log_{10}(C_i^*) \leq 3$ can exist in the gas or particle phase based on the local organic aerosol loading and absorptive partitioning theory (Pankow, 1994) while ROCP4ALK-ROCP6ALK exist meaningfully in the gas-phase only (Appendix A). The low volatility alkanes, $C_i^* \leq 1$ μg m^{-3}, are assumed to be primarily in the particulate phase and have a minor potential to react and contribute to O_3 formation (Fig. S5) so do not participate in gas-phase radical chemistry (Appendix B). Most of the L/S/IVOC emissions are expected to be unresolved at the individual species level (Robinson et al., 2007) and are characterized through other means such as volatility analysis (e.g., Lu et al., 2018).

Gas-phase chemistry for the alkane species with 10 μg m^{-3} $\leq C_i^* \leq 10^7$ μg m^{-3} (ROCP1ALK-ROCP6ALK and HC10) is based on GECKO-A predictions for C_{10}-C_{26} n-alkanes (Lannuque et al., 2018) and known H-shift pathways (Praske et al., 2018). The chemical reactions representing the major product channels and types of functionalities added to the parent hydrocarbon (RH) are:

$$RH_{M=7,6,5,4,3,2,1,\ n_O=0} + HO \rightarrow RO_2 + H_2O \quad (R1)$$

$$RO_2 + NO \rightarrow (1\text{-}\beta_1)\ R(OH)O_2 + \beta_1\ RNIT_{M\text{-}2.15,3} + (1\text{-}\beta_1)\ NO_2 \quad (R2)$$

$$RO_2 + NO_3 \rightarrow R(OH)O_2 + NO_2 \quad (R3)$$

$$RO_2 + HO_2 \rightarrow ROOH_{M\text{-}3.02,2} \quad (R4)$$

$$R(OH)O_2 \rightarrow R(O)OOH_{M\text{-}3.40,3} + HO_2 \quad (R5)$$

$$R(OH)O_2 + NO \rightarrow \beta_2\ R(OH)NIT_{M\text{-}4.33,4} + (1\text{-}\beta_2)\ R(OH)KET_{M\text{-}2.96,2} + (1\text{-}\beta_2)\ NO_2 + (1\text{-}\beta_2)\ HO_2 \quad (R6)$$

$$R(OH)O_2 + NO_3 \rightarrow R(OH)KET_{M\text{-}2.96,2} + NO_2 + HO_2 \quad (R7)$$

$$R(OH)O_2 + HO_2 \rightarrow R(OH)OOH_{M\text{-}5.38,3} \quad (R8)$$

where stable products are subscripted with their saturation concentration in $log_{10}(C_i^*)$ (relative to a parent hydrocarbon with $log_{10}(C_i^*)$ = M) and the number of oxygens per molecule (n_O). The initial product, RO_2, is the prompt peroxy radical resulting from hydrogen abstraction followed by O_2 addition (R1). RO_2 reactions lead to stable products like organic nitrates (RNIT) and peroxides (ROOH) (R2, R4) that can further react (following Sect. 3.2 for S/IVOCs and RACM2 for VOCs). The alkoxy radical generated from the prompt RO_2 can also undergo a 1,5 H-shift followed by addition of O_2 leading to a new hydroxy-peroxy radical, $R(OH)O_2$ (R2, R3). The $R(OH)O_2$ can undergo standard bimolecular peroxy radical fates leading to multifunctional nitrates (R(OH)NIT), ketones (R(OH)KET), and peroxides (R(OH)OOH) or a 1,6 H-shift at a rate of 0.188 s^{-1} (Vereecken and Nozière, 2020) producing a ketohydroperoxide (R(O)OOH) and HO_2 (R5) as described by Praske et al. (2018). Following GECKO-A (Lannuque et al., 2018), the yield of organic nitrates in reaction R2, β_1, is 0.28 for S/IVOC alkanes and 0.26 for HC10, consistent with the plateau at ~0.3 observed for C_{13} and larger alkanes (Yeh and Ziemann, 2014).

The yield of organic nitrates for the hydroxy-peroxy radical, β_2, is 0.14 for S/IVOC alkanes and 0.12 for HC10 (Lannuque et al., 2018). Rate constants are provided in Appendix B.

Products are often 2-3 orders of magnitude lower in C_i^* than their parent and can be 4-5 orders of magnitude lower in the case of the multifunctional nitrates and peroxides. For the alkane systems, product C_i^* are based on vapor pressures obtained from GECKO-A output using the Nannoolal method (Nannoolal et al., 2008; Nannoolal et al., 2004). With one exception, all stable products from the VOC, HC10 (M=7), are expected to remain in the gas phase and thus map to the standard gas-phase species ONIT (organic nitrates), OP2 (organic peroxides), and KET (ketones) inherited from RACM2. The hydroxyhydroperoxide from HC10 oxidation is predicted to be sufficiently functionalized to be semivolatile. That C_{10} multifunctional peroxide along with all the stable products from alkane-like S/IVOCs are mapped to new CRACMM species of matching C_i^* and molar oxygen to carbon ($n_O : n_C$) ratio (secondary, oxygenated L/S/IVOC species, Sect. 3.2).

According to the SOA SAR (Fig. S5) as well as the prompt (one HO reaction) mechanism predictions (Table 1), SVOCs of ROCP2ALK and lower volatility have SOA yields that are near 100% by mole (up to 150% by mass), and the atmospherically relevant SOA yields will depend on competition between phase partitioning, reaction, and deposition. Much of the alkane-like L/SVOC contribution to ambient OA will be in the form of direct emission of the lower volatility species as primary organic aerosol (POA). The mechanism-predicted prompt SOA yields for ROC3PALK and ROCP4ALK by mass (Table 1) are very similar to the emission-weighted SAR-based prediction of 0.83 and 0.55 by mass (Fig. S5). The mechanism-based prompt SOA yields for the more volatile alkane-like ROC species (ROCP5ALK, ROCP6ALK, and HC10) are lower than those predicted by the SOA SAR (28%, 18%, and 6% by mass). Note that the HC10 class is estimated to contain substantial emissions (Shown in Sect. 4 and accompanying Fig. 6b), some of which are poorly identified in SPECIATE (representative compound score of 1, Section 2.1).

The alkane-like ROC species differ from the previous CMAQ S/IVOC species implemented in AERO6/7 (× symbols Fig. 1, 3) in terms of the trend in n_C with volatility as they are all conceptualized as alkane-like structures because those are the representative structures currently populated with emissions in the S/IVOC range. SVOCs with $log_{10}(C_i^*[\mu g\ m^{-3}]) < 2.5$ are lumped into ROCN2ALK-ROCP2ALK species based on volatility regardless of their functionality resulting in some higher $n_O : n_C$ species being included (Fig. S6). CMAQ AERO6/7 previously assumed a slight increase in $n_O : n_C$ and corresponding decrease in n_C as volatility decreased (Fig. 1, Fig. S6). CRACMM alkane-like SVOCs with k_{OH} from OPERA are also less reactive than AERO6/7 SVOCs (Fig. 3).

The reaction products of ethane (ETH), C3 alkanes and other slowly-reacting species ($3.5\times10^{-13} \le k_{OH} < 3.4\times10^{-12}$ cm^3 molec^{-1} s^{-1}, HC3), and C5 alkanes and other moderately reacting species ($3.4\times10^{-12} \le k_{OH} \le 6.8\times10^{-12}$ cm^3 molec^{-1} s^{-1}, HC5) (Fig. 3) are obtained directly from RACM2 with the addition of a very small yield of SOA from HC3 (2.8×10^{-5} by mole) and HC5 (

1.3×10^{-3} by mole) (Table 1). Ethane is the only explicit alkane in CRACMM its rate constant with the hydroxyl radical is updated to follow recent recommendations (Burkholder et al., 2019). In addition, CRACMM includes a new species called SLOWROC with a lifetime of about one month ($k_{OH} < 3.5\times10^{-13}$ cm^3 $molec^{-1}$ s^{-1}) to prevent loss of emitted carbon that may contribute to the ambient atmospheric ROC burden (effective carbons per molecule of 2.1). SLOWROC also contains many HAPs (Sect. 4). Due to the highly empirical nature of SLOWROC, the molecular weight is based on an emission-weighted value rather than a representative compound. Oxidation of SLOWROC produces the ethylperoxy radical (ETHP) and a small yield of SOA (0.10% by mole).

Effective SOA yields for the alkane-like VOC ($log_{10}(C_i^*[\mu g\ m^{-3}]) \geq 6.5$) systems except HC10 use the simple SAR for SOA and are driven by isopropyl acetate and methyl butanoate (estimated SOA yields of 2.8 and 2.2% by mass) in the case of HC3, by isopentane (estimated SOA yield of 1.9% by mass) in the case of HC5, and by two long-lived aromatic species in the case of SLOWROC. HC3, HC5, and SLOWROC SOA is mapped to species ASOAT, a general, nonvolatile SOA species with molecular weight of 200 g mol^{-1} (Table 1). HC3, HC5, and SLOWROC are estimated to contribute 0.003%, 0.062%, and 0.0002% by mass, respectively of the total OA potential for anthropogenic and biomass burning emissions in the U.S. for 2017 conditions.

3.2 Secondary oxygenated L/S/IVOCs

Gas-phase oxidation of S/IVOC alkanes readily leads to oxygenated L/S/IVOC products with $n_O:n_C$ ratios up to 0.3 (Reactions R1-R8). The products of these prompt reactions continue to be processed in the atmosphere, resulting in further functionalization as well as fragmentation (cleaving of the carbon backbone) with implications for increasing or decreasing SOA, respectively. Functionalization products of the secondary oxygenated L/S/IVOC chemistry can sequester radicals, but fragmentation products, like formaldehyde, can eventually release radicals via photolysis (Edwards et al., 2014).

The chemistry of secondary oxygenated L/S/IVOCs is parameterized using the 2-D VBS framework (Donahue et al., 2012) with some modifications. The decrease in $log_{10}(C_i^*)$ per oxygen in the 2-D VBS box model was calculated using the parameterization from Donahue et al. (2011) with the oxygen-oxygen interaction term set to 2.3, the carbon-oxygen interaction parameter set to -0.3 to correct for the behavior of diacids, and the carbon-carbon interaction term set to 0.475 . As identified in Donahue et al. (2011), the resulting decrease in $\log_{10}C^*$ per oxygen is 1.7 as $n_O:n_C$ approaches zero and and is 1.93 at $n_O:n_C$ approaches 0.6. These values are consistent with the effect of adding carboxylic acids to an alkane-like molecule (Pankow and Asher, 2008). Homogeneous, gas-phase HO reaction rate constants were specified based on the parameterization proposed by Donahue et al. (2013): $k_{OH}(cm^3 molec^{-1} s^{-1}) \simeq 1.2\times10^{-12}(n_C + 9n_O - 10(n_O:n_C)^2)$. Following the reaction with HO, the probability of functionalization was parameterized as $f^{func} = 1 - (n_O:n_C)^{0.4}$, with subsequent probabilities of adding one, two, or three oxygens set at 30%, 50%, and 20%, respectively, following the 2-D VBS functionalization kernel derived for photo-oxidation of POA and IVOCs (Zhao et al., 2016). The sensitivity of yields to NO_x and formation of organic nitrates

were not explicitly addressed in the 2-D VBS-based aging mechanism, although both are addressed by CRACMM more broadly and some products mapped to secondary L/S/IVOCs contain nitrate functionality. Rather than recycling hydroxyl radicals as is standard practice for VBS-style reactions that are only meant to capture SOA, CRACMM sequesters HO_X in oxygenated L/S/IVOC products as might be expected when peroxides form. For example, reactions of type R1 followed by type R4 sequester two HO_X for each initiating reaction.

L/S/IVOC products predicted by the 2-D VBS were lumped into a reduced series of fifteen mechanism species spanning C_i^* of 10^{-2} through 10^6 μg m^{-3} and $n_O:n_C$ of 0.1 through 0.8 for use in CRACMM: ROCN2OXY2, ROCN2OXY4, ROCN2OXY8, ROCN1OXY1, ROCN1OXY3, ROCN1OXY6, ROCP0OXY2, ROCP0OXY4, ROCP1OXY1, ROCP1OXY3, ROCP2OXY2, ROCP3OXY2, ROCP4OXY2, ROCP5OXY1, and ROCP6XY1. These species follow a similar naming convention as the S/IVOC alkanes, where numbers after N and P indicate the negative or positive $log_{10}(C_i^*)$ value and the name ends in $10\times n_O:n_C$ (e.g., ROCN2OXY2 is $C_i^* = 10^{-2}$ μg m^{-3} with $n_O:n_C$ =0.2). VBS products of known n_C and n_O were mapped to the available CRACMM model species, first by interpolating to the two nearest $log_{10}(C_i^*)$ points, and then to the two nearest species in $n_O:n_C$ space. The number of $n_O:n_C$ levels represented at a given volatility in CRACMM increases with decreasing C_i^* to reflect increasing diversity in chemical functionality and size of products with lower saturation concentrations.

The portion of reacted mass following the fragmentation pathway, $f^{frag} = (n_O:n_C)^{0.4}$, was assumed to form fragments of sizes varying from one up to n_C carbons. The distribution of fragments was estimated assuming the probability of attack on any carbon as $1/n_C$. Fragments with greater than seven carbons were functionalized using the same oxygen addition probabilities and remapping to lumped model species as above. Stable fragmentation products with six or fewer carbons were mapped back to existing gas-phase species from RACM2 based on their carbon number as follows: C_1 to formaldehyde (HCHO), C_2 to acetaldehyde (ACD), C_3 to higher aldehydes (ALD), C_4 to methyl ethyl ketone (MEK), C_5 to dicarbonyls (DCB1), C_6 from low $n_O:n_C$ reactants to hydroxy ketones (HKET), and C_6 from high $n_O:n_C$ reactants to higher ketones (KET). The choice of functionality of the product species (e.g. aldehydes versus ketones) is entirely determined by the RACM2 species that were already available at each carbon number. Future measurements of the low molecular weight species produced by the oxidation of larger compounds would help constrain this choice and motivate the addition of new CRACMM species. A new semivolatile peroxide (OP3), equivalent to a $C_8H_{16}O_4$ species with C_i^* of ~10 μg m^{-3}, in CRACMM provides an oxygenated peroxide species between the L/S/IVOC oxygenated series and RACM2's higher organic peroxides (OP2). In addition, radical products are mapped to RACM2 peroxy radical species as follows: C_1 to methyl peroxy radical (MO2), C_2 to ethyl peroxy radicals (ETHP), C_3 to isopropylperoxy radicals (HC3P), C_4 to peroxy radicals from methyl ethyl ketone (MEKP), C_5 to pentan-3-ylperoxy (HC5P) radicals, and C_6 to ketone-derived peroxy radicals (KETP). OP3 can photolyze or react with HO.

Overall, the CRACMM scheme performs similarly to the medium-yield 2D-VBS scheme optimized for S/IVOCs by Zhao et al. (2016) (Fig. 4). For precursors with $n_O:n_C$ > 0.05 and 12 hours of chemical processing, the 2-D VBS and CRACMM aging schemes are almost the same in terms of OA yield (Fig. 4a-c) with values ranging from near 0.1 to above 1 as a function of volatility (Table 1). Some deviations occur between the schemes for the most oxygenated and volatile precursors ($n_O:n_C$ > 0.45 and $log_{10}(C_{OA}/C_i^*) \leq 0$, where C_{OA} is the mass-based concentration of the condensed-phase partitioning medium) for which CRACMM predicts a stronger dependence of yield on precursor volatility and also predicts less OA formation. Both CRACMM and the 2-D VBS predict consistent trends in OA yield as a function of precursor properties with more oxygenated and volatile precursors having lower yields due to an increased likelihood of fragmentation. At very long processing times CRACMM predicts OA yields will decrease (which has been observed in experimental systems in the work by He et al. (2022)) while the 2-D VBS indicates yields continue to increase from 2.5 days (Fig. 4) to 5.5 days (Fig. S7). In CRACMM $n_O:n_C$ ratios are predicted to increase with time, which can be due to both functionalization (Heald et al., 2010) and fragmentation (Kroll et al., 2009) reactions. CRACMM generally predicts lower $n_O:n_C$ ratios in OA products from oxygenated ROC (0.1 to 0.5 for least oxygenated and 0.6 to 0.7 for most oxygenated precursors) than the 2-D VBS (Fig. 4d-f).

3.3 Primary oxygenated IVOCs

Volatile chemical products emit significant amounts of oxygenated IVOCs (Seltzer et al., 2021; McDonald et al., 2018). Many of these oxygenated species are structurally different than what is conceptualized in the secondary oxygenated L/S/IVOCs (Section 3.2) since they include siloxanes and ethers, while secondary oxygenated species are primarily alcohols, peroxides, nitrates, and ketones. Emitted oxygenated IVOCs have a significantly lower potential to form SOA than hydrocarbon IVOCs of similar volatility (Pennington et al., 2021). In addition, oxygenated species generally differ from hydrocarbon-like emissions in their ability to form O_3, peroxyacetyl nitrate (PAN), and formaldehyde (Coggon et al., 2021) and should be represented separately from hydrocarbon-like species.

Two new types of oxygenated IVOCs with direct emissions are included as distinct species in CRACMM (Fig. 1-3 purple): propylene glycol (PROG) and oxygenated IVOCs (ROCIOXY). 1,2-propylene glycol is one of the most prevalent species in consumer product purchases (Stanfield et al., 2021) and is associated with increased allergic symptoms when inhaled (Choi et al., 2010). Propylene glycol is represented in CRACMM with chemistry based on MCM following the work of Coggon et al. (2021). The ROCIOXY class includes non-aromatic, saturated IVOCs with $n_O:n_C$ > 0.1 and all species containing silicon. Decamethylcyclopentasiloxane is the most abundant individual species in ROCIOXY, and ROCIOXY has an emission-weighted effective carbon number of 9.5. Due to the highly aggregated nature of ROCIOXY, the k_{OH} and molecular weight are emission-weighted properties rather than based on a representative compound. ROCIOXY produces the ethylperoxy radical with an 85.2% molar yield and SOA with a 14.9% molar yield (Table 1) upon reaction with HO in CRACMM. While the SOA yield may appear high, the lifetime of ROCIOXY is 40 hours at typical daytime HO concentrations which should limit the amount of SOA in urban source regions, similar to siloxane behavior in the work of Pennington et al. (2021). Future versions

of CRACMM emission processing could redirect alcohols, carbonyls, and other oxygenated S/IVOCs from ROCIOXY to the secondary oxygenated L/S/IVOC series (Sect. 3.2) and readjust the effective ROCIOXY SOA yield.

3.4 Furans

FURAN is a new lumped ROC species introduced in CRACMM with the most abundant individual species in the category being furfural followed by furan. Furans were not previously an independent category in RACM2, and Carter (2020a) recommended mapping 2-furfural to ~C8 hydrocarbons (now HC10) and furan to the lumped o-xylene (XYO in RACM2). Given the abundance of furans (140 Gg yr^{-1} of emission, primarily from wood burning for 2017 U.S. conditions), unique functional group structure, HO reactivity (Koss et al., 2018), and O_3 formation potential (Coggon et al., 2019), FURAN was implemented in CRACMM as a new species (Fig. 1-3 blue). Furans have been shown to form SOA with yields between 1.85% to 8.5% by mass depending on the structure (Gómez Alvarez et al., 2009) and the simple SAR predicts a yield of 2.6% by mass (Fig. S5). The furan SOA yield is about a factor of 4 lower than that of xylenes but products such as furanone (FURANONE, a new species in CRACMM) are also formed in aromatic systems like benzene (Section 3.5). The CRACMM species, FURAN, includes small amounts of other species with 2 double bonds (Fig. S3) including 2.4 Gg yr^{-1} of anthropogenic dienes.

The FURAN chemistry in CRACMM is based on a 5-species weighted average using furan emission factors reported by Koss et al. (2018) and the furan chemistry outlined by Wang et al. (2021) and Coggon et al. (2019). FURAN will predominantly react with hydroxyl radicals leading to gas-phase products including dicarbonyls (DCB1, DCB3), organic nitrates (ONIT), peroxides (OP2), furanone (FURANONE), and aldehydes (ALD) in addition to radicals (Appendix B). CRACMM assigns SOA from FURAN to further reactions in the ring-retaining product channel, FURANONE, consistent with products detected by Jiang et al. (2019). The effective SOA yield from FURAN is approximately 5% by mass (Bruns et al., 2016) when branching between high- and low-NO_X reactions is equal. The yield of SOA from FURANONE in CRACMM is set to 4% by mole or 8% by mass (Table 1).

3.5 Aromatics

Aromatic hydrocarbons (Fig. 1-3 blue) were reorganized in CRACMM to reduce the number of aromatic VOC model species and increase the number of aromatic IVOC species. Instead of 4 aromatic VOC categories based on reactivity (k_{OH}), CRACMM uses two categories of xylene-like hydrocarbon species based on reactivity: m-xylene and more reactive aromatics (XYM) and aromatics less reactive than m-xylene (XYE). Toluene (TOL), a HAP (Sect. 4), is now explicit in CRACMM, and benzene (BEN) was already explicit in RACM2. The three new IVOC aromatic hydrocarbons ($n_O : n_C = 0$) are: naphthalene and other polycyclic aromatic hydrocarbons (NAPH), single-ring aromatics of $log_{10}(C_i^*) \approx 5$ (ROCP5ARO), and single-ring aromatics of $log_{10}(C_i^*) \approx 6$ (ROCP6ARO). The ROCP5ARO and ROCP6ARO categories were previously found to be important for

representing SOA from vehicle combustion sources (Lu et al., 2020), and the emissions for 2017 indicated insufficient mass and SOA formation potential to warrant another aromatic species at $log_{10}(C_i^*) \approx 4$.

MCM v3.3.1 chemistry (Bloss et al., 2005; Jenkin et al., 2003) was used to obtain a basic mechanism for aromatic reaction for seven hydrocarbon-like aromatics in CRACMM (BEN, TOL, XYE, XYM, NAPH, ROCP6ARO and ROCP5ARO). The MCM epoxide yield (which includes unidentified species mass, Birdsall and Elrod (2011)) was set to zero and product mass redirected to the bicyclic peroxy channel following Xu et al. (2020). In addition, the organic nitrate yield (β, Reaction R11) from RO_2+NO is 0.2% in CRACMM (Xu et al., 2020). A fraction of the bicyclic peroxy radical channel is assumed to undergo autoxidation (Wang et al., 2017; Molteni et al., 2018; Xu et al., 2020). The following reactions describe this chemistry for a parent aromatic species, AROM:

$$AROM_{M,0} + HO \rightarrow (1\text{-}\alpha_{PL})\ ARO_2 + \alpha_{PL}\ PL_{M\text{-}2.14,1} + \alpha_{PL}\ HO_2 \quad (R9)$$

$$ARO_2 + HO_2 \rightarrow \alpha_H/(1\text{-}\alpha_{PL})\ ROOH^H_{M\text{-}2.48,2} + (1\text{-}\alpha_H\text{-}\alpha_{PL}\text{-}\alpha_A)/(1\text{-}\alpha_{PL})\ ROOH^B_{M\text{-}4.529,5} + \alpha_A/(1\text{-}\alpha_{PL})\ ROOH^A_{M\text{-}7.558,7} \quad (R10)$$

$$ARO_2 + NO \rightarrow \beta\ \alpha_H/(1\text{-}\alpha_{PL})\ RNIT^H_{M\text{-}2.23,3} + \beta\ (1\text{-}\alpha_H\text{-}\alpha_{PL}\text{-}\alpha_A)/(1\text{-}\alpha_{PL})\ RNIT^B_{M\text{-}4.279,6} + \beta\ \alpha_A/(1\text{-}\alpha_{PL})\ RNIT^A_{M\text{-}7.308,8} + (1\text{-}\beta)\ NO_2 + (1\text{-}\beta)\ \alpha_H/(1\text{-}\alpha_{PL})\ ROP^H_{M\text{-}1.35,1} + (1\text{-}\beta)\ (1\text{-}\alpha_H\text{-}\alpha_{PL})/(1\text{-}\alpha_{PL})\ ROP^B \quad (R11)$$

$$ARO_2 + NO_3 \rightarrow NO_2 + \alpha_H/(1\text{-}\alpha_{PL})\ ROP^H_{M\text{-}1.35,1} + (1\text{-}\alpha_H\text{-}\alpha_{PL})/(1\text{-}\alpha_{PL})\ ROP^B \quad (R12)$$

$$ARO_2 + RRO_2 \rightarrow RRO_2P + \alpha_H/(1\text{-}\alpha_{PL})\ ROP^H_{M\text{-}1.35,1} + (1\text{-}\alpha_H\text{-}\alpha_{PL})/(1\text{-}\alpha_{PL})\ ROP^B \quad (R13)$$

Stable, individual species are subscripted with their $log_{10}(C_i^*)$ relative to the parent volatility of M (estimated with SIMPOL (Pankow and Asher, 2008) based on expected functionality) and number of oxygens per molecule. The phenolic product (PL) yield (α_{PL}, 53% for benzene and 16-18% otherwise) is from MCM (o-xylene if a species was not available) and independent of NO level, in good agreement with experimental data for conditions below a few hundred ppb NO (Bates et al., 2021). The PL product is mapped to phenol (for benzene), cresols (for toluene and xylenes), or a lumped secondary oxygenated product (described in Sect. 3.2) based on volatility and $n_O{:}\,n_C$ (for all other aromatics). Aromatic peroxy radical (ARO_2) products included peroxides, organic nitrates, and alkoxy radical decomposition products (ROP). ROP products are produced by H-abstraction (H), traditional HO addition resulting in bicylic peroxy radicals (B), and/or autoxidation (A). The fraction of all AROM + HO through the H-abstraction route (α_H) is from MCM with the product mapped to benzaldehyde in the case of toluene and xylenes or a product based on expected volatility and $n_O{:}\,n_C$ (H-abstraction not applicable for benzene). ROP^B products from the bicylic peroxy radical alkoxy radical decomposition channel follow MCM and include glyoxal and/or methylglyoxal, furanones, dicarbonyl(s), and HO_2. α_A is the fraction of products undergoing autoxidation and is a subset of the bicyclic RO_2 products. Coefficients in Reactions R9-R13 (α_H, α_{PL}, α_A) are relative to total AROM + HO except the fraction of RO_2 + NO branching to organic nitrates (β) in Reaction R11.

Aromatic peroxy radicals can react with other organic peroxy radicals (RRO_2) with methyl peroxy radicals and acetylperoxy radicals being the most abundant and always represented in RACM2 (Stockwell et al., 1990). The RRO_2 products (RRO_2P) are based on MCM at yields specified independently of the ARO_2 product channels. Specifically, methyl peroxy radicals

(RRO_2 as RACM2 species MO_2), result in 0.68 formaldehyde, 0.37 HO_2, and 0.32 higher alcohols (RRO_2P = 0.68 HCHO + 0.37 HO2 + 0.32 MOH). Acetylperoxy radicals (RRO_2 as RACM2 species ACO_3) result in 0.7 methyl peroxy radicals and 0.3 acetic acid (RRO_2P = MO2 + ORA2).

Reactions R9-R13 produce condensible gases and SOA precursors. In the case of volatile aromatics like benzene, toluene, and xylenes, further reaction of the phenolic product along with autoxidation are proposed as the major SOA channels in CRACMM since traditional bimolecular RO_2 products are generally not of sufficiently low volatility. For aromatic IVOCs, peroxides, nitrates, and aldehydes from bimolecular RO_2 reactions can be semivolatile and partition based on their saturation concentration. Further oxidation of furanone produced from aromatic oxidation (e.g., Reaction 477, Appendix B) also results in small amounts of SOA (Sect. 3.4). For products in Reactions R9-R13 that are mapped to a corresponding surrogate of matching volatility and $n_O{:}\,n_C$, further chemical processing follows the secondary oxygenated S/IVOC chemistry in Sect. 3.2.

CRACMM retains the three phenolic species of RACM2 (hydroxy substituted benzenes like phenol and benzene diols, PHEN; cresols, CSL; and methylcatechols, MCT) with the same gas-phase chemistry as RACM2 except for the addition of one, nonvolatile SOA product for PHEN and CSL. The yield of SOA from phenols and cresols is set to reproduce the high-NO_X SOA yields from benzene and toluene oxidation observed in chamber experiments by Ng et al. (2007) with wall loss corrections based on Zhang et al. (2014) (see the supplement information for a detailed derivation). The molar SOA yield using this method is estimated as 15% by mole for phenols and 20% by mole for cresols (Table 1), within the range of 24-52% by mass for phenols and 27-49% by mass for cresols as summarized by Bruns et al. (2016). Future work should expand upon this phenolic SOA treatment as improvements in the phenoxy-phenylperoxy radical chemistry have been shown to modulate O_3 formation and could improve predictions for laboratory conditions over MCM, RACM2, and SAPRC by breaking the catalytic radical cycles (Bates et al., 2021). Products like methylcatechols could also lead to SOA with implications for O_3 and HO production in aromatic systems.

The bicyclic peroxy radical fate in aromatic hydrocarbon systems is not well characterized but includes autoxidation. Molteni et al. (2018) estimate molar yields of autoxidation products from aromatic oxidation of just under 3% by mole and that value is used for the aromatic IVOC systems in CRACMM (α_A=0.03). Higher values are not needed to produce significant SOA in IVOCs systems since traditional bimolecular RO_2 fates result in sufficiently functionalized products to contribute to SOA. Specifically, with α_A=0.03, CRACMM predicts SOA yields for ROCP5ARO, ROCP6ARO, and NAPH of 37%, 21% and 21% by mole respectively (Table 1). However, such low levels of autoxidation, even when combined with phenolic (PHEN and CSL) SOA, are insufficient to explain observed SOA production for the more volatile aromatics, particularly in RO_2 + HO_2 dominant conditions where SOA yields are around 27% by mole based on chamber experiments. Xu et al. (2020) indicate bicyclic peroxy radicals in the benzene system may predominantly form alkoxy radicals (even in RO_2 + HO_2 conditions) that continue to highly oxygenated organic molecules (HOM) in addition to other products. Given the current lack of carbon closure

for gas-phase aromatic chemistry (Xu et al., 2020) and low-volatility of laboratory generated $RO_2 + HO_2$ aromatic SOA (Ng et al., 2007), the amount of autoxidation in the benzene, toluene, and xylene aromatic systems is set in CRACMM to reproduce observed $RO_2 + HO_2$ chamber SOA yields when combined with the phenolic channel (see supplementary information for molar yield derivation). The resulting estimates for the fraction of AROM + HO reaction leading to autoxidation (α_A) are estimated as 19% by mole for benzene and 23% by mole for toluene and xylenes. This results in the phenolic channel contributing 30% of the SOA in the benzene system and 13% in the toluene systems for $RO_2 + HO_2$ conditions, similar to the previously published estimate of 20% for low-NO_x conditions for benzene, toluene, and m-xylene (Nakao et al., 2011) and 20-40% for toluene (Schwantes et al., 2017) as well as the relative abundance of phenolic products in benzene versus toluene systems.

In general, autoxidation of the bicyclic RO_2 in the aromatic systems is assumed to involve one H-shift followed by O_2 addition and result in peroxides and nitrates about seven $log_{10}(C_i^*)$ values lower in volatility than the parent aromatic (products in Reactions R10-R11). The autoxidation product in benzene and toluene systems with only one H-shift would have a C_i^* of 10 μg m^{-3}, making it semivolatile according to SIMPOL (Pankow and Asher, 2008). To improve consistency with Ng et al. yields and nonvolatile partitioning behaviors under low-NO_X conditions at low organic aerosol concentrations (<10 μg m^{-3}), the products from autoxidation in the toluene and benzene systems are assumed to result from two H-shifts followed by O_2 addition leading to two additional hydroperoxide functional groups and autoxidation products with C_i^* = 0.01 μg m^{-3}. Xylene-like (XYM and XYE) autoxidation products assume one H-shift with O_2 addition resulting in autoxidation products with C_i^* = 1 μg m^{-3}. $ROOH^B$ products from XYM and XYE are slightly lower in volatility than those from benzene and toluene and mapped to the new multifunctional C_8 peroxide (OP3, see Sect. 3.2 and Table 1) resulting in SOA from channels other than autoxidation and phenolic routes for xylenes. SOA yields for benzene, toluene, and xylenes summarized in Table 1 generally reproduce wall-loss corrected laboratory values (Ng et al., 2007; Zhang et al., 2014) due to the imposed autoxidation channel. Benzene and toluene are predicted to have lower SOA yields than the IVOC aromatics NAPH, ROCP5ARO, and ROCP6ARO. However, the amount of autoxidation for aromatic IVOCs was not adjusted to match literature SOA yields since many traditional bimolecular products were already in the S/IVOC range and thus SOA for aromatic IVOCs could be underestimated compared to laboratory work (Srivastava et al., 2022).

Figure 5 shows the molar flows to organic aerosol in the combined aromatic, phenolic, and furan systems based on anthropogenic and biomass burning emissions in the U.S. for 2017 and equal $RO_2 + HO_2$ vs $RO_2 + NO$ branching. Most (69%) phenol mass is directly emitted with the balance from benzene oxidation. In contrast, cresols are predominantly chemically produced (80% of source) rather than directly emitted. Approximately 22% of furanone is produced directly from furan oxidation but most furanone is predicted to be from oxidation of aromatic hydrocarbons like toluene and xylenes with smaller contributions from IVOC aromatics. About 32% of the aromatic system SOA is predicted to come from phenols, cresols, and furanone through the ASOATJ species. Peroxides (OP3) may be a substantial contributor to SOA mass. Autoxidation, leading to species such as ROCN1OXY6, also make meaningful contributions to the predicted SOA mass. By acknowledging further

oxidation of phenolic species as contributors to overall aromatic hydrocarbon SOA, all phenolic emissions can now be considered SOA precursors. In addition, adding phenolic sources of SOA increases the overall amount of SOA from ROC emissions compared to previous CMAQ aerosol representations that did not include phenols or cresols as SOA precursors.

3.6 Sesquiterpenes

Sesquiterpenes ($C_{15}H_{24}$) are a new radical system in CRACMM (previously only considered for SOA formation in CMAQ, Fig. 1-3 green) with chemistry built using β-caryophyllene from MCM (Jenkin et al., 2012) and autoxidation based on literature. β-caryophyllene is an IVOC ($log_{10}(C_i^*)$ of 5.05 μg m^{-3}) and MCM chemistry readily predicts sesquiterpene products that are S/IVOCs, consistent with the semivolatile nature of observed SOA (Griffin et al., 1999). Sesquiterpenes, SESQ, react with NO_3, O_3, and HO:

$SESQ_{5.05,0} + NO_3 \rightarrow SESQNRO_2$ (R14)

$SESQNRO_2 + HO_2 \rightarrow ROOH_{0.34,5}$ (R15)

$SESQNRO_2 + NO \rightarrow KET_{2.72,2} + 2\ NO_2$ (R16)

$SESQNRO_2 + NO_3 \rightarrow KET_{2.72,2} + 2\ NO_2$ (R17)

$SESQ_{5.05,0} + O_3 \rightarrow (1-\alpha_A)\ KET_{2.72,2} + \alpha_A\ PA_{-2,3}$ (R18)

$SESQ_{5.05,0} + HO \rightarrow SESQRO_2$ (R19)

$SESQRO_2 + HO_2 \rightarrow ROOH_{0.34,3}$ (R20)

$SESQRO_2 + NO_3 \rightarrow KET_{2.72,2}$ (R21)

$SESQRO_2 + NO \rightarrow \beta\ ONIT_{0.59,4} + (1-\beta)\ KET_{2.72,2} + (1-\beta)\ NO_2$ (R22)

Where α_A is the fraction of ozonolysis products undergoing autoxidation and β is the fraction of RO_2 +NO products resulting in organic nitrates (β = 0.25). The ozonolysis reaction (R18) is highly simplified and predicted to result in a ketone and autoxidation product, PA, of specified volatility and degree of oxygenation. Autoxidation is based on Richters et al. (2016) and α_A set to 1.8% by mole. Observations indicate sesquiterpenes are not major contributors by mass to ambient SOA in the Amazon (Yee et al., 2018), southeastern U.S., or boreal forest (Lee et al., 2020). As a result, CRACMM does not retain the unique identity of sesquiterpene products and all stable products in reactions R14-R22 are mapped to the corresponding secondary oxygenated S/IVOC of corresponding volatility and degree of oxygenation with further chemistry specified in Sect. 3.2.

CRACMM predicts prompt (first generation) sesquiterpene SOA that is less volatile than previous CMAQ work (Carlton et al., 2010; Griffin et al., 1999), is NO_x and oxidant dependent, and has the potential for higher yields through multigenerational chemistry. The yield of prompt SOA under RO_2+HO_2 dominant conditions is predicted to be 50% (OA = 1 μg m^{-3}) to 91% (OA = 10 μg m^{-3}) by mole for HO and NO_3 oxidation. These low-NO NO_3 yields are within the range of those observed in NO_3 oxidation experiments (SOA yields of 56-109% by mole of C, Jaoui et al. (2013)) albeit laboratory values corresponded to a higher concentration of organic aerosol (60-110 μg m^{-3}) and the RO_2 fate was not characterized. Under higher NO_X

conditions (RO_2+NO dominant) and moderate organic aerosol loading (OA = 10 μg m^{-3}), prompt SOA yields are expected to be ~12% by mole from HO oxidation similar to the carbon-based yields of aerosol from laboratory work (19% by mole for β-caryophyllene, Jaoui et al. (2013)). Nitrate oxidation is not expected to produce significant SOA when RO_2 react with NO or NO_3 (Reaction R16-R17), and prompt SOA yields from ozonolysis are 2.7% by mole, lower than the observed yield of 28% by mole C for ozonolysis (Jaoui et al., 2013). Thus, further chemical processing of first-generation sesquiterpene-derived ketones (mapped to CRACMM species ROCP3OXY2, chemistry in Sect. 3.2) likely results in lower volatility species that increase SOA yields beyond the prompt values, especially under high-NO_x and ozonolysis conditions.

3.7 Monoterpenes

CRACMM retains the two monoterpene categories of RACM2 with α-pinene and Δ-limonene as the major representative compounds in each class (API and LIM, respectively, Fig. 1-3 green). The two classes differ in the number of double bonds per species which is expected to influence reactivity and SOA formation potential (Hoffmann et al., 1997). In addition, species with two double bonds in their initial structure likely experience faster autoxidation (Møller et al., 2020). The two classes of monoterpenes (API vs LIM) have different sources of emissions with α-pinene being predominantly from vegetation but limonene having the potential for significant anthropogenic emissions from volatile chemical products (Coggon et al., 2021) in addition to biogenic sources. A new representation of API and LIM reaction with HO, NO_3, and O_3 was created to account for autoxidation leading to HOM and SOA. In addition, bimolecular peroxy radical reactions leading to dimers of extremely low volatility (CRACMM species ELHOM) with the potential to contribute to new particle formation via nucleation (Bianchi et al., 2019) were added.

When a monoterpene species, MT, reacts with an oxidant like HO (or NO_3), it directly forms a collection of peroxy radicals (MRO_2 and MRO_2^A), a fraction of which (α_A) can undergo autoxidation and form HOM:

$$MT + Oxidant \rightarrow (1- \alpha_A)\ MRO_2 + \alpha_A\ MRO_2^A. \quad (R23)$$

Autoxidation is implemented as a fixed yield rather than competitive fate since autoxidation in monoterpene + HO systems proceeds rapidly (rates of 3 to >10 s^{-1}) and only via specific peroxy radical isomers (Piletic and Kleindienst, 2022; Zhao et al., 2018; Berndt et al., 2016; Xu et al., 2019). This assumption of a fixed yield is valid for bimolecular RO_2 lifetimes (time scale for RO_2 reaction with NO or HO_2) greater than ~1 second (NO < ~1 ppb) which is consistent with most current conditions near earth's surface except for select urban locations, more often in winter, (Porter et al., 2021) and episodically near sources. The fraction of prompt API + HO peroxy radicals undergoing autoxidation and forming monoterpene-derived HOM (tracked as CRACMM species, HOM) (α_A) is set to 2.5% by mole (Berndt et al., 2016; Piletic and Kleindienst, 2022) with the uncertainty in the yield around a factor of two. Limonene is expected to have rapid H-shift reactions (Møller et al., 2020) and higher amounts of autoxidation products than α-pinene (Jokinen et al., 2015), and α_A is 5.5% for LIM + HO (Piletic and Kleindienst, 2022) (Table S7).

The peroxy radicals from monoterpene (API and LIM) reactions with HO undergo traditional bimolecular RO_2 fates leading to peroxides, alkoxy radical products, and nitrates:

$$MRO_2 + HO_2 \rightarrow ROOH \quad \text{(R24)}$$

$$MRO_2 + NO \rightarrow (1 - \beta)\, NO_2 + \alpha_{ALD} \times (1- \beta)\, ROP_{ALD} + (1-\alpha_{ALD}) \times (1- \beta)\, ROP_{FRAG} + \beta\, RNIT \quad \text{(R25)}$$

MRO_2 also reacts with MO2 and ACO3 (See Sect. 3.5) (Appendix B). Peroxides from MRO_2 reaction with HO_2 (Reaction R24) map to a new organic peroxide, OPB, added specifically to represent the C_{10} hydroperoxides from monoterpene oxidation. Further reaction or photolysis of OPB is assumed to produce products like existing organic peroxide reactions in RACM2 with products fed back to the lumped aldehydes (ALD), ketones (KET), and a saturated C_{10} RO_2 (HC10P). To better conserve carbon and track the identity of monoterpene-derived nitrates CRACMM includes a new C_{10} organic nitrate, TRPN (Reaction R25, RNIT product). The OPB peroxides and TRPN nitrates are assumed to remain in the gas phase (see representative structures in Appendix A).

The yield of organic nitrates (β, R25) is 18% for API (Nozière et al., 1999) and 23% for LIM based on MCM v3.3.1. (Saunders et al., 2003). Further reaction of the terpene nitrates produces LVOCs with a 100% molar yield (Zare et al., 2019; Browne et al., 2014) with products mapped to then new lumped CRACMM species for monoterpene HOM. While the yield of SOA from TRPN reaction is 100% by mole, chemical sinks will compete with deposition resulting in less than 100% of TRPN converted to SOA in chemical transport models.

In addition to terpene nitrates, major organic products from RO_2 + NO (Reaction R25) are alkoxy radicals which decompose to either aldehydes and HO_2 (ROP_{ALD}) with a yield of α_{ALD} or other smaller carbon number fragmentation products and HO_2 (ROP_{FRAG}). In the case of LIM (α_{ALD} = 64%), the alkoxy radical decomposition products are assumed to be smaller fragments (HCHO and UALD), but α_{ALD} = 1 for α-pinene according to MCM. Since the aldehydes from API and LIM could undergo autoxidation as hinted by Rolletter et al. (2020), new aldehydes, PINAL and LIMAL, were added for the monoterpene systems. Autoxidation for PINAL and LIMAL is added as competitive fate with plausible autoxidation rate constant for terpene systems ($k = 1\ s^{-1}$) for HO-initiated peroxy radicals formed at a yield of 23% (PINALP) or 70% (LIMALP) based on MCM v3.3.1. LIMAL and PINAL can also be lost via photolysis, and LIMAL can react with O_3. In general, rate constants in monoterpene systems (Appendix B) are from RACM2.

In the case of API and LIM reaction with nitrate radicals, Reactions analogous to R23-R25 generally apply but products are multifunctional and can release NO_2. Nitrate radical reactions are assumed to behave similarly in terms of autoxidation and use the same α_A as HO reactions which is likely in the case of limonene (Chen et al., 2021a) but an overestimate in the case of α-pinene (Kurtén et al., 2017). For reactions where multifunctional peroxy nitrates (or other multifunctional nitrates) are expected, the nitrate identity is prioritized for tracking and the product mapped to TRPN. Reaction of nitrate-derived MRO_2

with NO is expected to predominantly release all the nitrate as NO_2 ($\beta = 0$) and convert NO to NO_2 (additional NO_2 product alongside aldehyde production) while yielding a terpene aldehyde (PINAL or LIMAL) ($\alpha_{ALD} = 1$).

MRO_2^A from autoxidation in monoterpene + HO systems is implemented using two new peroxy radicals (labeled APIP2 and LIMP2) that are assumed to result in $C_{10}O_7$ radicals (Berndt et al., 2016) that can undergo traditional bimolecular fates. For all API and LIM reactions with HO and NO_3, the MRO_2^A + HO_2 product is mapped to HOM. In the case of MRO_2^A + NO, all products that release NO_2 (1-β) are also assumed to re-release HO via different fragmentation routes and the highly oxidized terpene nitrate as well as other carbon-containing products were mapped to HOM. MRO_2^A + MO2 and MRO_2^A + ACO3 aldehydes, ketones, and alcohols are also mapped to HOM. As a result, under all conditions, the yield of HOM from initial API or LIM reaction with HO or NO_3 is α_A.

The speciation of HOM changes slightly when MRO_2^A cross react with other monoterpene or isoprene RO_2. In addition to the traditional peroxy radical cross reactions with other organic peroxy radicals (MO2 and ACO3), the monoterpene-derived peroxy radicals undergoing autoxidation, MRO_2^A, react with the most abundant MRO_2 from α-pinene and limonene + HO to produce C_{20} dimers. These reactions followed the basic form:

$$MRO_2^A + MRO_2 \rightarrow (1-\alpha_{dim})\ HOM + 0.5\times(1-\alpha_{dim})\ ROH + 0.5\times(1-\alpha_{dim})\ ROP_{ALD} + 0.5\times(1-\alpha_{dim})\ HO + 0.5\times(1-\alpha_{dim})\ HO_2 + \alpha_{dim}\ ELHOM \quad (R26)$$

where α_{dim} is the fraction of MRO_2^A incorporated in dimers and set to 4% based on the work of Zhao et al. (2018). Other products include highly oxygenated monomers (mapped to HOM), aldehydes (mapped to PINAL or LIMAL), and alcohols with branching between those products also as specified by Zhao et al. (2018). In the case of nitrate-initiated MRO_2^A, NO_2 rather than HO is released. The same approach is used for monoterpene MRO_2^A + isoprene RO_2 with HCHO and MVK produced rather than PINAL or LIMAL. Dimer reactions are assumed to proceed quickly, and the rate constant was set to 1×10^{-10} cm^3 $molecule^{-1}$ s^{-1} based on the work of Molteni et al. (2019). In both the monoterpene and isoprene cross reactions, the dimer products are predicted to have a $log_{10}(C_i^*) < -3$ and are mapped to ELHOM.

The ozonolysis of monoterpenes in CRACMM also mimics reaction R23 where the oxidant in these reactions is O_3. Initially, the ozonolysis reaction will break a monoterpene double bond and yield Criegee intermediates that self-react to release hydroxyl radicals and produce peroxy radicals which were classified into the same two types of peroxy radical categories as with HO reactions: either autoxidizable or non-autoxidizable. The yield of peroxy radicals able to undergo autoxidation (MRO_2^A) for ozonolysis is set to 5% and 11% respectively in the API and LIM systems. These yields are doubled compared to HO to fall within the uncertainty of laboratory and computational studies that indicated autoxidation yields from O_3-initiated reactions are universally higher than autoxidation from HO-initiated chemistry (Jokinen et al., 2015; Ehn et al., 2014; Chen et al., 2021a). The formation of HO, H_2O_2, CO and aldehyde products from the ozonolysis reactions alongside MRO_2^A were

prescribed following MCM and RACM2 and further reaction of the MRO_2 and MRO_2^A peroxy radicals is the same as in the HO system.

Predicted SOA in the monoterpene systems comes from HOM and ELHOM products that are either promptly produced or from further reaction of terpene nitrates or terpene aldehydes. The yield of SOA from API reaction with HO or NO_3 is expected to be 2.5% by mole (4.6% by mass) from the initial autoxidation HOM but is further increased to 11% by mole (21% by mass) when the terpene nitrates further react under typical ambient conditions (Table 1). Under high-NOx conditions (RO_2+NO as the dominant bimolecular fate), the yield of SOA from API + HO approaches 37% by mass with most of the mass from terpene nitrate products highlighting the importance of the terpene nitrate fate which is currently assumed to be reaction with HO and functionalization. LIM SOA yields from HO and NO_3 are similar with values of 16% by mole or 30% by mass for typical conditions but as much as 50% by mass if RO_2+NO dominates and terpene nitrates react further. Yields also increase compared to the typical values if the terpene aldehydes react with HO which is estimated to yield SOA at 21% by mole (31% by mass) or 64% by mole (95% y mass) for PINAL and LIMAL, respectively. Terpene aldehyde photolysis, OPB (and OP3) reaction with HO, or LIMAL reaction with O_3 can also lead to trace amounts of SOA via a C_{10} RO_2 product (<1% molar yield, chemistry of Sect. 3.1 for HC10 peroxy radical).

The autoxidation derived HOM yield for α-pinene from CRACMM is similar to the computed yield predicted by Weber et al. (2020) using a more detailed CRI-HOM mechanism that invoked multi-generational peroxy radical chemistry in a global atmospheric chemistry model. Other models have applied numerous autoxidation mechanisms of varying complexity including a steady state HOM yield assumption similar to CRACMM (Gordon et al., 2016), a volatility basis set model (Schervish and Donahue, 2020), and a near explicit autoxidation mechanism involving 1773 reactions (Roldin et al., 2019). While the fixed HOM yields implemented in CRACMM consolidate the mechanism, additional species and reactions are considered here including NO_3 oxidation chemistry, the chemistry of reactive monoterpenes like limonene, and many accretion reactions that may produce ELHOM. Further refinements to the autoxidation mechanism will be considered in future CRACMM versions including an implementation of the temperature dependence of H-shift reactions, potentially revised volatilities for HOM and ELHOM, and fragmentation reactions of highly oxidized peroxy radicals that may limit HOM production.

The CRACMM approach to monoterpene organic nitrates differs from previous CMAQ approaches where organic nitrates were incorporated into the particle via heterogenous uptake driven by hydrolysis reactions (Pye et al., 2015; Zare et al., 2019). CRACMM indicates a potentially significant role for TRPN in forming SOA but via a different mechanism than previous work which assumed a 3-hour lifetime against condensed phase hydrolysis (k_{HET} (defined in footnote of Appendix B) of 1.13×10^{-7} s^{-1}). TRPN could also release NO_X upon chemical reaction (Saunders et al., 2003) and fragment into smaller molecules (Weber et al., 2020) which are not considered here. Future versions of CRACMM should incorporate monoterpene nitrate hydrolysis and release NO_X upon reaction where appropriate.

Note that the identity of terpene nitrates when they are lumped into HOM or ELHOM is not retained. Lower volatility nitrates, peroxides, ketones, and alcohols from terpene oxidation are lumped together based on volatility with HOM having an effective $log_{10}(C_i^*)$ of 0 to -3 and a representative structure with $log_{10}(C_i^*)$ of -2.2. ELHOM are nominally highly oxygenated C_{20} dimers with an effective $log_{10}(C_i^*)$ of -5 but species with C_{15} structures are also mapped to ELHOM based on their volatility (estimated as $log_{10}(C_i^*) < -3$). Given the importance of volatility as a driver of new particle formation events (McFiggans et al., 2019), the resolution in volatility for highly oxidized products should be investigated in future work in the context of predicting new particle formation events.

3.8 Isoprene and aqueous aerosol pathways

The treatment of isoprene chemistry in CRACMM version 1.0 is the same as in RACM2-AERO6 as implemented in CMAQ v5.3.3. Notably, the CMAQ implementation includes formation of isoprene epoxydiols (IEPOX) as a tracer. An investigation of isoprene chemistry in CRACMM using the Automated MOdel REduction (AMORE) condensation of a detailed isoprene mechanism (Wennberg et al., 2018) with isoprene nitrate hydrolysis (Vasquez et al., 2020), is available in the work of Wiser et al. (in prep.) and as CRACMM1AMORE in CMAQv5.4.

Precursors to SOA from aqueous reactions include IEPOX, glyoxal (GLY), and methylglyoxal (MGLY) and follow CMAQ AERO7. GLY is a lumped species and emissions include glycolaldehyde (total U.S. 2017 GLY emissions: 418 Gg yr^{-1}). MGLY is also lumped and includes 2-oxobutanal and other carbonyl aldehydes (total U.S. 2017 MGLY emissions: 1129 Gg yr^{-1}). SOA from IEPOX uptake follows the reactive uptake formulation of Pye et al. (2013) with the Henry's law coefficient for IEPOX (3.0×10^7 M atm^{-1}) and organosulfate condensed-phase formation rate constant (8.83×10^{-3} M^{-2} s^{-1}) from the work of Pye et al. (2017). New in CRACMM compared to standard AERO7 in CMAQ are separate species for the organosulfate (AISO3OS) vs. non-sulfated (2-methyltetrol, AISO3NOS) IEPOX-derived SOA to facilitate tracking of sulfur. Reactive uptake of GLY and MGLY on aqueous particles uses a fixed uptake coefficient (2.9×10^{-3}) (Liggio et al., 2005) as in CMAQ version 5.2-5.3.3 (Pye et al., 2015). Cloud-processed SOA from GLY and MGLY is based on the reaction with aqueous HO and the work of Carlton et al. (Carlton et al., 2008). Glyoxal SOA may include formation of salt-like structures in the aerosol phase (Paciga et al., 2014), but for simplicity, the oligomeric structure of Loeffler et al. (2006) is used as the representative structure of all glyoxal and methylglyoxal SOA. Note that the molecular weight of GLY and MGLY SOA specified in CRACMM differs from the representative structure. Aqueous reaction products leading to SOA in CRACMM, as implemented in CMAQ, are not currently allowed to volatilize to the gas phase which likely occurs for a subset of IEPOX products (Riedel et al., 2015; D'Ambro et al., 2019).

3.9 Acrolein and 1,3-butadiene

Acrolein (ACRO) is a major oxidation product of 1,3-butadiene (BDE13) and both species were added explicitly in CRACMM due to their importance for health (Scheffe et al., 2016) (see Sect. 4). For BDE13 reaction with HO, which is likely its dominant removal pathway (Agency for Toxic Substances and Disease Registry, 2012; Tuazon et al., 1999), the SAPRC18 Mechgen utility (Carter, 2020b) was used to generate products that are mapped to the analogous CRACMM species. SAPRC18 Mechgen is convenient since the products are already aggregated to a similar degree as RACM2 and CRACMM. A peroxy radical specific to BDE13 reaction with HO (BDE13P) is used so that formation of acrolein (from all channels except BDE13P+HO_2) could be explicitly predicted. For BDE13 + O_3, a Criegee biradical is predicted to be a significant product in SAPRC18 and MCMv3.3.1. Criegee biradicals are not implemented in CRACMM due to their short lifetime, so MCMv3.3.1 was used to determine the likely products from Criegee decomposition. For simplicity, BDE13 reaction with nitrate follows the diene + NO_3 products from RACM2 with acrolein instead of MACR specified as the product. Products from reaction of ACRO with HO and NO_3 are taken from RACM2's lumped MACR species. In the case of ACRO ozonolysis, prompt products as well as the expected Criegee biradical products are from MCM. ACRO photolysis products are from SPARC18 Mechgen.

3.10 Additional rate constant updates

The inorganic chemistry of RACM2 is retained in CRACMM with updated rate constants for some reactions. In CRACMM, rate expressions for 26 inorganic reactions and 2 organic reactions (carbon monoxide and methane with HO, ethane was also updated as mentioned in Sect. 3.1) were updated compared to RACM2 values (IUPAC, 2010; Sander et al., 2011; Goliff et al., 2013) to follow the NASA/JPL evaluation number 19 (Burkholder et al., 2019) and IUPAC recommendations (Atkinson et al., 2004). Photolysis rate coefficients were updated for 5 chemical species: C3 and higher aldehydes (ALD), acetone (ACT), methyl ehtyl ketone (MEK), higher ketones (KET), and formaldehyde (HCHO). The photolysis rate coefficient for ALD is set to that of propionaldehyde from the NASA/JPL evaluation number 19 (Burkholder et al., 2019). CRACMM adds the acetone photolysis pathway producing methyl peroxy radical and carbon monoxide in addition to the existing RACM2 pathway that produces methyl peroxy and acetyl peroxy radicals. Quantum yields of ACT are updated following the NASA/JPL evaluation number 19 (Burkholder et al., 2019). In addition, the temperature and pressure effects on ACT photolysis rate coefficients now follow Blitz et al. (2004). Photolysis rate coefficients and products of MEK and KET use quantum yield from Raber and Moortgat (1996) and absorption cross sections from Brewer et al. (2019). The photolysis pathway for formaldehyde in RACM2 contained an error in quantum yield data resulting in overestimated photolysis rate coefficients, which are now corrected in CRACMM using data from the NASA/JPL evaluation number 19. These general kinetic updates are expected to lead to minor decreases in O_3 formation compared to RACM2-AERO6.

4 ROC Hazardous Air Pollutants

Hazardous air pollutants are known or suspected to cause serious adverse health or environmental effects and are therefore a priority to represent in chemical mechanisms. However, the number of HAPs routinely considered should be moderated for computational efficiency. While 189 substances are designated as HAPs by the U.S. EPA, HAP species such as polycylic organic matter (POM) and glycol ethers contain many individual compounds such that the actual number of individual species meeting the definition of a HAP is well over 3,000 (U.S. Environmental Protection Agency, 2022c). The SPECIATE database, which includes a HAP identifier, was used as the initial source of identification for the species-level emission inventory and supplemented with additional data sources. POM was identified based on species with more than 1 benzene ring and $n_O : n_C = 0$ in their representative structure (an additional 56 species to the HAP category in SPECIATE). The POM requirement of a boiling point above 100° C was found to be duplicative with the aromaticity criteria based on the work of Achten and Andersson (2015). The identifier of 1-bromopropane, a newly designated HAP (U.S. Environmental Protection Agency, 2022a), was updated. SPECIATE was also cross referenced with individual glycol ethers (U.S. Environmental Protection Agency, 2022c) (4 additional HAPs). CAS numbers of individual species and their representative structures were cross-referenced with the toxicity value file input to the Human Exposure Model (U.S. Environmental Protection Agency, 2021a) identifying an additional 39 HAPs. Overall, 491 HAPs were identified in SPECIATE of which 188 had nonzero ROC emissions in the 2017 inventory used here.

To assess the coverage of HAPs and their toxicity in CRACMM, toxicity potentials were estimated using chronic inhalation metrics from the U.S. Environmental Protection Agency (2021b). EPA's process for estimating a cancer risk is based on the unit risk estimate (URE) which is the estimated number of excess tumors per person due to inhalation of 1 μg m^{-3} of the pollutant over a lifetime. Non-cancer (mutagenicity, developmental toxicity, neurotoxicity, and/or reproductive toxicity) risk uses a reference concentration (RfC) which is an estimate of the concentration that could be inhaled over a lifetime without an appreciable risk. Species in SPECIATE were matched to the inhalation RfC and URE values (U.S. Environmental Protection Agency, 2021a) by CAS number. A few SPECIATE species (2,4-toluene diisocyanate, an m & p-xylene mixture, an m & p-cresol mixture, and a chrysene mixture) were manually mapped to relevant exposure risk values. In cases where a species in SPECIATE did not have a CAS or unique structure, a representative structure was used for mapping. A relative non-cancer toxicity potential was estimated based on the emitted mass of a species divided by the RfC, and a relative cancer toxicity potential was estimated as the product of the emissions and URE (Simon et al., 2010). For species designated as HAPs but not included in the toxicity value table (U.S. Environmental Protection Agency, 2021a), a RfC of 20 mg m^{-3} and URE of $1x10^{-8}$ μg^{-1} m^3, corresponding to the maximum RfC and minimum URE values for known HAPs, were used to provide what is potentially a conservative underestimate of risk potential.

Nine species in CRACMM cover 50% of the total cancer and 60% of the total noncancer emission-weighted toxicity estimated for the anthropogenic and biomass burning emissions for 2017 U.S. conditions (Fig. 6a: ACD, ETEG, ACRO, TOL, NAPH, MOH, HCHO, BDE13, and BEN). Toluene (chemistry in Sect. 3.5) is now separated from other aromatics and explicit due to its role as a HAP and significant emissions on an individual basis (430 Gg yr^{-1} in 2017, Fig. 6b) as well as to facilitate comparison with routine measurements. Ethylene glycol, toluene, and methanol are, however, not particularly strong drivers of cancer and noncancer inhalation toxicity risk potential (Fig. 6b). NAPH (chemistry in Sect. 3.5), ACRO (chemistry in Sect. 3.9), and BDE13 (chemistry in Sect.3.9) are new mechanism species and are estimated to carry significant emission-weighted toxicity (Scheffe et al., 2016) (Fig. 6b). NAPH emissions are dominated by naphthalene (74%) but include POM as well, making it an aggregate of HAPs. Naphthalene alone accounts for 70% of the cancer and 98% of the non-cancer emission-weighted toxicity of NAPH. In the case of ACRO, significant secondary production (not shown in Fig. 6b) is expected, and acrolein has been previously shown to be the largest contributor to noncancer inhalation risk in the U.S. (Scheffe et al., 2016). Given acetaldehyde and formaldehyde are also produced by oxidation of biogenic and anthropogenic emissions, the actual coverage of toxicity by the 9 major HAP species is likely much higher than estimated based on the emissions alone. Previous work including secondary production estimated that acetaldehyde, benzene, formaldehyde, methanol, acrolein, 1,3-butadiene, and naphthalene represented over 84% of the cancer risk and 93% of the non-cancer respiratory risk effects in the U.S. in 2011 (Scheffe et al., 2016).

The lumped, slowly reacting ROC (SLOWROC, Sect. 3.1) is 61% HAP by mass with enough emission-weighted toxicity to make it the second leading contributor to cancer and noncancer health risk potential out of all CRACMM species (Fig. 6b). Species within SLOWROC have a lifetime against chemical reaction of about 1 month and are typically discarded from chemical transport model calculations for that reason. SLOWROC includes ethylene oxide and 1,2-dibromoethane, among many other species, that individually contribute to high levels of potential cancer risk (2^{nd} and 10^{th} highest emission-weighted toxicity out of all 188 individual HAPs in this work). Hydrogen cyanide is the most abundant individual species in SLOWROC and is the second largest contributor to noncancer health risk potential for all HAPs considered. In standard CRACMM applications, SLOWROC concentrations could be used to indicate areas warranting additional investigation, but individual compound tracers would be required for studies specifically addressing the health impacts of these longer-lived pollutants. In CMAQv5.4, additional individual HAPs needed for air toxic assessments (e.g., Scheffe et al., 2016), can be added to a chemical mechanism as tracers with reactive decay.

In total, twenty-nine ROC species in CRACMM contain some amount of HAP emissions (Fig. 6a). In terms of species with significant HAP emissions by mass, the two lumped, single-ring aromatic hydrocarbon categories (XYE and XYM) are 61 and 67% HAP by mass with ethylbenzene (in XYE) and indene (in XYM) being the largest contributors to cancer risk potential and m-xylene (in XYM) and o-xylene (in XYE) being the largest contributors to noncancer health risk potential. The gas-phase chemistry of XYE is based on ethylbenzene (Sect. 3.5), so XYE could become an explicit HAP in CRACMM with

changes only to emission mapping (redirecting single-ring species in XYE other than ethylbenzene to XYM). The two aromatic IVOCs are about 10% HAP by emitted mass with 2,4-toluene diisocyanate (ROCP5ARO) and aniline (ROCP6ARO) being the largest HAP contributors by mass as well as in terms of noncancer health risk potential (#5 and #10 out of 188 species). ALD (35% HAP) includes the HAP propionaldehyde. OLT (5% HAP by mass) includes acrylonitrile resulting in moderate cancer and noncancer health risk potential. Despite the low contributions by mass of HAPs to FURAN, FURAN shows moderate contributions to cancer risk potential due to the inclusion of chloroprene.

HAPs added in CRACMM provide greater explicit coverage of species contributing to chronic inhalation health risks, and many of the species classified as HAPs also contribute substantially to criteria pollutant formation. In total, HAPs are estimated to account for about 8% of the total OA formation potential for 2017 U.S. anthropogenic and biomass burning emissions (using SAR methods from Sect. 2.1). HAPs, with major contributors being formaldehyde, toluene, acetaldehyde, m-xylene, 1,3-butadiene, ethylbenzene, o-xylene, acrolein, ethylene glycol, and phenol, are predicted to contribute 31% of the O_3 formation potential for 2017 U.S. anthropogenic and biomass burning emissions. Based on their potential for emission-weighted cancer toxicity ©, noncancer toxicity (N), and O_3 formation potential (O), priority HAPs to consider for purposes of protecting public health are: formaldehye (CNO), ethylene oxi©(C), naphth©ne (C), 1,3-butadiene (CN),©nzene (C), acrolein (N), hydrogen cyanide (N), toluene 2,4-diisocyanate (N), acetaldehyde (O), toluene (O), m-xylene (O), and methanol (O).

5 Implications for the Chemical Evolution of ROC

In this section, CRACMM ROC species are visualized in terms of the carbon oxidation state and degree of oxygenation to understand if there are critical gaps in the atmospheric representation of ROC. The mean carbon oxidation state (OS_C) of a species increases upon oxidation and compounds generally move towards lower n_C and higher OS_C as they are chemically processed in the atmosphere (Kroll et al., 2011). This view emphasizes SOA as a chemical intermediate on the path toward smaller and more functionalized compounds with carbon dioxide (OS_C = 4) as the ultimate endpoint. Using the CRACMM representative structures (Appendix A), each stable ROC species was plotted in the OS_C vs n_C space (Fig. 7) using the OS_C definition of Kroll et al. (2011) considering the number of carbon, hydrogen (n_H), and oxygen (n_O) per molecule and expanded to include nitrogen (n_N) and sulfur (n_S) (assuming sulfate and nitrate functionality) as follows:

$$OS_C = 2\times n_O : n_C - n_H : n_C - 5\times n_N : n_C - 6\times n_S : n_C \quad (1).$$

CRACMM species cover the atmospherically relevant range of ROC oxidation state and n_C (Fig. 7). The largest n_C species in CRACMM are alkane-like with 20 to 30 carbons and a low oxidation state consistent with observations of particulate vehicle exhaust and ambient hydrocarbon-like organic aerosol (Kroll et al., 2011). Other OA species in CRACMM generally fall in the range of n_C and OS_C reported for ambient observations of biomass burning organic aerosol, fresh ambient (less oxygenated) SOA, and aged (more oxygenated) ambient SOA. These ambient observations are based on bulk analysis (Kroll et al., 2011),

and thus the observed ranges shown do not identify each possible SOA contributor at the molecular level. Monoterpene SOA, specifically C_{10} HOM monomers and C_{20} HOM dimers, have an oxidation state of -0.4 and -0.9, respectively, similar to laboratory data (Kroll et al., 2011). Monoterpene SOA has also been linked with the less oxidized (fresh ambient SOA) aerosol mass spectrometer (AMS) surrogate (Xu et al., 2018).

Two species in CRACMM, the glyoxal and methylglyoxal SOA from uptake in aqueous particles (AGLYJ) and clouds (AORGC), have overlap with the observed ambient aged SOA which is often identified via positive matrix factorization analysis as a more oxidized oxygenated organic aerosol (MO-OOA) (Zhang et al., 2011). The MO-OOA factor has been linked to SOA from aqueous processing (Xu et al., 2017), and 10% by mass of the MO-OOA in the southeast U.S. has been attributed to low molecular weight carboxylic acids, of which dicarboxylic acids are primarily from aqueous processing (Chen et al., 2021b). Aqueous isoprene SOA species such as isoprene-derived organosulfates and 2-methyltetrols (n_C = 5) match properties of known major isoprene SOA constituents (Kroll et al., 2011; Surratt et al., 2010), and aqueous isoprene SOA (not shown in Fig. 7) is often resolved separately from MO-OOA. If the aged SOA region described by MO-OOA does represent an intermediate through which significant amounts of carbon should pass, additional chemical pathways beyond those from glyoxal and methylgyloxal may be needed in CRACMM.

Other mechanisms besides CRACMM (top of Fig. 7) focus on the more volatile range of ROC. MCM and SAPRC18 include a sesquiterpene species with 15 carbons, but otherwise focus on smaller carbon number species. The range in n_C for alkane-like species in current mechanisms was highlighted in Section 3.1 and never exceeds 12. In terms of aromatics, the largest aromatic in MCM is a C_{11} diethyltoluene. SAPRC18 includes some naphthalene-like species with 12 carbons, and RACM2 represents single ring aromatics with ~9 carbon (Fig. 1, XYM). CB6 has a xylene species with 8 carbons, and RACM2 and CB6 both include monoterpenes as their largest species by n_C. CRACMM S/IVOCs with alkane, aromatic, and oxygenated structures populate the higher carbon number (n_C > 10) space that includes known organic aerosol species as well as precursors with high SOA yields and is not covered by current mechanisms due to their focus on gas-phase endpoints.

As a complement to OS_C, van Krevelen diagrams of $n_H{:}\,n_C$ versus $n_O{:}\,n_C$ for individual and bulk species have been used to provide insight into the evolution of ambient organic aerosol (Heald et al., 2010). Since hydrogen and oxygen are generally the most abundant non-carbon elements in organic aerosol, these diagrams can help identify types of chemical functionalization. Primary emissions, particularly for alkane-like sources like vehicles tend to reside near an $n_H{:}\,n_C$ of two and $n_O{:}\,n_C$ of zero. Atmospheric processing generally moves OA towards higher $n_O{:}\,n_C$ and lower $n_H{:}\,n_C$ with the trajectory determined by the abundance of alcohol and peroxide (slope of zero) vs ketone and aldehyde (slope of -2) groups (Heald et al., 2010). Mean atmospheric transformation of OA has been observed to occur along a slope of -0.5 (Ng et al., 2011) to -0.6 (Chen et al., 2015) which reflects either carboxylic acids or a combination of alcohols, peroxides, ketones, and aldehydes.

Figure 8 (black line) shows the observed trend and range in $n_O:n_C$ from the ambient atmosphere from multiple field campaigns extended to $n_O:n_C$ of zero for primary source measurements.

The 26 individual particulate organic species in CRACMM span the full range of observed $n_O:n_C$ in bulk OA with excellent coverage for $n_O:n_C < 0.5$ (Fig. 8). The highest observed $n_O:n_C$ conditions (~1.2) were only present in remote regions sampled by aircraft as described in the work by Chen et al. (2015). While CRACMM includes species with high $n_O:n_C$, those species (glyoxal SOA, isoprene organosulfate SOA, and non-sulfated isoprene SOA) tend to have much higher $n_H:n_C$ than the ambient trend suggests. Note that $n_O:n_C$ based on measurement techniques may not include all the oxygen in organosulfate compounds and oxidation state is likely a more robust way to measure degree of oxidation than $n_O:n_C$ based on techniques like an AMS (Canagaratna et al., 2015). Particularly for the $n_O:n_C > 0.5$ OA species, CRACMM indicates more hydrogen than ambient observations suggest. If the ambient observations are correct, future versions of CRACMM could resolve the overestimate in $n_H:n_C$ by: (1) shifting the representative compound structures (for species like ROCN2OXY8) to reflect more ketones, (2) adjusting the assumed change in volatility per oxygen in the secondary oxygenated chemistry (Sect. 3.2), and/or (3) adding more chemical channels resulting in condensible ketones, carboxylic acids, or other high $n_O:n_C$, low $n_H:n_C$ products (e.g., photolysis of SOA, Baboomian et al. (2020)). Combined with the information from the oxidation state plot (Fig. 7), CRACMM may need SOA species that are both lower in H and higher in O and at smaller carbon numbers with implications for aerosol hygroscopicity and mass (Pye et al., 2017).

Chen et al. (2015) noted that SOA produced in laboratory experiments was generally too low in $n_H:n_C$ at a given $n_O:n_C$ and tended to reside below the black ambient line in Fig. 8. CRACMM species are above the ambient trendline suggests that our conceptual picture of atmospheric processing to SOA, informed by known gas-phase chemistry and 2-D VBS approaches, does not match what is observed in laboratory experiments. One possible reason is the preferential sampling of certain chemical space in laboratory experiments (Porter et al., 2021).

Figures 7 and 8 suggest that chemistry leading to OA needs to be considered in mechanism development to obtain an accurate representation of gas and particulate ROC including the correct properties of OA. Accurate properties of OA are critical for estimating hygroscopicity with implications for climate (Haywood and Boucher, 2000) as well as fine particle mass (Pye et al., 2017). The linkages between gas and particulate endpoints are further emphasized by examining emissions from anthropogenic and biomass burning sources of ROC by volatility class and their propagation to endpoints (Fig. 9). Total emissions of ROC in 2017 (excluding biogenic VOCs) are estimated at 21 Tg yr^{-1} with VOCs as the most abundantly emitted volatility class of compounds. VOCs dominate ROC HO reactivity accounting for 81% of the total. In addition, the total U.S. O_3 formation potential is estimated as 47 Tg yr^{-1} with VOCs accounting for 90% of it (based on the MIR SAR, Fig. 9). Thus, across all anthropogenic and biomass burning sources and locations for 2017, VOCs are the dominant contributors to gas-phase endpoints such as HO reactivity and O_3; however, emitted IVOCs (generally excluded from mechanism development)

make appreciable contributions to estimated gas-phase endpoints (18% of HO reactivity and 10% of the O_3 formation potential). As a class, the O_3 from IVOCs (about 4.5 Tg yr^{-1}) exceeds the O_3 estimated for any individual CRACMM species in Figure 1. In terms of effective MIR, IVOCs (effective MIR of 1.1 g O_3 g^{-1} ROC) are comparable to HC10 and exceed that of BEN, HC3, and ETH. L/SVOCs are not substantial contributors to HO reactivity or O_3 formation (~1%) due to slower reaction rates (k_{OH}, Fig. 3) and alkane-like structures with less potential for O_3 formation (effective MIR 0.14 to 0.27 g O_3 g^{-1} ROC). The OA potential from ROC emissions in the U.S. (excluding biogenic emissions) is estimated as 5 Tg yr^{-1} and emphasizes the need to consider L/S/IVOCs. Traditional VOCs (effective SOA yield of 5%), are important (14% of total) contributors to OA potential, but OA potential is dominated by IVOCs (38%) and S/IVOCs (48%) due to their initially lower volatility and ability to become condensible with only small additions in functionality.

6 Discussion

CRACMM provides an integrated approach to the representation of O_3, organic aerosol, and many HAPs in air. These endpoints are linked as O_3, SOA, and secondary HAPs such as formaldehyde and acrolein are products of gas-phase precursor emissions including primary HAPs. This section highlights reasons why mechanism development remains important and provides specific recommendations for future work based on lessons from CRACMM development.

First, the magnitude and compound identity of ROC emissions is an active area of research and mechanisms need to interface with this emerging information. Improving emissions characterization without the accompanying mechanism linkages hinders accurate source apportionment and effective air quality management decisions. Much of the work on emissions speciation is identifying new species in the IVOC range which has been historically neglected by gas-phase mechanisms but is necessary for both O_3 and SOA prediction. Emissions speciation work should continue to characterize source profiles in databases and other forums at the highest level of individual compound detail available using representative structures when necessary so compounds can be easily mapped to mechanisms. In addition, efforts to accurately determine the emissions of individual HAPs, especially formaldehyde, acetaldehyde, toluene, m-xylene, and methanol which are important for O_3, should be leveraged in the preparation of emission inputs for regional chemical transport models even when HAPs are not the primary objective. Development of emissions and mechanisms should continue to be an iterative process in which new measurement techniques better quantify and identify emissions resulting in new or refined mechanism species. Simultaneously, mechanisms can indicate which emitted species are high priority to constrain due to their role in secondary pollutant formation or health impacts.

Second, current chemical transport model mechanisms do not characterize the full range of atmospheric ROC and such analysis could help identify missing sources of SOA, HO reactivity, formaldehyde, and other secondary HAPs. The ability to account for all reactive tropospheric carbon and perform a ROC budget analysis in current mechanisms is limited due to the focus on

the more volatile range of ROC which excludes lower volatility primary ROC. In addition, some carbon in secondary ROC, including species in the volatile range, is discarded in mechanisms like SAPRC07 and RACM2 because of product lumping for computational efficiency. For example, the largest organic peroxide in RACM2 is OP2 with two carbons. So, peroxides formed from RO_2+HO_2 reactions for xylene-like aromatics ($n_C = 9$) result in a loss of seven carbon per reaction. In the RACM2 monoterpene system, eight carbons or 80% of the parent carbon is lost each time a peroxide is formed; and SAPRC07 loses 4 carbon for each monoterpene peroxide formed. While conservation of emitted mass was a priority for the design of CRACMM and more secondary mechanism species were added at the higher carbon numbers (e.g., a C_8 and C_{10} peroxide), the chemical scheme in CRACMM is like RACM2 and SAPRC07 in that it does not conserve mass upon reaction for all chemical systems. However, by curating structural identifiers (SMILES) for all species in CRACMM, conservation of carbon can now be calculated and the importance of lost (or gained) carbon can be examined. The CMAQv5.4 implementation of CRACMM includes an updated chemical mechanism processor that creates an optional diagnostic file containing the elemental balance for each CRACMM reaction. Future work will aim to calculate mass balance across the mechanism and use it as a diagnostic tool to guide development.

Third, current gas-phase mechanisms do not couple radical chemistry with SOA formation and linking the development provides additional constraints for ozone-forming reactions as well as secondary inorganic aerosol production. Particles and ozone are inherently linked systems (Ivatt et al., 2022; Womack et al., 2019). Molar yields for SOA are often comparable to molar yields of existing gas-phase product channels, and SOA mass should be removed from volatile gas-phase products. Properly sequestering products like peroxides in the particle will remove them as a potential photolytic source of radicals that release HO_X back to the atmosphere. Similarly, sequestering one organic nitrate in the particle-phase could remove one HO_X and one NO from the gas-phase system. Autoxidation, implemented in CRACMM primarily to produce SOA, effectively sequesters radicals since they are generally of sufficiently low volatility to condense. CRACMMv1.0 targeted SOA systems for development, but CRACMM updates impact O_3 as will be demonstrated for the Northeast U.S. in future companion work (Place et al., in prep.). Future versions of CRACMM should continue to consider chemical channels that lead to both gas-phase and particulate products to better constrain O_3.

Fourth, linking gas-phase chemistry with SOA formation for the first time enabled the treatment of new SOA precursors with implications for the magnitude and source attribution of OA. Organic aerosol is dynamic with properties that evolve as a function of precursor and chemical regime and thus need to be considered as part of a holistic treatment of atmospheric chemistry. The interconnected nature of aromatic, phenolic, and furan systems highlights why mechanism development should consider SOA production alongside gas-phase chemistry. Developing phenolic and furanone gas-phase chemistry without consideration of SOA (as in CMAQv5.3.3) neglects a significant SOA source. Specifying SOA yields for phenolic and aromatic hydrocarbon precursors without recognizing they are also secondary would duplicate SOA mass. As a result, both phenolic and non-phenolic routes to SOA need to be specified consistently. The attribution of aromatic SOA to these two

routes will affect how much SOA is predicted overall and how it is attributed to various sources. In the case of benzene SOA, the more SOA comes from phenol vs non-phenol channels, the higher the total SOA potential of U.S. emissions (as phenol > benzene emissions) and larger attribution to sources with high phenol to benzene ratios such as wildland fires and residential wood combustion. Previous work estimated oxidation of phenol, naphthalene, and benzene alone can account for 80% of the SOA from residential wood combustion (Bruns et al., 2016). The importance of connecting SOA with multigenerational gas-phase chemistry also applies to the monoterpene system where the fate of terpene nitrates and aldehydes will significantly modulate SOA formation. In the case of monoterpene SOA, the allocation of SOA between initial autoxidation, terpene nitrate, and aldehyde channels will affect the NOx dependence of total monoterpene SOA and therefore how much is considered controllable vs. noncontrollable. The allocation of SOA among different later generation species should continue to be evaluated and revised as new information becomes available which will improve source apportionment of fine particle mass.

Fifth, new measurement techniques, observational studies, and computational methods are continually improving the characterization of many chemical systems, and their results need to be translated to model mechanisms. Autoxidation, a novel, atmospherically relevant chemical pathway discovered just under a decade ago (Crounse et al., 2013), will be considered in CMAQ for the first time in CRACMMv1.0. Just this year, a new class of atmospherically relevant compounds, hydrotrioxides were identified (Berndt et al., 2022). Even for traditional systems, information continues to emerge. For example, benzene mechanisms have been historically built on data that characterized about half of the product mass with recent work used to inform CRACMMv1.0 reaching ~80% carbon closure (Xu et al., 2020). Measurement techniques and the availability of observational data will only further improve, providing more complete data to design and evaluate mechanisms going forward.

Finally, the chemistry of the atmosphere in the U.S. and elsewhere is changing, and previously acceptable representations of chemistry may need modification. Autoxidation is one example of a pathway likely to grow in importance, but indications of change can be seen in multiple systems. Deposition of nitrogen has shifted from primarily oxidized nitrogen (nitrate) to reduced nitrogen (ammonia) (Li et al., 2016). Fine particle mass is no longer dominated by summertime sulfate (Chan et al., 2018), and the temperature dependence of summertime urban Northeast U.S. $PM_{2.5}$ is now being modulated by organic aerosol (Vannucci and Cohen, 2022). Particulate sulfur is also becoming increasingly recognized as organic (Riva et al., 2019; Moch et al., 2018). At the same time sulfate and nitrate in cloud water have been decreasing at a mountaintop site in the Northeast U.S., total organic carbon in cloud water may be increasing (Lawrence et al., 2022). Organic compounds in air are changing with total U.S. emissions of anthropogenic ROC going from ~30% lower than NO_x in 2002 to exceeding NO_x by ~40% in 2019 (Pye et al., 2022). The composition of ROC is also changing to more oxygenated forms resulting in an average reduction in the O_3 formation potential of an individual VOC of about 20% due to mixture effects (Venecek et al., 2018). Questions chemical transport modeling and mechanisms are being asked to answer are also changing with increasing interest in wildland fires (McClure and Jaffe, 2018), volatile chemical products (Seltzer et al., 2022), and per- and poly-fluoroalkyl substances (D'Ambro et al., 2021) among them. Changes in air pollution sources and questions of interest as well as chemical regimes

over time require continued mechanism development, and CRACMM is now available as a community framework for further development.

Code and data availability

EPA's CompTox Chemicals Dashboard is available at: https://comptox.epa.gov/dashboard (U.S. Environmental Protection Agency, 2021d). OPERA predictions of species properties can be obtained from the Chemicals Dashboard or for any species with a SMILES using the EPA's Chemical Transformation Simulator at https://qed.epa.gov/cts/ (U.S. Environmental Protection Agency, 2022f). SPECIATE is distributed at https://www.epa.gov/air-emissions-modeling/speciate. RDKit version 2020.09.01 was used in python (RDKit, 2020). The implementation of RACM2-AERO6 is available in CMAQ v5.3.3 (U.S. Environmental Protection Agency Office of Research and Development, 2019). RACM2 and CRACMMv1 in CMAQ v5.4 (released October 2022) are available on github (https://github.com/USEPA/CMAQ) and Zenodo (U.S. EPA Office of Research and Development, 2022). Supporting data for CRACMM, including the SPECIATE database mapped to CRACMM, input to the Speciation Tool, profile files output from Speciation Tool for input to SMOKE, python code for mapping species to CRACMM, chemical mechanism, and mechanism metadata is available at https://github.com/USEPA/CRACMM. Specific analyses and scripts used in this manuscript such as the 2017 U.S. species-level inventory and code for figures are archived on data.gov and available at https://doi.org/10.23719/1527956.

Author contributions

HOTP designed the overall scope and drafted the initial document with input from coauthors. Main text figures were prepared by BNM (Fig. 4) and HOTP (all others). HOTP, BNM, and KMS prepared supplement figures. Chemistry of various ROC systems was designed by HOTP (aromatics, sesquiterpenes, primary oxygenated IVOCs, and other miscellaneous SOA systems), BKP (monoterpenes), BNM (secondary oxygenated ROC), KMS (S/IVOC alkanes), ELD (1,3 butadiene and acrolein), IRP (monoterpenes), RHS (S/IVOC alkanes, furans), MMC (furans, propylene glycol), and LX (aromatics). HOTP, BKP, BNM, KMS, ELD, SF, GS, BH, and JB coded the CMAQ implementation of CRACMM. HOTP, KMS, ELD, IRP, and SF determined representative compound structures for SPECIATE. HOTP, KMS, CA, KMF, and GP developed the 2017 emissions inventory and resulting SOA and ozone analysis. ES, GS, BH, and WRS updated rate constants and photolysis reactions in reactions ported from RACM2. HOTP performed the HAP analysis. All coauthors contributed to developing the mechanism and editing the manuscript.

Competing interests

The authors declare that they have no conflict of interest.

Disclaimer

The views expressed in this article are those of the authors and do not necessarily represent the views or policies of the U.S. Environmental Protection Agency, Department of Energy (DOE), or Oak Ridge Institute of Science and Education (ORISE).

Acknowledgements

This work was supported by the U.S. Environmental Protection Agency Office of Research and Development. This research was supported in part by an appointment to the U.S. Environmental Protection Agency (EPA) Research Participation Program administered by the ORISE through an interagency agreement between the U.S. DOE and the U.S. Environmental Protection Agency. ORISE is managed by ORAU under DOE contract number DE-SC0014664. We thank internal reviewers at EPA for providing comments on a draft of this manuscript. We thank Kelley Barsanti for useful discussion about emissions and mechanism development and Chris Nolte for perspectives on model development. We thank Rohit Mathur and Sergey Napelenok for comments on a draft version of the manuscript. MMC, RHS, and LX acknowledge support through the EPA-STAR program, Grant # 84001001 and the CIRES cooperative agreement NA17OAR4320101. LX also acknowledges NASA grant 80NSSC21K1704.

Tables

Table 1: Pathways to SOA in CRACMM by system. Some systems include a representation of autoxidation (Auto? = Yes). Actual SOA formation in CRACMM is modulated by oxidant concentration (HO, NO_3, O_3), RO_2 bimolecular fate (NO/HO_2), bimolecular RO_2 lifetime (τ_{RO2}), abundance of the partitioning medium (OA), photolysis (hν), and/or aqueous environment (see heterogeneous reactions in Appendix B). When autoxidation is represented but τ_{RO2} is not listed here, autoxidation is assumed to be sufficiently fast that it is not modulated by ambient conditions. All SOA is modulated by temperature through gas-phase reaction rates and effect of temperature on volatility (not explicitly listed). For estimated yield calculations, typical population-weighted values (Porter et al., 2021) of the bimolecular RO_2 fate (equal RO_2+HO_2 and RO_2+NO), the bimolecular lifetime (10s), and the amount of organic partitioning medium (10 μg m^{-3}) are assumed (if applicable). Estimated yields exclude multigenerational oxidation of secondary oxygenated ROC species unless explicitly mentioned.

System	Precursor	Main SOA Species	Scientific Basis	Auto?	Factors affecting SOA	Est. Yield (Mole Frac.)	Est. Yield (Mass Frac.)
Alkane-like systems (Sect. 3.1)							
~C27 SVOCs[a,b]	ROCP1ALK	secondary oxygenated L/S/IVOCs	GECKO (Lannuque et al., 2018) + literature (Praske et al., 2018; Vereecken and Nozière, 2020)	Yes	HO, HO_2/NO, τ_{RO2}, OA	1.0	0.75
~C24 SVOCs[a,b]	ROCP2ALK	secondary oxygenated L/S/IVOCs	GECKO (Lannuque et al., 2018) + literature (Praske et al., 2018; Vereecken and Nozière, 2020)	Yes	HO, HO_2/NO, τ_{RO2}, OA	0.98	0.87
~C21 IVOCs[a,b]	ROCP3ALK	secondary oxygenated L/S/IVOCs	GECKO (Lannuque et al., 2018) + literature (Praske et al., 2018; Vereecken and Nozière, 2020)	Yes	HO, HO_2/NO, τ_{RO2}, OA	0.86	0.72
~C18 IVOCs[a]	ROCP4ALK	secondary oxygenated L/S/IVOCs	GECKO (Lannuque et al., 2018) + literature (Praske et al., 2018; Vereecken and Nozière, 2020)	Yes	HO, HO_2/NO, τ_{RO2}, OA	0.48	0.51
~C14 IVOCs[a]	ROCP5ALK	secondary oxygenated L/S/IVOCs	GECKO (Lannuque et al., 2018) + literature (Praske et al., 2018; Vereecken and Nozière, 2020)	Yes	HO, HO_2/NO, τ_{RO2}, OA	0.13	0.15
~C12 IVOCs[a]	ROCP6ALK	secondary oxygenated L/S/IVOCs	GECKO (Lannuque et al., 2018) + literature (Praske et al., 2018; Vereecken and Nozière, 2020)	Yes	HO, HO_2/NO, τ_{RO2}, OA	0.040	0.043
~C10 VOCs	HC10	secondary oxygenated L/S/IVOCs	GECKO (Lannuque et al., 2018) + literature (Praske et al., 2018; Vereecken and Nozière, 2020)	Yes	HO, HO_2/NO, τ_{RO2}, OA	0.0059	0.0083
~C_5 VOCs	HC5	ASOAT	Emission-based SAR	No	HO	0.0013	0.0037
~C_3 VOCs	HC3	ASOAT	Emission-based SAR	No	HO	2.8×10^{-5}	0.00013
Long-lived species[a]	SLOWROC	ASOAT	Emission-based SAR	No	HO	0.0010	0.0027
Oxygenated L/S/IVOCs (Sect. 3.2-3.3)							

Secondary oxygenated L/SVOCs[c]	ROCP0OXY02 ROCN1OXY06 ROCN1OXY03 ROCN1OXY01	secondary oxygenated L/S/IVOCs	Multigeneration 2-D VBS	No	HO, OA	[d]	1.02-1.16[d]
Secondary oxygenated SVOCs[c]	ROCP1OXY01 ROCP0OXY04	secondary oxygenated L/S/IVOCs	Multigeneration 2-D VBS	No	HO, OA	[d]	0.85-0.89[d]
Secondary oxygenated SVOCs[c]	ROCP2OXY02 ROCP1OXY03	secondary oxygenated L/S/IVOCs	Multigeneration 2-D VBS	No	HO, OA	[d]	0.63-0.64[d]
Secondary oxygenated IVOCs[c]	ROCP3OXY02	secondary oxygenated L/S/IVOCs	Multigeneration 2-D VBS	No	HO, OA	[d]	0.52[d]
Secondary oxygenated IVOCs[c]	ROCP4OXY02	secondary oxygenated L/S/IVOCs	Multigeneration 2-D VBS	No	HO, OA	[d]	0.37[d]
Secondary oxygenated IVOCs[c]	ROCP5OXY01	secondary oxygenated L/S/IVOCs	Multigeneration 2-D VBS	No	HO, OA	[d]	0.36[d]
Secondary oxygenated IVOCs[c]	ROCP6OXY01	secondary oxygenated L/S/IVOCs	Multigeneration 2-D VBS	No	HO, OA	[d]	0.23[d]
Multi-functional ~C8 peroxides	OP3	AOP3	New lumped, semivolatile species; Chemistry like RACM OP2	No	OA, hν, HO	0.50[e]	0.50[e]
Emitted oxygenated IVOCs[a]	ROCIOXY	ASOAT	Emission-based SAR	No	HO	0.15	0.12
Aromatics and furans (Sect. 3.4-3.5)							
Furanone[a]	FURANONE	ASOAT	Literature on furans (Bruns et al., 2016)	No	HO	0.040	0.080
Less volatile aromatic IVOCs[a]	ROCP5ARO	secondary oxygenated L/S/IVOCs ASOAT	MCM (Bloss et al., 2005) + literature (Xu et al., 2020; Molteni et al., 2018)	Yes	HO, HO_2, NO, OA	0.37[f]	0.47[f]
More volatile aromatic IVOCs[a]	ROCP6ARO	secondary oxygenated L/S/IVOCs, ASOAT	MCM (Bloss et al., 2005) + literature (Xu et al., 2020; Molteni et al., 2018)	Yes	HO, HO_2, NO, OA	0.21[f]	0.25[f]
Naphthalene and PAHs	NAPH	secondary oxygenated L/S/IVOCs ASOAT	MCM (Bloss et al., 2005) + literature (Xu et al., 2020; Molteni et al., 2018)	Yes	HO, HO_2, NO, OA	0.21[f]	0.34[f]

Benzene	BEN	AROCN1OXY6, ASOAT	MCM (Bloss et al., 2005) + literature (Xu et al., 2020; Molteni et al., 2018; Ng et al., 2007)	Yes	HO, HO_2, NO, OA	0.18[f,g]	0.44[f,g]
Toluene	TOL	AROCN1OXY6, ASOAT	MCM (Bloss et al., 2005) + literature (Xu et al., 2020; Molteni et al., 2018; Ng et al., 2007)	Yes	HO, HO_2, NO, OA	0.15[f,g]	0.33[f,g]
More reactive aromatic VOCs	XYM	AROCP0OXY4, ASOAT, AOP3	MCM (Bloss et al., 2005) + literature (Xu et al., 2020; Molteni et al., 2018; Ng et al., 2007)	Yes	HO, HO_2, NO, OA	0.28[f,g]	0.54[f,g]
Less reactive aromatic VOCs	XYE	AROCP0OXY4, ASOAT, AOP3	MCM (Bloss et al., 2005) + literature (Xu et al., 2020; Molteni et al., 2018; Ng et al., 2007)	Yes	HO, HO_2, NO, OA	0.28[f,g]	0.50[f,g]
Phenol and aromatic diols[a]	PHEN	ASOAT	Literature including benzene constraints (Bruns et al., 2016; Ng et al., 2007; Zhang et al., 2014)	No	HO	0.15	0.28
Cresols[a]	CSL	ASOAT	Literature including xylene+toluene constraints (Bruns et al., 2016; Ng et al., 2007; Zhang et al., 2014)	No	HO	0.20	0.29
Sesquiterpenes (Sect. 3.6) + Monoterpenes (Sect. 3.7)							
Sesquiterpenes	SESQ	secondary oxygenated L/S/IVOCs	MCM (Jenkin et al., 2012) + literature (Richters et al., 2016)	Yes	HO, NO_3, O_3, HO_2, NO, OA	HO: 0.52, O_3: 0.028, NO_3: 0.46	HO: 0.60, O_3: 0.034, NO_3: 0.45
α-pinene and similar	API	AHOM, AELHOM	Literature (Nozière et al., 1999; Berndt et al., 2016; Piletic and Kleindienst, 2022; Zhao et al., 2018; Jokinen et al., 2015)	Yes	HO, NO_3, O_3, HO_2, NO	HO, NO_3: 0.11,[h] O_3: 0.13[h]	HO, NO_3: 0.21,[h] O_3: 0.24[h]
limonene and similar	LIM	AHOM, AELHOM	Literature (Piletic and Kleindienst, 2022; Zhao et al., 2018; Jokinen et al., 2015)	Yes	HO, NO_3, O_3, HO_2, NO	HO, NO_3: 0.16,[h] O_3: 0.21[h]	HO, NO_3: 0.30,[h] O_3: 0.38[h]
Pinonaldehyde[a]	PINAL	AHOM	MCM (Saunders et al., 2003) + RACM2 photolysis + assumed autoxidation	Yes	HO, τ_{RO2}	Phot: see HC10 HO: 0.21	HO: 0.31
Limonene-like aldehydes[a]	LIMAL	AHOM	MCM (Saunders et al., 2003) + RACM2 photolysis + assumed autoxidation	Yes	HO, O_3, τ_{RO2}	Phot: See HC10 HO: 0.64, O_3: <1%	HO: 0.95
Terpene peroxides	OPB	see HC10	New volatile biogenic peroxide, Chemistry like RACM2 OP2	No	HO, hν	HO: <1%	--
Terpene nitrates	TRPN	AHOM	Literature (Zare et al., 2019)	No	HO, NO_3, O_3	1.0	1.16
Aqueous Systems (Sect. 3.8)							

Isoprene epoxydiols	IEPOX	AISO3NOS, AISO3OS	CMAQ AERO6-7 (Pye et al., 2017; Pye et al., 2013)	No	Particle pH, liquid water, sulfate, size distribution	Variable	Variable
Glyoxal + methylglyoxal uptake to particles	GLY, MGLY	AGLY	CMAQ AERO6-7 (Pye et al., 2015)	No	Particle size distribution	Variable	Variable
Glyoxal + methylglyoxal uptake in clouds	GLY, MGLY	AORGC	CMAQ AERO5-7 (Carlton et al., 2008)	No	HO	Variable	Variable

[a]New SOA precursor system compared to CMAQ AERO6-7 (Appel et al., 2021).

[b]ROCN2ALK, ROCN1ALK, ROCP0ALK, ROCP1ALK, ROCP2ALK, and ROCP3ALK can partition directly to particles and form POA (See Sect. 3.1). Yields here are for chemical reaction.

[c]While these species are envisioned as secondary, oxygenated semivolatile emissions from sources such as biomass burning could be mapped to this system based on volatility.

[d]Calculated for 12 hours of reaction time across multiple generations. Only mass-based yields are provided. See Fig. 4.

[e]Based on semivolatile partitioning of OP3. Further reaction of OP3 with HO produces <1% molar yield of SOA.

[f]SOA yield includes furanone route contributions.

[g]SOA yield includes phenolic (PHEN or CSL) route contributions.

[h]SOA yield includes complete further reaction of TRPN but not aldehydes (PINAL or LIMAL).

Figures

Figure 1: Emission-weighted number of carbon per molecule of individual ROC species grouped by CRACMM species. Violin plots (with shaded colors for families of species in Sect. 3 that are either new or substantially updated compared to RACM2.) are weighted by the magnitude of U.S. anthropogenic and biomass burning emissions in 2017. Overlaid boxplots indicate the 25th percentile, median, and 75th percentile values. Whiskers extend from the minimum to maximum properties for species with emissions >100 Mg yr^{-1}. CMAQ v5.3.3 values are for RACM2 with the aerosol module AERO6 or represent an individual HAP from CMAQ. In some cases, the CMAQv5.3.3 values represent similar species from RACM2 (e.g., HC8 values at CRACMM HC10). Emission magnitudes by species are available in supporting data Table D2.

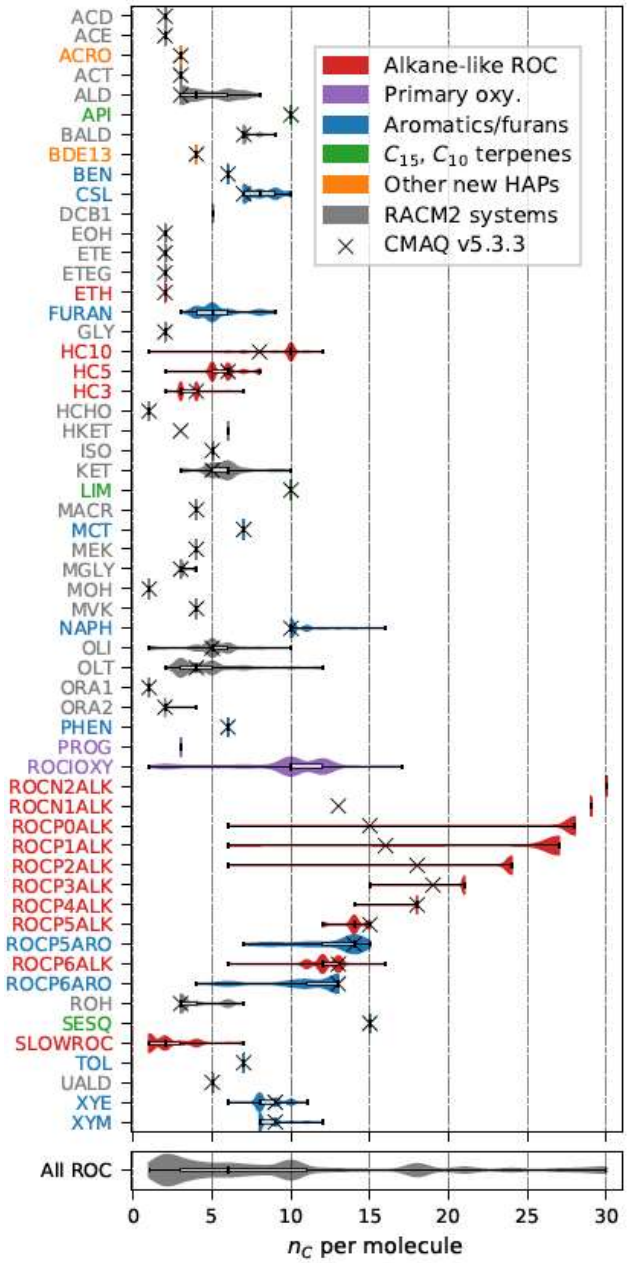
ACD
ACE
ACRO
ACT
ALD
API
BALD
BDE13
BEN
CSL
DCB1
EOH
ETE
ETEG
ETH
FURAN
GLY
HC10
HC5
HC3
HCHO
HKET
ISO
KET
LIM
MACR
MCT
MEK
MGLY
MOH
MVK
NAPH
OLI
OLT
ORA1
ORA2
PHEN
PROG
ROCIOXY
ROCN2ALK
ROCN1ALK
ROCP0ALK
ROCP1ALK
ROCP2ALK
ROCP3ALK
ROCP4ALK
ROCP5ALK
ROCP5ARO
ROCP6ALK
ROCP6ARO
ROH
SESQ
SLOWROC
TOL
UALD
XYE
XYM
All ROC
Alkane-like ROC
Primary oxy.
Aromatics/furans
C_{15}, C_{10} terpenes
Other new HAPs
RACM2 systems
CMAQ v5.3.3
0
5
10
15
20
25
30
n_C per molecule

Figure 2: Same as Fig. 1 except the property displayed is the saturation concentration in $\log_{10}(C_i^*)$.

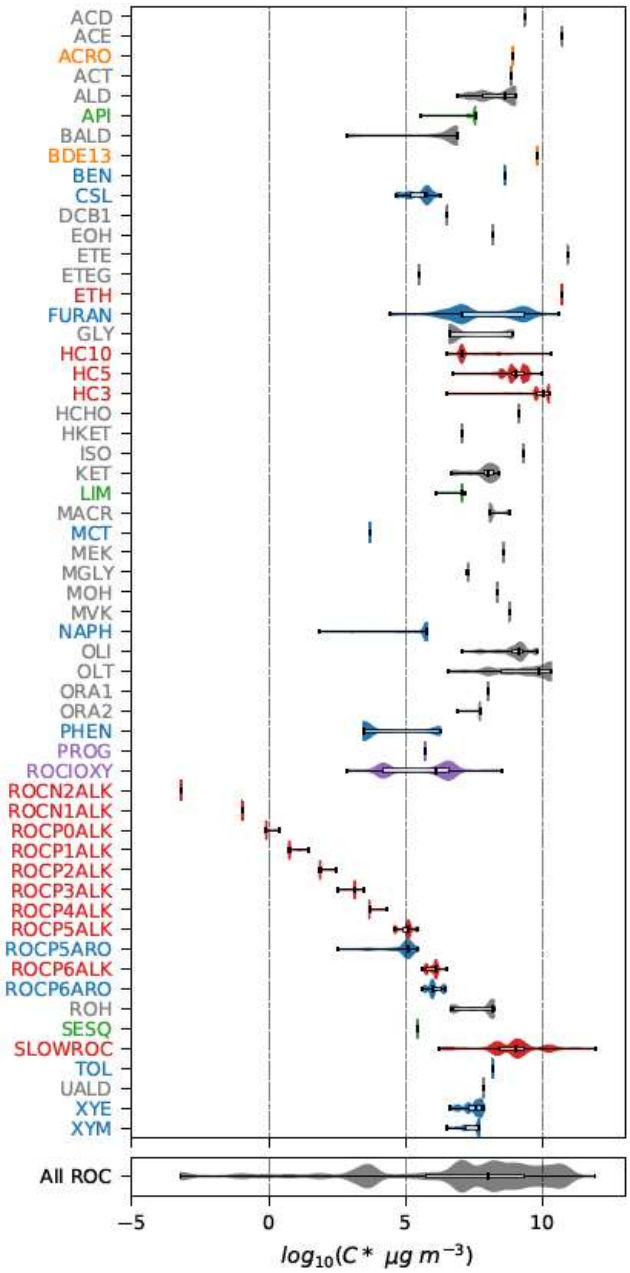

1160

Figure 3: Same as Fig. 1 except the property displayed is the HO rate constant estimated by OPERA.

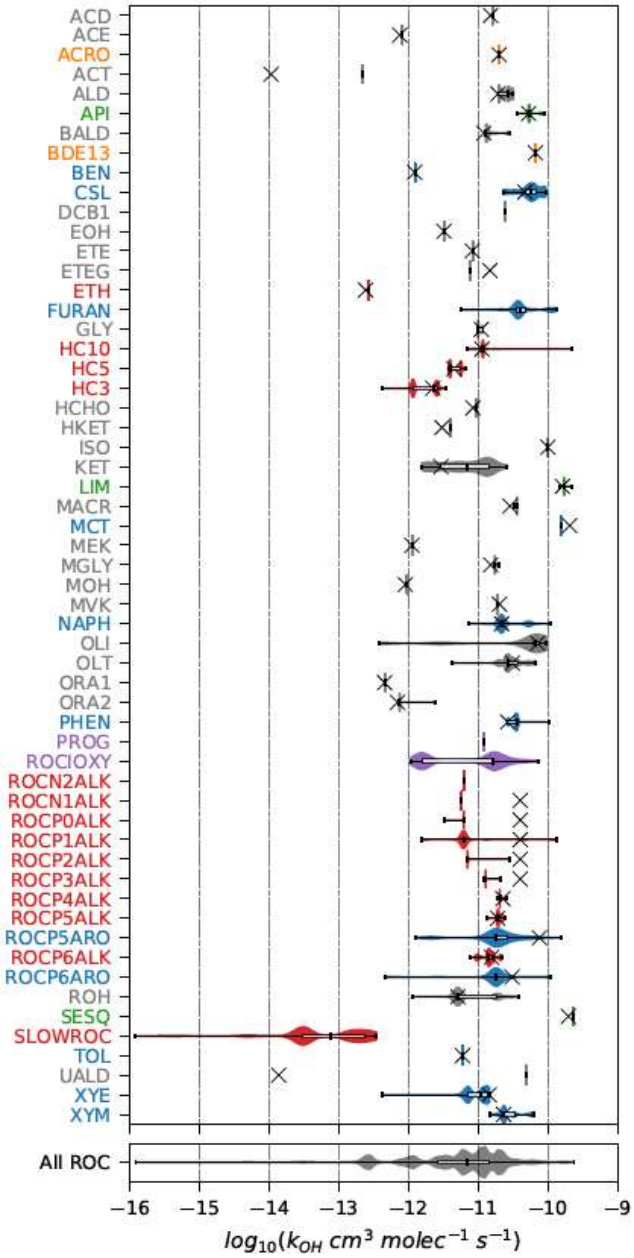

Figure 4: Organic aerosol yield and bulk n_O: n_C predicted by the CRACMM oxygenated ROC aging mechanism (Sect. 3.2) and the 2D-VBS configuration reported by Zhao et al. (2016). The x axis is defined as $log_{10}(C_0^*/C_{OA})$ where C_{OA} is the background OA concentration and C_0^* is the saturation concentration of the precursor. The aging of each species is simulated at a constant HO concentration of 10^6 molec cm^{-3} for 12 hours (darker colors) and 2.5 days (lighter colors) at four different C_{OA} conditions (0.1, 1, 10, and 100 µg m^{-3}). In cases where multiple predictions are present for the same saturation ratio, values are averaged.

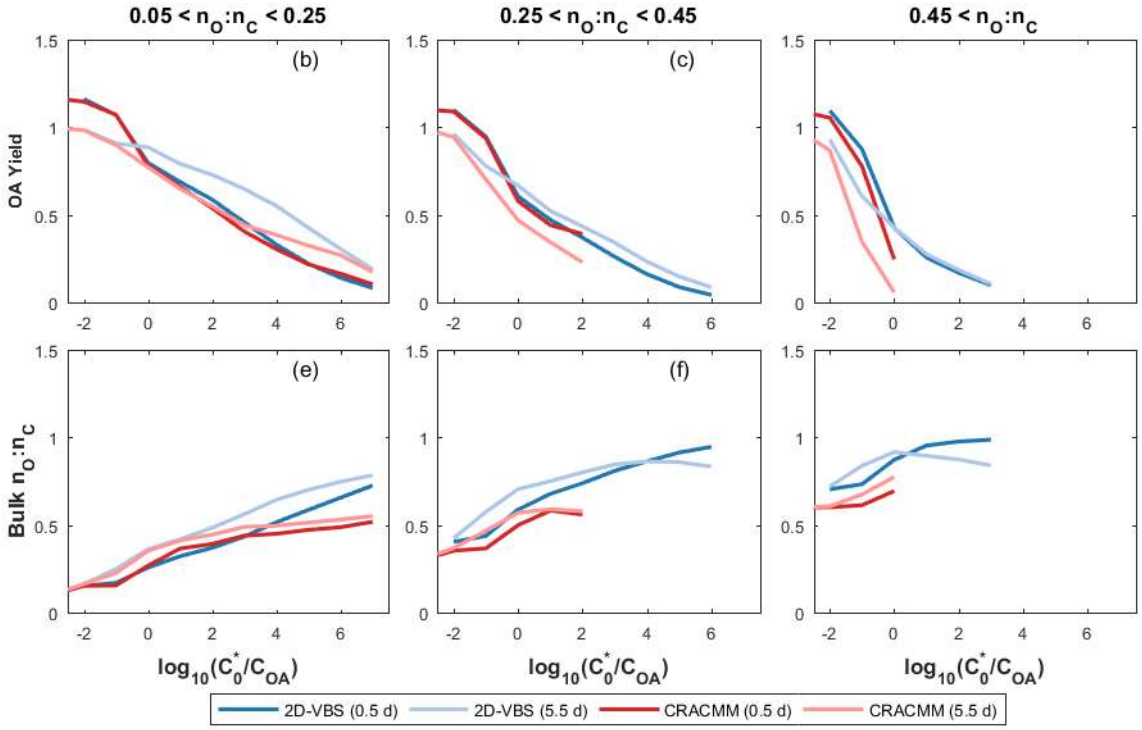

Figure 5: Molar flows to organic aerosol in the aromatic + phenolic + furan systems for 2017 U.S. emissions. Bimolecular RO_2 reactions are split equally between RO_2+NO and RO_2+HO_2 with the fraction of products undergoing autoxidation as specified in CRACMM. Partitioning of semivolatile species is calculated for 10 µg m^{-3} of organic aerosol. Precursor species include: toluene (TOL), m-xylene and more reactive aromatic VOCs (XYM), benzene (BEN), ethylbenzene and less reactive aromatic VOCs (XYE), phenolic species (PHEN), cresols (CSL), naphthalene and PAHs (NAPH), and other IVOC aromatics of higher (ROCP6ARO) and lower (ROCP5ARO) volatility. Aqueous pathways to SOA from glyoxal and methylglyoxal are not shown. Products that do not lead to OA are not shown but are indicated by the outflow from a species being smaller than the inflow. Red flows indicate emissions. Purple flows indicate hydroxyl radical oxidation chemistry. Blue flows indicate partitioning to the condensed phase.

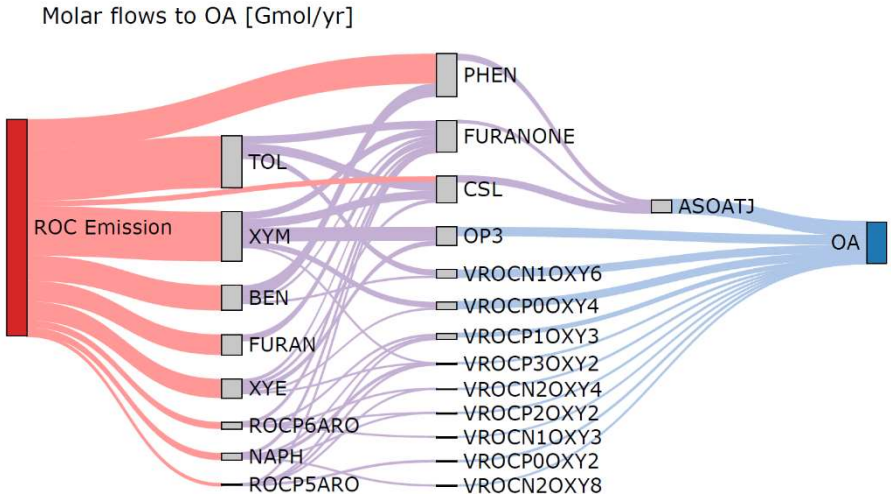

Figure 6: Distribution of hazardous air pollutants (HAPs) across CRACMM emitted species. Panel (a) indicates the mass fraction of 2017 U.S. anthropogenic and biomass burning ROC emissions by CRACMM species that are HAPs (blue). Panel (b) indicates the magnitude of emissions in Tg yr^{-1} by CRACMM species (bars) and the emission-weighted toxicity for cancer (x) or noncancer (+) health effects. Cancer and noncancer toxicity are normalized for purposes of display such that the species with the maximum value in each category is 3. Health risks are only shown for CRACMM species that contain non-zero emissions of HAPs. This data is available in the supplementary archive as Table D3.

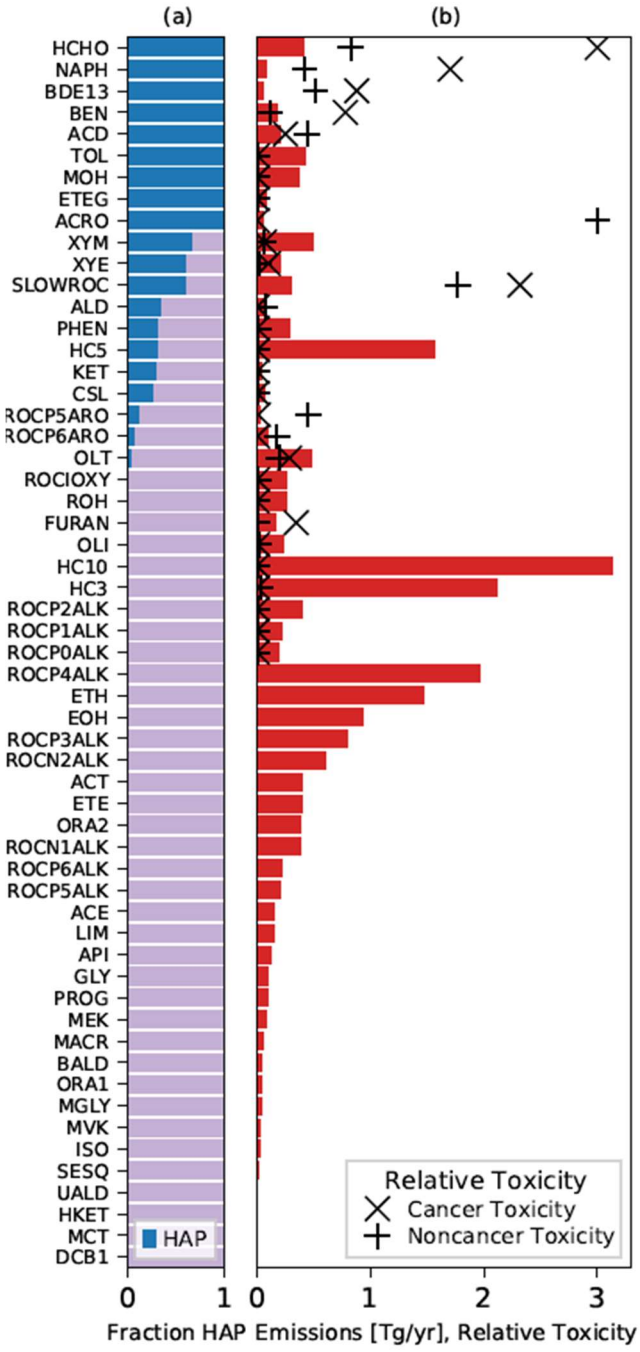

Figure 7: Mean carbon oxidation state (OS_C) and number of carbon atoms per molecule (n_C) for all stable ROC species. Filled circles indicate at least one particulate species present in CRACMM. Black circles indicate the presence of at least one gas species in CRACMM. Grey ellipses indicate approximate ranges of observation-based bulk OS_C and n_C from the work by Kroll et al. (2011) for hydrocarbon-like OA (vehicle emissions and ambient hydrocarbon-like organic aerosol), biomass burning OA, fresh ambient SOA, and aged ambient SOA. Grey bars indicate n_C coverage in mechanisms other than CRACMM.

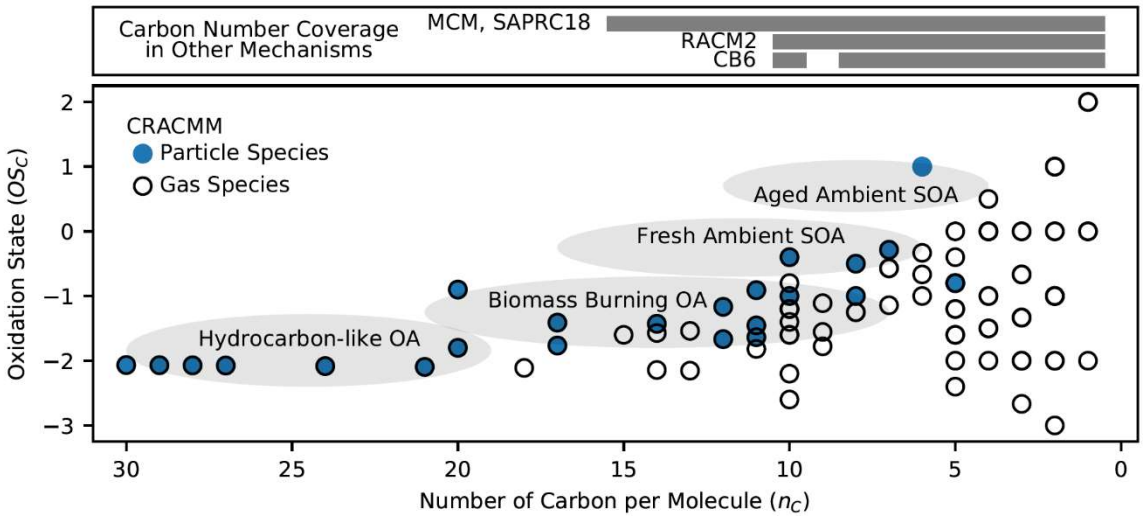

Figure 8: Molar hydrogen to carbon ($n_H{:}\,n_C$) and oxygen to carbon ($n_O{:}\,n_C$) ratios of CRACMM particulate ROC species. Color indicates the mean carbon oxidation state (OS_C). The observed trajectory trendline with slope of -0.6 is based on ambient measurements assembled by Chen et al. (2015) and extended to laboratory systems with $n_O{:}\,n_C$ near zero. Three CRACMM species are labeled: glyoxal SOA (AGLY), isoprene-derived organosulfates (AISO3OS), and non-sulfated isoprene SOA represented as 2-methyltetrols (AISO3NOS).

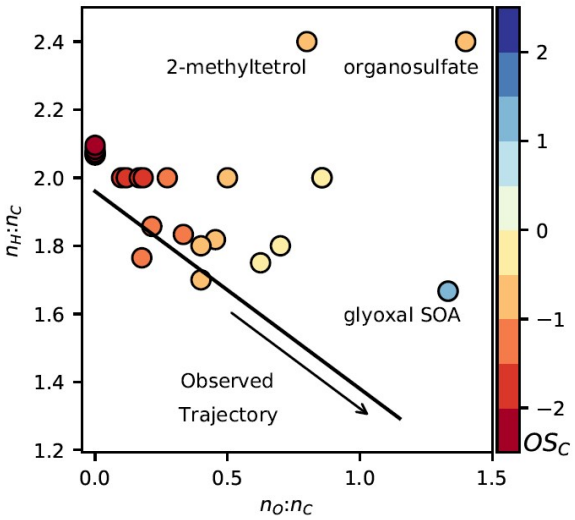

Figure 9: Anthropogenic and wood-burning ROC emissions and their relative potential HO reactivity (OH_R), ozone (O_3) formation, and OA for 2017 U.S. conditions by volatility class. Biogenic VOCs (BVOC) are not considered here. Ozone and OA formation potentials are calculated using the MIR and OA simple SAR approaches from Sect. 2.1. Metrics are aggregated from the individual species level to volatility classes: low volatility organic compounds (LVOC), semivolatile organic compounds (SVOC), intermediate volatility organic compounds (IVOC), and volatile organic compounds (VOC).

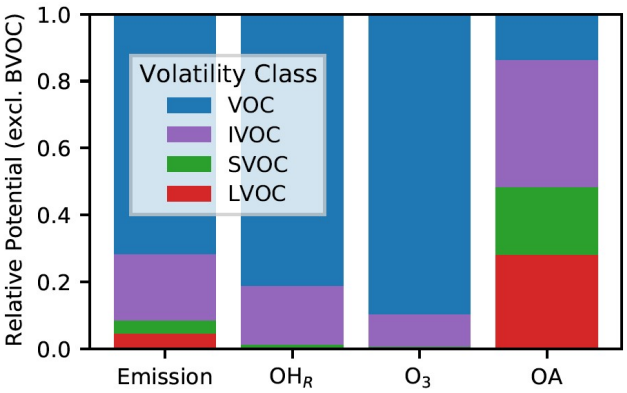

Appendix A: ROC Species in CRACMM and their description, phase (Phs) in which they can exist (G=gas, P=particle), and SMILES for representative compound structure. Appendix A along with additional ROC species information is also available in csv format in the data archive associated with this work (Table D1). Species properties such as molecular weights are determined from the representative structure except in the case of highly empirical species (SLOWROC, ROCIOXY, ASOAT). In CMAQ, aerosol species reside in Aitken, accumulation, and/or coarse modes and are appended with the letter to indicate the size mode. Prepending of species with a V or A (e.g., in Appendix B) indicates gas or particulate phase.

Species	Description	Phs	Representative Compound
ACD	Acetaldehyde	G	CC=O
ACE	Acetylene	G	C#C
ACO3	Acetyl peroxy radicals	G	CC(=O)O[O]
ACRO	Acrolein	G	C=CC=O
ACT	Acetone	G	CC(C)=O
ACTP	Peroxy radicals formed from ACT	G	CC(=O)CO[O]
ADCN	Aromatic-NO_3 adduct from PHEN	G	OC1=C[C]C(O[N+]([O-])=O)C=C1
ADDC	Aromatic-HO adduct from CSL	G	CC1=CC(O)=CC([O])C1
AGLY	SOA from reactive uptake of glyoxal on particles	P	OC2OC(C1OC(O)C(O)O1)OC2O
AISO3NOS	Non-sulfated SOA from IEPOX uptake	P	C(O)C(O)(C)C(O)CO
AISO3OS	Organosulfate SOA from IEPOX uptake	P	C(O)C(OS(O)(=O)(=O))(C)C(O)CO
ALD	C3 and higher aldehydes	G	CCC=O
AORGC	SOA from cloud processing of GLY and MGLY	P	OC2OC(C1OC(O)C(O)O1)OC2O
API	Alpha-pinenes and cyclic terpenes with one double bond	G	CC1=CCC2CC1C2(C)C
APINP1	Peroxy radicals from API+NO_3 that do not undergo autoxidation	G	[O]OC1(C)C(ON(=O)=O)CC2CC1C2(C)C
APINP2	Peroxy radicals from API+NO_3 that undergo autoxidation	G	[O]OC1(C)C(ON(=O)=O)CC2CC1C2(C)C
APIP1	Peroxy radicals from API+HO that do not undergo autoxidation	G	[O]OC1(C)C(O)CC2CC1C2(C)C
APIP2	Peroxy radicals from API+HO that undergo autoxidation	G	[O]OC1(C)C(O)CC2CC1C2(C)C
ASOAT	An empirical SOA	P	CC(=O)C(C(C(C(CO)O)O)O)O
BAL1	Peroxy radicals formed from BALD	G	[O]OC1=CC=C(C)C=C1
BAL2	Peroxy radicals formed from BALD	G	[O]OC1=CC=CC=C1
BALD	Benzaldehyde and other aromatic aldehydes	G	O=CC1=CC=CC=C1
BALP	Peroxy radicals formed from BALD	G	O=C(O[O])C1=CC=CC=C1
BDE13	1,3-butadiene	G	C=CC=C
BDE13P	Peroxy radicals from BDE13	G	C=CC(O[O])CO
BEN	Benzene	G	C1=CC=CC=C1
BENP	Peroxy radicals formed from benzene	G	[O]OC1C=CC2OOC1C2O
CHO	Phenoxy radical formed from CSL	G	[O]C1C=C(C)C(O)C(=C1)C
CO	Carbon monoxide	G	[C-]#[O+]
CSL	Cresol and other hydroxy substituted aromatics	G	CC(C)(O)C1=CC=CC=C1
DCB1	Unsaturated dicarbonyls	G	O=CC=C(C)C=O
DCB2	Unsaturated dicarbonyls	G	O=CC(=CC(=O)C)C
DCB3	Unsaturated dicarbonyls	G	O=CC=CC=O
ELHOM	Extremely-low volatility highly oxygenated molecules from terpenes	GP	OC1CC2C(OOC2(C)C)C(OOC3(C)C4C(C)(C)C(C4)CC3O)C1(C)OO
EOH	Ethanol	G	CCO
ETE	Ethene	G	C=C
ETEG	Ethylene glycol	G	OCCO
ETEP	Peroxy radicals formed from ETE	G	OCCO[O]
ETH	Ethane	G	CC
ETHP	Peroxy radicals formed from ethane and other species	G	CCO[O]

FURAN	Furans and other dienes	G	O=CC1=CC=CO1
FURANO2	Peroxy radicals from FURAN oxidation	G	OC1C=CC(O1)(O[O])(C=O)
FURANONE	Ring-retaining ketone product from FURAN oxidation	G	C1=CC(=O)OC1O
GLY	Glyoxal and glycoaldehydes	G	O=CC=O
HC10	Alkanes and other species with HO rate constant greater than 6.8×10^{-12} molec cm^{-3} sec^{-1}	G	CCCCCCCCCC
HC10P	Peroxy radicals formed from HC10	G	CCCCCCCC(CC)O[O]
HC10P2	Hydroxy peroxy radicals from HC10P alkoxy product	G	CCCCC(O[O])CCC(O)CC
HC3	Alkanes and other species with HO rate constant less than 3.4×10^{-12} molec cm^{-3} sec^{-1}	G	CCC
HC3P	Peroxy radicals formed from HC3	G	CC(C)O[O]
HC5	Alkanes and other species with HO rate constant between 3.4×10^{-12} and 6.8×10^{-12} molec cm^{-3} sec^{-1}	G	CCCCC
HC5P	Peroxy radicals formed from HC5	G	CCC(O[O])CC
HCHO	Formaldehyde	G	C=O
HKET	Hydroxy ketone	G	CC(=O)CO
HOM	Highly oxygenated molecules from terpenes	GP	OC1CC2C(OOC2(C)C)C(OO)C1(C)OO
IEPOX	Isoprene epoxydiols	G	OCC1OC1(C)CO
ISHP	Beta-hydroxy hydroperoxides from ISOP+HO_2	G	C=CC(OO)(CO)C
ISO	Isoprene	G	CC(=C)C=C
ISON	Beta-hydroxyalkylnitrates from ISOP+NO alkylnitrates from ISO+NO_3	G	OCC(C)(C=C)ON(=O)=O
ISOP	Peroxy radicals formed from ISO+HO	G	OCC(O[O])C(C)=C
KET	Ketones	G	CCC(=O)CC
KETP	Peroxy radicals formed from KET	G	CCC(C(C)O[O])=O
LIM	Δ-limonene and other cyclic diene-terpenes	G	CC(=C)[C@@H]1CCC(C)=CC1
LIMAL	Limonene aldehyde and similar LIM-derived aldehydes	G	O=CCC(CCC(=O)C)C(=C)C
LIMALP	Peroxy radicals from LIMAL	G	O=CCC(CCC(=O)C)C(C)(CO)O[O]
LIMNP1	Peroxy radicals from LIM+NO_3 that do not undergo autoxidation	G	[O-][N+](=O)OC1CC(CCC1(C)O[O])C(=C)C
LIMNP2	Peroxy radicals from LIM+NO_3 that undergo autoxidation	G	[O-][N+](=O)OC1CC(CCC1(C)O[O])C(=C)C
LIMP1	Peroxy radicals from LIM+HO that do not undergo autoxidation	G	[O]OC1(C)CCC(CC1O)C(=C)C
LIMP2	Peroxy radicals from LIM+HO that undergo autoxidation	G	[O]OC1(C)CCC(CC1O)C(=C)C
MACP	Peroxy radicals formed from MACR+HO	G	CC(=C)C(=O)O[O]
MACR	Methacrolein and other C_4 aldehydes	G	CC(=C)C=O
MAHP	Hydroperoxides from MACP+HO_2	G	C=C(C)C(OO)=O
MCP	Peroxy radical formed from MACR+HO which does not form MPAN	G	OCC(C)(O[O])C=O
MCT	Methyl catechol	G	CC1=CC(O)=C(O)C=C1
MCTO	Alkoxy radical formed from MCT+HO and MCT+NO_3	G	CC1=CC(O)=CC([O])=C1
MCTP	Radical formed from MCT+O_3 reaction	G	CC(/C=C\[C](O[O])O)=C/C(O)=O
MEK	Methyl ethyl ketone	G	CCC(C)=O
MEKP	Peroxy radicals formed from MEK	G	[O]OCCC(=O)C
MGLY	Methylglyoxal and other α-carbonyl aldehydes	G	CC(=O)C=O
MO2	Methyl peroxy radical	G	CO[O]
MOH	Methanol	G	CO
MPAN	Peroxymethacryloylnitrate and other higher peroxyacylnitrates from isoprene oxidation	G	O=N(=O)OOC(=O)C(=C)C
MVK	Methyl vinyl ketone	G	CC(=O)C=C
MVKP	Peroxy radicals formed from MVK	G	CC(=O)C(O)CO[O]
NALD	Nitrooxyacetaldehyde	G	O=CCON(=O)=O
NAPH	Naphthalene and other PAHs	G	C1=CC2=CC=CC=C2C=C1
NAPHP	Peroxy radicals from NAPH oxidation	G	C12=CC=CC=C1C3OOC(C3O[O])C2(O)

OLI	Internal alkenes	G	CC=C(C)C
OLIP	Peroxy radicals formed from OLI	G	[O]OC(C)(C)C(C)O
OLND	NO_3-alkene adduct reacting via decomposition	G	CC(O[O])CO[N+]([O-])=O
OLNN	NO_3-alkene adduct reacting to form carbonitrates + HO2	G	CC(O[O])CO[N+]([O-])=O
OLT	Terminal alkenes	G	CC=C
OLTP	Peroxy radicals formed from OLT	G	CC(CO)O[O]
ONIT	Organic nitrates	G	CCC(C)O[N+](=O)[O-]
OP1	Methyl hydrogen peroxide	G	COO
OP2	Higher organic peroxides	G	CCOO
OP3	Semivolatile organic peroxide	GP	CCC(=O)CC(OO)C(O)CC
OPB	Terpene-derived peroxides	G	OOC1(C)C(O)CC2CC1C2(C)C
ORA1	Formic acid	G	OC=O
ORA2	Acetic acid and higher acids	G	CC(O)=O
ORAP	Peroxy radical formed from ORA2 + HO reaction	G	[O]OCC(=O)O
PAA	Peroxyacetic acids and higher analogs	G	CC(=O)OO
PAN	Peroxyacetyl nitrate and higher saturated PANs	G	CC(=O)OON(=O)=O
PHEN	phenol and benzene diols	G	OC1=CC(O)=CC=C1
PINAL	Pinonaldehyde and similar APIN-derived aldehydes	G	O=CCC1CC(C(=O)C)C1(C)C
PINALP	Peroxy radicals from PINAL oxidation	G	O=CCC1(O[O])CC(C(=O)C)C1(C)C
PPN	Peroxypropionyl nitrate	G	CCC(=O)OO[N+](=O)[O-]
PROG	Propylene glyocol and other 3 carbon dialcohols	G	CC(O)CO
RCO3	Higher saturated acyl peroxy radicals	G	CCC(=O)O[O]
ROCIOXY	Intermediate volatility oxygenated ROC species (directly emitted)	G	C[Si]1(C)O[Si](C)(C)O[Si](C)(C)O[Si](C)(C)O[Si](C)(C)O1
ROCN1ALK	Alkane-like ROC, $C_i^* = 10^{-1} \mu g\ m^{-3}$	GP	CCCCCCCCCCCCCCCCCCCC(C)CCCC(C)CCCC
ROCN1OXY1	Oxygenated ROC, $C_i^* = 10^{-1} \mu g\ m^{-3}$ and $n_O : n_C$ of 0.1	GP	CCCCCCCCCCCCCCCCCCCC(=O)O
ROCN1OXY3	Oxygenated ROC, $C_i^* = 10^{-1} \mu g\ m^{-3}$ and $n_O : n_C$ of 0.3	GP	C(CCCCCC(=O)O)CCCCC(=O)O
ROCN1OXY6	Oxygenated ROC, $C_i^* = 10^{-1} \mu g\ m^{-3}$ and $n_O : n_C$ of 0.6	GP	C(CCC(C(=O)O)O)CCC(=O)O
ROCN2ALK	Alkane-like ROC, $C_i^* = 10^{-2} \mu g\ m^{-3}$	GP	CCCCCCCCCCCCCCCCCCCCCCCCCCCCCC
ROCN2OXY2	Oxygenated ROC, $C_i^* = 10^{-2} \mu g\ m^{-3}$ and $n_O : n_C$ of 0.2	GP	C#CCCC[C@H](CCCCCCCCCCC(=O)O)O
ROCN2OXY4	Oxygenated ROC, $C_i^* = 10^{-2} \mu g\ m^{-3}$ and $n_O : n_C$ of 0.4	GP	C(CCCCC(=O)O)CCCC(C(=O)O)O
ROCN2OXY8	Oxygenated ROC, $C_i^* = 10^{-2} \mu g\ m^{-3}$ and $n_O : n_C$ of 0.8	GP	CC(=O)C(C(C(C(CO)O)O)O)O
ROCP0ALK	Alkane-like ROC, $C_i^* = 10^{0} \mu g\ m^{-3}$	GP	CCCCCCCCCCCCCCCCC(C)CCCCCCCCCC
ROCP0OXY2	Oxygenated ROC, $C_i^* = 10^{0} \mu g\ m^{-3}$ and $n_O : n_C$ of 0.2	GP	CCCCCCCCCCCC(=O)CC(=O)O
ROCP0OXY4	Oxygenated ROC, $C_i^* = 10^{0} \mu g\ m^{-3}$ and $n_O : n_C$ of 0.4	GP	C(CCCCC(=O)O)CCCC(=O)O
ROCP1ALK	Alkane-like ROC, $C_i^* = 10^{1} \mu g\ m^{-3}$	GP	CCCCCCCCCCCCCCCCCCCCCCCCCCC
ROCP1ALKP	Peroxy radicals from ROCP1ALK oxidation	G	CCCCCCCCCCCCCCCCCCCCCCCCCC(CC)O[O]
ROCP1ALKP2	Hydroxy peroxy radicals from ROCP1ALK alkoxy product	G	CCCCCCCCCCCCCCCCCCCCCC(O[O])CCC(O)CC
ROCP1OXY1	Oxygenated ROC, $C_i^* = 10^{1} \mu g\ m^{-3}$ and $n_O : n_C$ of 0.1	GP	CCCCCCCCCCCCCCCCC(=O)O
ROCP1OXY3	Oxygenated ROC, $C_i^* = 10^{1} \mu g\ m^{-3}$ and $n_O : n_C$ of 0.3	GP	C(CCCCCO)CCCCC(=O)O
ROCP2ALK	Alkane-like ROC, $C_i^* = 10^{2} \mu g\ m^{-3}$	GP	CCCCCCCCCCCCCCCCCCCCCCCCC
ROCP2ALKP	Peroxy radicals from ROCP2ALK oxidation	G	CCCCCCCCCCCCCCCCCCCCCC(CC)O[O]
ROCP2ALKP2	Hydroxy peroxy radicals from ROCP2ALK alkoxy product	G	CCCCCCCCCCCCCCCCCCCC(O[O])CCC(O)CC
ROCP2OXY2	Oxygenated ROC, $C_i^* = 10^{2} \mu g\ m^{-3}$ and $n_O : n_C$ of 0.2	GP	CCCCCCCCCCCC(=O)O
ROCP3ALK	Alkane-like ROC, $C_i^* = 10^{3} \mu g\ m^{-3}$	GP	CCCCCCCCCCCCCCCCCCCCC
ROCP3ALKP	Peroxy radicals from ROCP3ALK oxidation	G	CCCCCCCCCCCCCCCCCCC(CC)O[O]
ROCP3ALKP2	Hydroxy peroxy radicals from ROCP3ALK alkoxy product	G	CCCCCCCCCCCCCCCC(O[O])CCC(O)CC
ROCP3OXY2	Oxygenated ROC, $C_i^* = 10^{3} \mu g\ m^{-3}$ and $n_O : n_C$ of 0.2	GP	C(CCCCCO)CCCCC=O

ROCP4ALK	Alkane-like ROC, $C_i^* = 10^4 \mu g\ m^{-3}$	G	CCCCCCCCCCCCCCCCCC
ROCP4ALKP	Peroxy radicals from ROCP4ALK oxidation	G	CCCCCCCCCCCCCCCCC(CC)O[O]
ROCP4ALKP2	Hydroxy peroxy radicals from ROCP4ALK alkoxy product	G	CCCCCCCCCCCCC(O[O])CCC(O)CC
ROCP4OXY2	Oxygenated ROC, $C_i^* = 10^4 \mu g\ m^{-3}$ and $n_O{:}\ n_C$ of 0.2	G	CCCCCC(CC)C(=O)O
ROCP5ALK	Alkane-like ROC, $C_i^* = 10^5 \mu g\ m^{-3}$	G	CCCCCCCCCCCCCC
ROCP5ALKP	Peroxy radicals from ROCP5ALK oxidation	G	CCCCCCCCCCCC(CC)O[O]
ROCP5ALKP2	Hydroxy peroxy radicals from ROCP5ALK alkoxy product	G	CCCCCCCCC(O[O])CCC(O)CC
ROCP5ARO	Aromatic ROC, $C_i^* = 10^5 \mu g\ m^{-3}$	G	CCCCCCCCC1=CC=CC=C1
ROCP5AROP	Peroxy radicals from ROCP5ARO oxidation	G	CCCCCCCCC1(OO2)C=CC(O[O])C2C1O
ROCP5OXY1	Oxygenated ROC, $C_i^* = 10^5 \mu g\ m^{-3}$ and $n_O{:}\ n_C$ of 0.1	G	CCCCCCCCCCC=O
ROCP6ALK	Alkane-like ROC, $C_i^* = 10^6 \mu g\ m^{-3}$	G	CCCCCCCCCCCCC
ROCP6ALKP	Peroxy radicals from ROCP6ALK oxidation	G	CCCCCCCCCCC(CC)O[O]
ROCP6ALKP2	Hydroxy peroxy radicals from ROCP6ALK alkoxy product	G	CCCCCCCC(O[O])CCC(O)CC
ROCP6ARO	Aromatic ROC, $C_i^* = 10^6 \mu g\ m^{-3}$	G	CCCCCCC1=CC=C(C)C=C1
ROCP6AROP	Peroxy radicals from ROCP6ARO oxidation	G	OC1C2C(CCCCCC)(O[O])C=CC1(C)OO2
ROCP6OXY1	Oxygenated ROC, $C_i^* = 10^6 \mu g\ m^{-3}$ and $n_O{:}\ n_C$ of 0.1	G	CCCCCCCCC=O
ROH	C3 and higher alcohols	G	CCCO
SESQ	Sesquiterpenes	G	C/C1=C/CCC(=C)C2CC(C)(C)C2CC\1
SESQNRO2	Peroxy radicals from SESQ reaction with nitrate radicals	G	[O]OC1(C)CCC2C(CC2(C)C)C(=C)CCC1O[N+](=O)[O-]
SESQRO2	Peroxy radicals from SESQ reaction with HO	G	[O]OC1(C)CCC2C(CC2(C)C)C(=C)CCC1O
SLOWROC	Slowly reacting ROC with $k_{OH} < 3.5\times10^{-13}$ molec cm^{-3} sec^{-1}	G	C#N
TOL	Toluene	G	CC1=CC=CC=C1
TOLP	Peroxy radicals formed from TOL	G	[O]OC1C=CC2(C)OOC1C2O
TRPN	Terpene nitrates	G	O=N(=O)OC1(C)C(O)CC2CC1C2(C)C
UALD	Unsaturated aldehydes	G	CC=C(C)C=O
UALP	Peroxy radicals formed from UALD	G	CC(O[O])C(C)(O)C=O
XYE	O- and p-xylene and other less reactive volatile aromatics with $k_{OH} < 1.46\times10^{-11}$ molec cm^{-3} sec^{-1}	G	CCC1=CC=CC=C1
XYEP	Peroxy radicals formed from XYE	G	[O]OC1C=CC2(CC)OOC1C2O
XYM	M-xylene and other more reactive volatile aromatics with $k_{OH} > 1.46\times10^{-11}$ molec cm^{-3} sec^{-1}	G	CC1=CC(C)=CC=C1
XYMP	Peroxy radicals formed from XYM	G	[O]OC1C=CC2(C)OOC1(C)C2O

Appendix B: Chemistry of CRACMM v1.0. For photolysis and heterogenous reactions (rate constant values not provided), rates depend on radiation, predicted concentrations, and/or other conditions, so a reference to the underlying data and formulation is provided. Rate constant values (k), if provided, are specified at 298.15 K, M=2.4615×10^{19} molecules cm^{-3}, and 1.00 atm. This information is also available in the supporting data archive and in CMAQv5.4. Partitioning of condensible organics is not listed here, and CMAQ assumes equilibrium partitioning calculated via operator splitting separate from the kinetic chemistry.

N	CMAQ Label	Reaction	Rate Constant Formula[a,b,c]	k (molec cm^{-3} sec^{-1} or s^{-1})
1	R001	O3 → O3P	σ from Sander et al. (2011); φ = 1.0 - φ of O_3 (Reaction 2)	Not Applicable
2	R002	O3 → O1D	σ and φ from Sander et al. (2011)	Not Applicable
3	R003	H2O2 → 2.000*HO	σ from Sander et al. (2011); φ = 1.0	Not Applicable
4	R004	NO2 → O3P + NO	σ and φ from Sander et al. (2011)	Not Applicable
5	R005	NO3 → NO	σ and φ from Sander et al. (2011)	Not Applicable
6	R006	NO3 → O3P + NO2	σ and φ from Sander et al. (2011)	Not Applicable
7	R007	HONO → HO + NO	σ from Sander et al. (2011); φ = 1.0	Not Applicable
8	R008	HNO3 → HO + NO2	σ from Sander et al. (2011); φ = 1.0	Not Applicable
9	R009	HNO4 → 0.200*HO + 0.800*HO2 + 0.800*NO2 + 0.200*NO3	σ from Sander et al. (2011); φ = 1.0	Not Applicable
10	R010	HCHO → CO	σ and φ from Sander et al. (2011)	Not Applicable
11	R011	HCHO → 2.000*HO2 + CO	σ and φ from Sander et al. (2011)	Not Applicable
12	R012	ACD → HO2 + MO2 + CO	σ and φ from Sander et al. (2011)	Not Applicable
13	R013	ALD → HO2 + ETHP + CO	σ from Burkholder et al. (2019); φ from Heicklen et al. (1986) and IUPAC datasheet P3 (updated 16th May 2002)	Not Applicable
14	R014	ACT → MO2 + ACO3	σ and φ from Burkholder et al. (2019)	Not Applicable
15	R014a	ACT → 2.000*MO2 + CO	σ and φ from Burkholder et al. (2019)	Not Applicable
16	R015	UALD → 1.220*HO2 + 0.784*ACO3 + 1.220*CO + 0.350*HCHO + 0.434*ALD + 0.216*KET	σ and φ from Magneron et al. (2002); uses crotonaldehyde	Not Applicable
17	TRP01	PINAL → HO2 + HC10P + CO	Uses data for ALD (Reaction 13)	Not Applicable
18	TRP02	LIMAL → HO2 + HC10P + CO	Uses data for ALD (Reaction 13)	Not Applicable
19	R016	MEK → 0.100*MO2 + ETHP + 0.900*ACO3 + 0.100*CO	σ from Brewer et al. (2019); φ from IUPAC datasheet P8 (5th December 2005)	Not Applicable

N	CMAQ Label	Reaction	Rate Constant Formula[a,b,c]	k (molec cm^{-3} sec^{-1} or s^{-1})
20	R017	KET → 1.500*ETHP + 0.500*ACO3 + 0.500*CO	σ from Brewer et al. (2019); φ from IUPAC datasheet P8 (5th December 2005)	Not Applicable
21	R018	HKET → HO2 + ACO3 + HCHO	σ from Yujing and Mellouki (2000); φ from IUPAC datasheet P8 (5th December 2005)	Not Applicable
22	R019	MACR → 0.340*HO + 0.660*HO2 + 0.670*ACO3 + 0.330*MACP + 0.340*XO2 + 0.670*CO + 0.670*HCHO	σ and φ from Sander et al. (2011)	Not Applicable
23	R020	MVK → 0.300*MO2 + 0.300*MACP + 0.700*CO + 0.700*UALD	σ and φ from Sander et al. (2011)	Not Applicable
24	R021	GLY → 2.000*CO	σ and φ from Sander et al. (2011)	Not Applicable
25	R022	GLY → HCHO + CO	σ and φ from Sander et al. (2011)	Not Applicable
26	R023	GLY → 2.000*HO2 + 2.000*CO	σ and φ from Sander et al. (2011)	Not Applicable
27	R024	MGLY → HO2 + ACO3 + CO	σ and φ from Sander et al. (2011)	Not Applicable
28	R025	DCB1 → 1.500*HO2 + 0.250*ACO3 + 0.200*XO2 + CO + 0.500*GLY + 0.500*MGLY	Uses data for MGLY (Reaction 27)	Not Applicable
29	R026	DCB2 → 1.500*HO2 + 0.250*ACO3 + 0.200*XO2 + CO + 0.500*GLY + 0.500*MGLY	Uses data for MGLY (Reaction 27)	Not Applicable
30	R027	BALD → CHO + HO2 + CO	σ and φ from SAPRC07 (Carter, 2010)	Not Applicable
31	R028	OP1 → HO + HO2 + HCHO	σ from Sander et al. (2011); φ = 1.0	Not Applicable
32	R029	OP2 → HO + HO2 + ALD	Uses data for OP1 (Reaction 31)	Not Applicable
33	TRP03	OPB → HO + HO2 + ALD	Uses data for OP1 (Reaction 31)	Not Applicable
34	R029a	OP3 → HO + HO2 + ALD	Uses data for OP1 (Reaction 31)	Not Applicable
35	R030	PAA → HO + MO2	σ from Sander et al. (2011); φ = 1.0	Not Applicable
36	R031	ONIT → HO2 + NO2 + 0.200*ALD + 0.800*KET	σ from Talukdar et al. (1997); φ = 1.0	Not Applicable
37	R032	PAN → ACO3 + NO2	σ and φ from Sander et al. (2011)	Not Applicable
38	R033	PAN → MO2 + NO3	σ from Sander et al. (2011); φ = 1.0 - φ of PAN in Reaction 36	Not Applicable
39	R034	O3 + HO → HO2	$1.70\times10^{-12}\exp(-940.00/T)$	7.26×10^{-14}
40	R035	O3 + HO2 → HO	$1.00\times10^{-14}\exp(-490.00/T)$	1.93×10^{-15}
41	R036	O3 + NO → NO2	$3.00\times10^{-12}\exp(-1500.00/T)$	1.96×10^{-14}
42	R037	O3 + NO2 → NO3	$1.20\times10^{-13}\exp(-2450.00/T)$	3.24×10^{-17}
43	R038	O3P + O2 + M → O3	$6.10\times10^{-34}(T/300)^{-2.40}$	6.19×10^{-34}
44	R039	O3P + O3 →	$8.00\times10^{-12}\exp(-2060.00/T)$	7.99×10^{-15}
45	R040	O1D + O2 → O3P	$3.30\times10^{-11}\exp(55.00/T)$	3.97×10^{-11}
46	R041	O1D + N2 → O3P	$2.15\times10^{-11}\exp(110.00/T)$	3.11×10^{-11}
47	R042	O1D + H2O → 2.000*HO	$1.63\times10^{-10}\exp(60.00/T)$	1.99×10^{-10}
48	R043	HO + H2 → HO2	$2.80\times10^{-12}\exp(-1800.00/T)$	6.69×10^{-15}

N	CMAQ Label	Reaction	Rate Constant Formula[a,b,c]	k (molec cm^{-3} sec^{-1} or s^{-1})
49	R044	HO + HO2 →	$4.80\times10^{-11}exp(250.00/T)$	1.11×10^{-10}
50	R045	HO2 + HO2 → H2O2	k0= $3.00\times10^{-13}exp(460.0/T)$; k1= $2.10\times10^{-33}exp(920.0/T)$	2.53×10^{-12}
51	R046	HO2 + HO2 + H2O → H2O2	k0= $4.20\times10^{-34}exp(2660.0/T)$; k1= $2.94\times10^{-54}exp(3120.0/T)$	5.68E-30
52	R047	H2O2 + HO → HO2	$1.80\times10^{-12}exp(0.00/T)$	1.80×10^{-12}
53	R048	NO + O3P → NO2	ko= 9.10E-32$exp(0.0/T)(T/300)^{-1.50}$; ki = $3.00\times10^{-11}exp(0.0/T)(T/300)^{0.00}$; n= 1.00;F= 0.60	1.68×10^{-12}
54	R049	NO + HO → HONO	ko= 7.10E-31$exp(0.0/T)(T/300)^{-2.60}$; ki = $3.60\times10^{-11}exp(0.0/T)(T/300)^{-0.10}$; n= 1.00;F= 0.60	7.46×10^{-12}
55	R050	NO + HO2 → NO2 + HO	$3.44\times10^{-12}exp(260.00/T)$	8.23×10^{-12}
56	R051	NO + HO2 → HNO3	k0= $6.0950\times10^{-14}exp(270.0/T)(T/300)^{-1.00}$; k2= $6.8570\times10^{-34}exp(270.0/T)(T/300)^{1.00}$; k3= $-5.9680\times10^{-14}exp(270.00/T)$	4.56×10^{-14}
57	R052	NO + NO + O2 → 2.000*NO2	4.25E-39exp(663.50/T)	3.93E-38
58	R053	HONO + HO → NO2	$3.00\times10^{-12}exp(250.00/T)$	6.94×10^{-12}
59	R054	NO2 + O3P → NO	$5.30\times10^{-12}exp(200.00/T)$	1.04×10^{-11}
60	R055	NO2 + O3P → NO3	ko= 3.40E-31$exp(0.0/T)(T/300)^{-1.60}$; ki = $2.30\times10^{-11}exp(0.0/T)(T/300)^{-0.20}$; n= 1.00;F= 0.60	4.02×10^{-12}
61	R056	NO2 + HO → HNO3	ko= $1.80\times10^{-30}exp(0.0/T)(T/300)^{-3.00}$; ki = $2.80\times10^{-11}exp(0.0/T)(T/300)^{0.00}$; n= 1.00;F= 0.60	1.06×10^{-11}
62	R057	HNO3 + HO → NO3	k0= $2.40\times10^{-14}exp(460.0/T)$; k1= $2.70\times10^{-17}exp(2199.0/T)$; k3= $6.50\times10^{-34}exp(1335.0/T)$	1.54×10^{-13}
63	R058	NO3 + HO → HO2 + NO2	2.00×10^{-11}	2.00×10^{-11}
64	R059	NO3 + HO2 → 0.700*HO + 0.700*NO2 + 0.300*HNO3	3.50×10^{-12}	3.50×10^{-12}
65	R060	NO3 + NO → 2.000*NO2	$1.70\times10^{-11}exp(125.00/T)$	2.59×10^{-11}
66	R061	NO3 + NO2 → NO + NO2	$4.35\times10^{-14}exp(-1335.00/T)$	4.94×10^{-16}
67	R062	NO3 + NO3 → 2.000*NO2	$8.50\times10^{-13}exp(-2450.00/T)$	2.29×10^{-16}
68	R063	NO3 + NO2 → N2O5	ko= $2.40\times10^{-30}exp(0.0/T)(T/300)^{-3.00}$; ki = $1.60\times10^{-12}exp(0.0/T)(T/300)^{0.10}$; n= 1.00;F= 0.60	1.35×10^{-12}
69	R064	N2O5 → NO2 + NO3	$1.72\times10^{26}exp(-10840.00/T)$ *R063	3.76E-28

N	CMAQ Label	Reaction	Rate Constant Formula[a,b,c]	k (molec cm^{-3} sec^{-1} or s^{-1})
70	R065	N2O5 + H2O → 2.000*HNO3	1.00E-22	1.00E-22
71	R066	NO2 + HO2 → HNO4	ko= $1.90\times10^{-31}\exp(0.0/T)(T/300)^{-3.40}$; ki = $4.00\times10^{-12}\exp(0.0/T)(T/300)^{-0.30}$; n= 1.00;F= 0.60	1.31×10^{-12}
72	R067[d]	HNO4 → HO2 + NO2	$4.76\times10^{26}\exp(-10900.00/T)$ *R066	8.28E-28
73	R068	HNO4 + HO → NO2	$4.50\times10^{-13}\exp(610.00/T)$	3.48×10^{-12}
74	R069	SO2 + HO → HO2 + SULF + SULRXN	ko= $2.90\times10^{-31}\exp(0.0/T)(T/300)^{-4.10}$; ki = $1.70\times10^{-12}\exp(0.0/T)(T/300)^{0.20}$; n= 1.00;F= 0.60	9.58×10^{-13}
75	R070	CO + HO → HO2	k0= $1.44\times10^{-13}\exp(0.0/T)$; k1= $2.74\times10^{-33}\exp(0.0/T)$; $2.45\times10^{-12}\exp(-1775.00/T)$	2.11×10^{-13}
76	R071	HO + CH4 → MO2	$2.45\times10^{-12}\exp(-1775.00/T)$	6.36×10^{-15}
77	R072	ETH + HO → ETHP	$7.66\times10^{-12}\exp(-1020.00/T)$	2.50×10^{-13}
78	R073	HC3 + HO → HC3P + 0.000*ASOATJ	$7.68\times10^{-12}\exp(-370.00/T)$	2.22×10^{-12}
79	R074	HC5 + HO → HC5P + 0.001*ASOATJ	$1.01\times10^{-11}\exp(-245.00/T)$	4.44×10^{-12}
80	R076	ETE + HO → ETEP	ko= $1.00\times10^{-28}\exp(0.0/T)(T/300)^{-4.50}$; ki = $8.80\times10^{-12}\exp(0.0/T)(T/300)^{-0.85}$; n= 1.00;F= 0.60	8.20×10^{-12}
81	R077	OLT + HO → OLTP	$5.72\times10^{-12}\exp(500.00/T)$	3.06×10^{-11}
82	R078	OLI + HO → OLIP	$1.33\times10^{-11}\exp(500.00/T)$	7.11×10^{-11}
83	R080	ACE + HO → 0.650*HO + 0.350*HO2 + 0.350*CO + 0.650*GLY + 0.350*ORA1	ko= $5.50\times10^{-30}\exp(0.0/T)(T/300)^{0.00}$; ki = $8.30\times10^{-13}\exp(0.0/T)(T/300)^{2.00}$; n= 1.00;F= 0.60	7.47×10^{-13}
84	ROCARO31	BEN + HO → 0.470*BENP + 0.530*PHEN + 0.530*HO2	$2.33\times10^{-12}\exp(-193.00/T)$	1.22×10^{-12}
85	ROCARO41	TOL + HO → 0.820*TOLP + 0.180*CSL + 0.180*HO2	$1.81\times10^{-12}\exp(354.00/T)$	5.93×10^{-12}
86	ROCARO51	XYM + HO → 0.830*XYMP + 0.170*CSL + 0.170*HO2	2.33×10^{-11}	2.33×10^{-11}
87	ROCARO61	XYE + HO → 0.820*XYEP + 0.180*CSL + 0.180*HO2	7.16×10^{-12}	7.16×10^{-12}
88	R086	ISO + HO → ISOP	$2.70\times10^{-11}\exp(390.00/T)$	9.99×10^{-11}
89	R087	API + HO → 0.975*APIP1 + 0.025*APIP2	$1.21\times10^{-11}\exp(440.00/T)$	5.29×10^{-11}
90	R088	LIM + HO → 0.945*LIMP1 + 0.055*LIMP2	$4.20\times10^{-11}\exp(401.00/T)$	1.61×10^{-10}
91	TRP04	PINAL + HO → 0.230*PINALP + 0.770*RCO3	$5.20\times10^{-12}\exp(600.00/T)$	3.89×10^{-11}
92	TRP05	LIMAL + HO → 0.700*LIMALP + 0.300*RCO3	1.00×10^{-10}	1.00×10^{-10}
93	R089	HCHO + HO → HO2 + CO	$5.50\times10^{-12}\exp(125.00/T)$	8.36×10^{-12}
94	R090	ACD + HO → ACO3	$4.70\times10^{-12}\exp(345.00/T)$	1.50×10^{-11}
95	R091	ALD + HO → RCO3	$4.90\times10^{-12}\exp(405.00/T)$	1.91×10^{-11}
96	R092	ACT + HO → ACTP	$4.56\times10^{-14}\exp(-427.00/T)(T/300)^{3.65}$	1.06×10^{-14}
97	R093	MEK + HO → MEKP	$1.50\times10^{-12}\exp(-90.00/T)$	1.11×10^{-12}
98	R094	KET + HO → KETP	$2.80\times10^{-12}\exp(10.00/T)$	2.90×10^{-12}
99	R095	HKET + HO → HO2 + MGLY	3.00×10^{-12}	3.00×10^{-12}
100	R096	MACR + HO → 0.570*MACP + 0.430*MCP	$8.00\times10^{-12}\exp(380.00/T)$	2.86×10^{-11}
101	R097	MVK + HO → MVKP	$2.60\times10^{-12}\exp(610.00/T)$	2.01×10^{-11}
102	R098	UALD + HO → 0.313*ACO3 + 0.687*UALP	$5.77\times10^{-12}\exp(533.00/T)$	3.45×10^{-11}
103	R099	GLY + HO → HO2 + 2.000*CO	1.10×10^{-11}	1.10×10^{-11}

N	CMAQ Label	Reaction	Rate Constant Formula[a,b,c]	k (molec cm^{-3} sec^{-1} or s^{-1})
104	R100	MGLY + HO → ACO3 + CO	$9.26\times10^{-13}\exp(830.00/T)$	1.50×10^{-11}
105	R101	DCB1 + HO → 0.520*HO2 + 0.330*CO + 0.400*ALD + 0.780*KET + 0.100*GLY + 0.010*MGLY	$2.80\times10^{-11}\exp(175.00/T)$	5.04×10^{-11}
106	R102	DCB2 + HO → 0.520*HO2 + 0.330*CO + 0.130*MEK + 0.100*GLY + 0.010*MGLY + 0.780*OP2	$2.80\times10^{-11}\exp(175.00/T)$	5.04×10^{-11}
107	R103	DCB3 + HO → 0.560*HO2 + 0.210*MACP + 0.110*CO + 0.270*GLY + 0.010*MGLY + 0.790*OP2	1.00×10^{-11}	1.00×10^{-11}
108	R104	BALD + HO → BALP	$5.32\times10^{-12}\exp(243.00/T)$	1.20×10^{-11}
109	R105	PHEN + HO → 0.152*ASOATJ + 0.619*HO2 + 0.170*ADDC + 0.059*CHO + 0.619*MCT	$6.75\times10^{-12}\exp(405.00/T)$	2.63×10^{-11}
110	R106	CSL + HO → 0.200*ASOATJ + 0.584*HO2 + 0.160*ADDC + 0.056*CHO + 0.584*MCT	$4.65\times10^{-11}\exp(0.00/T)$	4.65×10^{-11}
111	R108	MCT + HO → MCTO	$2.05\times10^{-10}\exp(0.00/T)$	2.05×10^{-10}
112	R109	MOH + HO → HO2 + HCHO	$2.85\times10^{-12}\exp(-345.00/T)$	8.96×10^{-13}
113	R110	EOH + HO → HO2 + ACD	$3.00\times10^{-12}\exp(20.00/T)$	3.21×10^{-12}
114	R111	ROH + HO → HO2 + 0.719*ALD + 0.184*ACD	$2.60\times10^{-12}\exp(200.00/T)$	5.09×10^{-12}
115	R112	ETEG + HO → HO2 + ALD	1.47×10^{-11}	1.47×10^{-11}
116	R113	OP1 + HO → 0.350*HO + 0.650*MO2 + 0.350*HCHO	$2.90\times10^{-12}\exp(190.00/T)$	5.48×10^{-12}
117	R114	OP2 + HO → 0.010*HO + 0.440*HC3P + 0.070*XO2 + 0.080*ALD + 0.410*KET	$3.40\times10^{-12}\exp(190.00/T)$	6.43×10^{-12}
118	TRP06	OPB + HO → 0.010*HO + 0.440*HC10P + 0.070*XO2 + 0.080*ALD + 0.410*KET	$3.40\times10^{-12}\exp(190.00/T)$	6.43×10^{-12}
119	R114a	OP3 + HO → 0.010*HO + 0.440*HC10P + 0.070*XO2 + 0.080*ALD + 0.410*KET	$3.40\times10^{-12}\exp(190.00/T)$	6.43×10^{-12}
120	R115	ISHP + HO → HO + MACR + 0.904*IEPOX	1.00×10^{-10}	1.00×10^{-10}
121	R116	MAHP + HO → MACP	3.00×10^{-11}	3.00×10^{-11}
122	R117	ORA1 + HO → HO2	4.50×10^{-13}	4.50×10^{-13}
123	R118	ORA2 + HO → 0.640*MO2 + 0.360*ORAP	$4.00\times10^{-14}\exp(850.00/T)$	6.92×10^{-13}
124	R119	PAA + HO → 0.350*HO + 0.650*ACO3 + 0.350*XO2 + 0.350*HCHO	$2.93\times10^{-12}\exp(190.00/T)$	5.54×10^{-12}
125	R120	PAN + HO → XO2 + NO3 + HCHO	4.00×10^{-14}	4.00×10^{-14}
126	R121	PPN + HO → XO2 + NO3 + HCHO	4.00×10^{-14}	4.00×10^{-14}
127	R122	MPAN + HO → NO2 + HKET	3.20×10^{-11}	3.20×10^{-11}
128	R123	ONIT + HO → HC3P + NO2	$5.31\times10^{-12}\exp(-260.00/T)$	2.22×10^{-12}
129	TRP07	TRPN + HO → HOM	4.80×10^{-12}	4.80×10^{-12}
130	R124	NALD + HO → NO2 + XO2 + HKET	$5.60\times10^{-12}\exp(270.00/T)$	1.39×10^{-11}
131	R125	ISON + HO → NALD + 0.070*HKET + 0.070*HCHO	1.30×10^{-11}	1.30×10^{-11}
132	R126	ETE + O3 → 0.080*HO + 0.150*HO2 + 0.430*CO + HCHO + 0.370*ORA1	$9.14\times10^{-15}\exp(-2580.00/T)$	1.60×10^{-18}
133	R127	OLT + O3 → 0.220*HO + 0.320*HO2 + 0.080*MO2 + 0.060*ETHP + 0.040*HC3P + 0.020*HC5P + 0.068*H2O2 + 0.430*CO + 0.020*ETH + 0.015*HC3 + 0.006*HC5 + 0.032*BEN + 0.560*HCHO + 0.010*ACD + 0.440*ALD + 0.030*ACT + 0.020*BALD + 0.060*MEK + 0.010*HKET + 0.030*ORA1 + 0.060*ORA2	$4.33\times10^{-15}\exp(-1800.00/T)$	1.03×10^{-17}
134	R128	OLI + O3 → 0.460*HO + 0.070*HO2 + 0.320*MO2 + 0.070*ETHP + 0.040*HC3P + 0.090*ACO3 + 0.370*CO + 0.026*H2O2 + 0.010*ETH + 0.010*HC3 + 0.090*HCHO + 0.457*ACD + 0.730*ALD + 0.110*ACT + 0.017*KET + 0.044*HKET + 0.017*ORA2	$4.40\times10^{-15}\exp(-845.00/T)$	2.59×10^{-16}

N	CMAQ Label	Reaction	Rate Constant Formula[a,b,c]	k (molec cm^{-3} sec^{-1} or s^{-1})
135	R130	ISO + O3 → 0.250*HO + 0.250*HO2 + 0.080*MO2 + 0.100*ACO3 + 0.100*MACP + 0.090*H2O2 + 0.140*CO + 0.580*HCHO + 0.461*MACR + 0.189*MVK + 0.280*ORA1 + 0.153*OLT	$7.86\times10^{-15}\exp(-1913.00/T)$	1.29×10^{-17}
136	R131	API + O3 → 0.900*HO + 0.900*APIP1 + 0.050*APIP2 + 0.050*PINAL + 0.050*H2O2 + 0.140*CO	$5.00\times10^{-16}\exp(-530.00/T)$	8.45×10^{-17}
137	R132	LIM + O3 → 0.840*HO + 0.840*LIMP1 + 0.110*LIMP2 + 0.050*LIMAL + 0.050*H2O2 + 0.140*CO	$2.95\times10^{-15}\exp(-783.00/T)$	2.13×10^{-16}
138	TRP08	LIMAL + O3 → 0.040*HO + 0.670*HC10P + 0.790*HCHO + 0.330*KET + 0.040*HO2 + 0.200*CO	8.30×10^{-18}	8.30×10^{-18}
139	TRP09	TRPN + O3 → HOM	1.67×10^{-16}	1.67×10^{-16}
140	R132	MACR + O3 → 0.190*HO + 0.140*HO2 + 0.100*ACO3 + 0.220*CO + 0.500*MGLY + 0.450*ORA1	$1.36\times10^{-15}\exp(-2112.00/T)$	1.14×10^{-18}
141	R134	MVK + O3 → 0.160*HO + 0.110*HO2 + 0.280*ACO3 + 0.010*XO2 + 0.560*CO + 0.100*HCHO + 0.540*MGLY + 0.070*ORA1 + 0.070*ORA2 + 0.100*ALD	$8.50\times10^{-16}\exp(-1520.00/T)$	5.19×10^{-18}
142	R135	UALD + O3 → 0.100*HO + 0.072*HO2 + 0.008*MO2 + 0.002*ACO3 + 0.100*XO2 + 0.243*CO + 0.080*HCHO + 0.420*ACD + 0.028*KET + 0.491*GLY + 0.003*MGLY + 0.044*ORA1	1.66×10^{-18}	1.66×10^{-18}
143	R136	DCB1 + O3 → 0.050*HO + HO2 + 0.600*RCO3 + 0.600*XO2 + 1.500*CO + 0.050*HCHO + 0.050*GLY + 0.080*MGLY + 0.650*OP2	2.00×10^{-16}	2.00×10^{-16}
144	R137	DCB2 + O3 → 0.050*HO + HO2 + 0.600*RCO3 + 0.600*XO2 + 1.500*CO + 0.050*HCHO + 0.050*GLY + 0.080*MGLY + 0.700*DCB1 + 0.650*OP2	2.00×10^{-16}	2.00×10^{-16}
145	R138	DCB3 + O3 → 0.050*HO + HO2 + 1.500*CO + 0.480*GLY + 0.700*DCB1 + 0.250*ORA1 + 0.250*ORA2 + 0.110*PAA	9.00×10^{-17}	9.00×10^{-17}
146	R140	MCTO + O3 → MCTP	2.86×10^{-13}	2.86×10^{-13}
147	R141	ETE + NO3 → 0.800*OLNN + 0.200*OLND	$4.39\times10^{-13}\exp(-2282.00/T)(T/300)^{2.00}$	2.06×10^{-16}
148	R142	OLT + NO3 → 0.430*OLNN + 0.570*OLND	$1.79\times10^{-13}\exp(-450.00/T)$	3.96×10^{-14}
149	R143	OLI + NO3 → 0.110*OLNN + 0.890*OLND	$8.64\times10^{-13}\exp(450.00/T)$	3.91×10^{-12}
150	R145	ISO + NO3 → ISON	$3.03\times10^{-12}\exp(-446.00/T)$	6.79×10^{-13}
151	R146	API + NO3 → 0.975*APINP1 + 0.025*APINP2	$1.19\times10^{-12}\exp(490.00/T)$	6.16×10^{-12}
152	R147	LIM + NO3 → 0.945*LIMNP1 + 0.055*LIMNP2	1.22×10^{-11}	1.22×10^{-11}
153	TRP10	TRPN + NO3 → HOM	$3.15\times10^{-14}\exp(-448.00/T)$	7.01×10^{-15}
154	R148	HCHO + NO3 → HO2 + CO + HNO3	$2.00\times10^{-12}\exp(-2440.00/T)$	5.58×10^{-16}
155	R149	ACD + NO3 → ACO3 + HNO3	$1.40\times10^{-12}\exp(-1900.00/T)$	2.39×10^{-15}
156	R150	ALD + NO3 → RCO3 + HNO3	$3.76\times10^{-12}\exp(-1900.00/T)$	6.42×10^{-15}
157	R151	MACR + NO3 → 0.680*HCHO + 0.320*MACP + 0.680*XO2 + 0.680*MGLY + 0.320*HNO3 + 0.680*NO2	3.40×10^{-15}	3.40×10^{-15}
158	R152	UALD + NO3 → HO2 + XO2 + 0.668*CO + 0.332*HCHO + 0.332*ALD + ONIT	$5.02\times10^{-13}\exp(-1076.00/T)$	1.36×10^{-14}
159	R153	GLY + NO3 → HO2 + 2.000*CO + HNO3	$2.90\times10^{-12}\exp(-1900.00/T)$	4.95×10^{-15}
160	R154	MGLY + NO3 → ACO3 + CO + HNO3	$3.76\times10^{-12}\exp(-1900.00/T)$	6.42×10^{-15}
161	R155	PHEN + NO3 → 0.152*ASOATJ + 0.339*CHO + 0.850*ADDC + 0.424*ADCN + 0.424*HNO3	3.78×10^{-12}	3.78×10^{-12}
162	R156	CSL + NO3 → 0.200*ASOATJ + 0.320*CHO + 0.080*ADDC + 0.400*ADCN + 0.400*HNO3	1.06×10^{-12}	1.06×10^{-12}
163	R158	MCT + NO3 → MCTO + HNO3	2.01×10^{-10}	2.01×10^{-10}
164	R159	MPAN + NO3 → MACP + NO2	$2.20\times10^{-14}\exp(-500.00/T)$	4.11×10^{-15}
165	TRP11	PINALP → HOM	1.00	1.00

N	CMAQ Label	Reaction	Rate Constant Formula[a,b,c]	k (molec cm^{-3} sec^{-1} or s^{-1})
166	TRP12	LIMALP → HOM	1.00	1.00
167	R166	ACO3 + NO2 → PAN	ko= 9.70×10^{-29}exp(0.0/T)(T/300)$^{-5.60}$; ki = 9.30×10^{-12}exp(0.0/T)(T/300)$^{-1.50}$; n= 1.00;F= 0.60	8.68×10^{-12}
168	R167	PAN → ACO3 + NO2	1.11×10^{28}e-14000.00/T) *R166	3.90×10^{-48}
169	R168	RCO3 + NO2 → PPN	ko= 9.70×10^{-29}exp(0.0/T(T/300)$^{-5.60}$; ki = 9.30×10^{-12}exp(0.0/T(T/300)$^{-1.50}$; n= 1.00;F= 0.60	8.68×10^{-12}
170	R169	PPN → RCO3 + NO2	1.11×10^{28}e-14000.00/T) *R168	3.90×10^{-48}
171	R170	MACP + NO2 → MPAN	2.80×10^{-12}exp(181.00/T)	5.14×10^{-12}
172	R171	MPAN → MACP + NO2	1.60×10^{16}exp(-13486.00/T)	3.63×10^{-04}
173	R172	MO2 + NO → HO2 + NO2 + HCHO	2.80×10^{-12}exp(300.00/T)	7.66×10^{-12}
174	R173	ETHP + NO → HO2 + NO2 + ACD	2.60×10^{-12}exp(365.00/T)	8.84×10^{-12}
175	R174	HC3P + NO → 0.660*HO2 + 0.131*MO2 + 0.048*ETHP + 0.089*XO2 + 0.935*NO2 + 0.504*ACD + 0.132*ALD + 0.165*ACT + 0.042*MEK + 0.065*ONIT	4.00×10^{-12}	4.00×10^{-12}
176	R175	HC5P + NO → 0.200*HO2 + 0.051*MO2 + 0.231*ETHP + 0.235*XO2 + 0.864*NO2 + 0.018*HCHO + 0.045*ACD + 0.203*ALD + 0.033*MEK + 0.217*ACT + 0.033*KET + 0.272*HKET + 0.136*ONIT	4.00×10^{-12}	4.00×10^{-12}
177	R177	ETEP + NO → HO2 + NO2 + 1.600*HCHO + 0.200*ALD	9.00×10^{-12}	9.00×10^{-12}
178	R178	OLTP + NO → 0.780*HO2 + 0.970*NO2 + 0.780*HCHO + 0.012*ACD + 0.440*ALD + 0.060*ACT + 0.130*MEK + 0.030*ONIT	4.00×10^{-12}	4.00×10^{-12}
179	R179	OLIP + NO → 0.830*HO2 + 0.950*NO2 + 0.810*ACD + 0.680*ALD + 0.200*ACT + 0.090*KET + 0.020*HKET + 0.050*ONIT	4.00×10^{-12}	4.00×10^{-12}
180	ROCARO33	BENP + NO → 0.000*ONIT + 0.001*VROCP4OXY2 + 0.001*VROCN1OXY6 + 0.998*NO2 + 0.998*HO2 + 0.000*BALD + 0.998*GLY + 0.499*FURANONE + 0.249*DCB2 + 0.249*DCB3	2.70×10^{-12}exp(360.00/T)	9.03×10^{-12}
181	ROCARO43	TOLP + NO → 0.000*ONIT + 0.001*VROCP4OXY2 + 0.001*VROCN1OXY6 + 0.998*NO2 + 0.998*HO2 + 0.085*BALD + 0.548*GLY + 0.365*MGLY + 0.365*FURANONE + 0.548*DCB1	2.70×10^{-12}exp(360.00/T)	9.03×10^{-12}
182	ROCARO53	XYMP + NO → 0.000*ONIT + 0.001*VROCP3OXY2 + 0.001*VROCP0OXY4 + 0.998*NO2 + 0.998*HO2 + 0.048*BALD + 0.703*GLY + 0.247*MGLY + 0.351*FURANONE + 0.598*DCB2	2.70×10^{-12}exp(360.00/T)	9.03×10^{-12}
183	ROCARO63	XYEP + NO → 0.000*ONIT + 0.001*VROCP3OXY2 + 0.001*VROCP0OXY4 + 0.998*NO2 + 0.998*HO2 + 0.085*BALD + 0.548*GLY + 0.365*MGLY + 0.456*FURANONE + 0.456*DCB2	2.70×10^{-12}exp(360.00/T)	9.03×10^{-12}
184	R188	ISOP + NO → 0.880*HO2 + 0.880*NO2 + 0.200*HCHO + 0.280*MACR + 0.440*MVK + 0.120*ISON + 0.021*GLY + 0.029*HKET + 0.027*ALD	2.43×10^{-12}exp(360.00/T)	8.13×10^{-12}
185	R189	APIP1 + NO → 0.820*HO2 + 0.820*NO2 + 0.820*PINAL + 0.180*TRPN	4.00×10^{-12}	4.00×10^{-12}
186	TRP13	APIP2 + NO → 0.820*HO + 0.820*NO2 + HOM	4.00×10^{-12}	4.00×10^{-12}
187	TRP14	APINP1 + NO → 2.000*NO2 + PINAL	4.00×10^{-12}	4.00×10^{-12}

N	CMAQ Label	Reaction	Rate Constant Formula[a,b,c]	k (molec cm^{-3} sec^{-1} or s^{-1})
188	TRP15	APINP2 + NO → 0.820*NO2 + 0.820*HO + HOM	4.00×10^{-12}	4.00×10^{-12}
189	R190	LIMP1 + NO → 0.770*HO2 + 0.770*NO2 + 0.490*LIMAL + 0.280*HCHO + 0.280*UALD + 0.230*TRPN	4.00×10^{-12}	4.00×10^{-12}
190	TRP16	LIMP2 + NO → 0.770*HO + 0.770*NO2 + HOM	4.00×10^{-12}	4.00×10^{-12}
191	TRP17	LIMNP1 + NO → 2.000*NO2 + LIMAL	4.00×10^{-12}	4.00×10^{-12}
192	TRP18	LIMNP2 + NO → 0.770*NO2 + 0.770*HO + HOM	4.00×10^{-12}	4.00×10^{-12}
193	TRP19	PINALP + NO → 0.950*HO2 + 0.950*NO2 + 0.050*TRPN + 0.950*HCHO + 0.950*KET	$2.70\times10^{-12}\exp(360.00/T)$	9.03×10^{-12}
194	TRP20	LIMALP + NO → 0.940*HO2 + 0.940*NO2 + 0.060*TRPN + 0.940*HCHO + 0.940*KET	$2.70\times10^{-12}\exp(360.00/T)$	9.03×10^{-12}
195	R191	ACO3 + NO → MO2 + NO2	$8.10\times10^{-12}\exp(270.00/T)$	2.00×10^{-11}
196	R192	RCO3 + NO → ETHP + NO2	$8.10\times10^{-12}\exp(270.00/T)$	2.00×10^{-11}
197	R193	ACTP + NO → ACO3 + NO2 + HCHO	$2.90\times10^{-12}\exp(300.00/T)$	7.93×10^{-12}
198	R194	MEKP + NO → 0.670*HO2 + NO2 + 0.330*HCHO + 0.670*DCB1	4.00×10^{-12}	4.00×10^{-12}
199	R195	KETP + NO → 0.770*HO2 + 0.230*ACO3 + 0.160*XO2 + NO2 + 0.460*ALD + 0.540*MGLY	4.00×10^{-12}	4.00×10^{-12}
200	R196	MACP + NO → 0.650*MO2 + 0.350*ACO3 + NO2 + 0.650*CO + 0.650*HCHO	$2.54\times10^{-12}\exp(360.00/T)$	8.50×10^{-12}
201	R197	MCP + NO → NO2 + 0.500*HO2 + 0.500*HCHO + HKET	$2.54\times10^{-12}\exp(360.00/T)$	8.50×10^{-12}
202	R198	MVKP + NO → 0.300*HO2 + 0.700*ACO3 + 0.700*XO2 + NO2 + 0.300*HCHO + 0.700*ALD + 0.300*MGLY	$2.54\times10^{-12}\exp(360.00/T)$	8.50×10^{-12}
203	R199	UALP + NO → HO2 + NO2 + 0.610*CO + 0.030*HCHO + 0.270*ALD + 0.180*GLY + 0.700*KET + 0.210*MGLY	$2.54\times10^{-12}\exp(360.00/T)$	8.50×10^{-12}
204	R200	BALP + NO → BAL1 + NO2	4.00×10^{-12}	4.00×10^{-12}
205	R201	BAL1 + NO → BAL2 + NO2	4.00×10^{-12}	4.00×10^{-12}
206	R202	ADDC + NO → HO2 + NO2 + 0.320*HKET + 0.680*GLY + 0.680*OP2	$2.70\times10^{-12}\exp(360.00/T)$	9.03×10^{-12}
207	R203	MCTP + NO → MCTO + NO2	$2.70\times10^{-12}\exp(360.00/T)$	9.03×10^{-12}
208	R204	ORAP + NO → NO2 + GLY + HO2	4.00×10^{-12}	4.00×10^{-12}
209	R205	OLNN + NO → NO2 + HO2 + ONIT	4.00×10^{-12}	4.00×10^{-12}
210	R206	OLND + NO → 2.000*NO2 + 0.287*HCHO + 1.240*ALD + 0.464*KET	4.00×10^{-12}	4.00×10^{-12}
211	R207	ADCN + NO → 2.000*NO2 + GLY + OP2	$2.70\times10^{-12}\exp(360.00/T)$	9.03×10^{-12}
212	R208	XO2 + NO → NO2	4.00×10^{-12}	4.00×10^{-12}
213	R209	BAL2 + NO2 → ONIT	2.00×10^{-11}	2.00×10^{-11}
214	R210	CHO + NO2 → ONIT	2.00×10^{-11}	2.00×10^{-11}
215	R211	MCTO + NO2 → ONIT	2.08×10^{-12}	2.08×10^{-12}
216	R212	MO2 + HO2 → OP1	$4.10\times10^{-13}\exp(750.00/T)$	5.07×10^{-12}
217	R213	ETHP + HO2 → OP2	$7.50\times10^{-13}\exp(700.00/T)$	7.85×10^{-12}
218	R214	HC3P + HO2 → OP2	$1.66\times10^{-13}\exp(1300.00/T)$	1.30×10^{-11}
219	R215	HC5P + HO2 → OP2	$1.66\times10^{-13}\exp(1300.00/T)$	1.30×10^{-11}
220	R217	ETEP + HO2 → OP2	$1.90\times10^{-13}\exp(1300.00/T)$	1.49×10^{-11}
221	R218	OLTP + HO2 → OP2	$1.66\times10^{-13}\exp(1300.00/T)$	1.30×10^{-11}
222	R219	OLIP + HO2 → OP2	$1.66\times10^{-13}\exp(1300.00/T)$	1.30×10^{-11}
223	ROCARO32	BENP + HO2 → 0.602*OP2 + 0.398*VROCN1OXY6	$2.91\times10^{-13}\exp(1300.00/T)$	2.28×10^{-11}
224	ROCARO42	TOLP + HO2 → 0.720*OP2 + 0.281*VROCN1OXY6	$2.91\times10^{-13}\exp(1300.00/T)$	2.28×10^{-11}
225	ROCARO52	XYMP + HO2 → 0.048*OP2 + 0.675*OP3 + 0.277*VROCP0OXY4	$2.91\times10^{-13}\exp(1300.00/T)$	2.28×10^{-11}
226	ROCARO62	XYEP + HO2 → 0.085*OP2 + 0.634*OP3 + 0.281*VROCP0OXY4	$2.91\times10^{-13}\exp(1300.00/T)$	2.28×10^{-11}
227	R228	ISOP + HO2 → ISHP	$2.05\times10^{-13}\exp(1300.00/T)$	1.60×10^{-11}
228	R229	APIP1 + HO2 → OPB	1.50×10^{-11}	1.50×10^{-11}
229	TRP21	APIP2 + HO2 → HOM	1.50×10^{-11}	1.50×10^{-11}

N	CMAQ Label	Reaction	Rate Constant Formula[a,b,c]	k (molec cm^{-3} sec^{-1} or s^{-1})
230	TRP22	APINP1 + HO2 → TRPN	1.50×10^{-11}	1.50×10^{-11}
231	TRP23	APINP2 + HO2 → HOM	1.50×10^{-11}	1.50×10^{-11}
232	R230	LIMP1 + HO2 → OPB	1.50×10^{-11}	1.50×10^{-11}
233	TRP24	LIMP2 + HO2 → HOM	1.50×10^{-11}	1.50×10^{-11}
234	TRP25	LIMNP1 + HO2 → TRPN	1.50×10^{-11}	1.50×10^{-11}
235	TRP26	LIMNP2 + HO2 → HOM	1.50×10^{-11}	1.50×10^{-11}
236	TRP27	PINALP + HO2 → OPB	$2.91\times10^{-13}\exp(1300.00/T)$	2.28×10^{-11}
237	TRP28	LIMALP + HO2 → OPB	$2.91\times10^{-13}\exp(1300.00/T)$	2.28×10^{-11}
238	R231	ACO3 + HO2 → 0.440*HO + 0.440*MO2 + 0.150*ORA2 + 0.410*PAA	$4.30\times10^{-13}\exp(1040.00/T)$	1.41×10^{-11}
239	R232	RCO3 + HO2 → 0.440*HO + 0.440*ETHP + 0.150*ORA2 + 0.410*PAA	$4.30\times10^{-13}\exp(1040.00/T)$	1.41×10^{-11}
240	R233	ACTP + HO2 → 0.150*HO + 0.150*ACO3 + 0.150*HCHO + 0.850*OP2	$1.15\times10^{-13}\exp(1300.00/T)$	9.00×10^{-12}
241	R234	MEKP + HO2 → OP2	$1.15\times10^{-13}\exp(1300.00/T)$	9.00×10^{-12}
242	R235	KETP + HO2 → OP2	$1.15\times10^{-13}\exp(1300.00/T)$	9.00×10^{-12}
243	R236	MACP + HO2 → MAHP	$1.82\times10^{-13}\exp(1300.00/T)$	1.42×10^{-11}
244	R237	MCP + HO2 → MAHP	$1.82\times10^{-13}\exp(1300.00/T)$	1.42×10^{-11}
245	R238	MVKP + HO2 → OP2	$2.91\times10^{-13}\exp(1300.00/T)$	2.28×10^{-11}
246	R239	UALP + HO2 → OP2	$2.91\times10^{-13}\exp(1300.00/T)$	2.28×10^{-11}
247	R240	ADDC + HO2 → OP2	$3.75\times10^{-13}\exp(980.00/T)$	1.00×10^{-11}
248	R241	CHO + HO2 → CSL	1.00×10^{-11}	1.00×10^{-11}
249	R242	MCTP + HO2 → OP2	$3.75\times10^{-13}\exp(980.00/T)$	1.00×10^{-11}
250	R243	ORAP + HO2 → OP2	$1.15\times10^{-13}\exp(1300.00/T)$	9.00×10^{-12}
251	R244	OLNN + HO2 → ONIT	$1.66\times10^{-13}\exp(1300.00/T)$	1.30×10^{-11}
252	R245	OLND + HO2 → ONIT	$1.66\times10^{-13}\exp(1300.00/T)$	1.30×10^{-11}
253	R246	ADCN + HO2 → OP2	$3.75\times10^{-13}\exp(980.00/T)$	1.00×10^{-11}
254	R247	XO2 + HO2 → OP2	$1.66\times10^{-13}\exp(1300.00/T)$	1.30×10^{-11}
255	R248	MO2 + MO2 → 0.740*HO2 + 1.370*HCHO + 0.630*MOH	$9.50\times10^{-14}\exp(390.00/T)$	3.51×10^{-13}
256	R249	ETHP + MO2 → HO2 + 0.750*HCHO + 0.750*ACD + 0.250*MOH + 0.250*EOH	$1.18\times10^{-13}\exp(158.00/T)$	2.00×10^{-13}
257	R250	HC3P + MO2 → 0.894*HO2 + 0.080*MO2 + 0.026*ETHP + 0.026*XO2 + 0.827*HCHO + 0.198*ALD + 0.497*KET + 0.050*GLY + 0.250*MOH + 0.250*ROH	$9.46\times10^{-14}\exp(431.00/T)$	4.02×10^{-13}
258	R251	HC5P + MO2 → 0.842*HO2 + 0.018*MO2 + 0.140*ETHP + 0.191*XO2 + 0.777*HCHO + 0.251*ALD + 0.618*KET + 0.250*MOH + 0.250*ROH	$1.00\times10^{-13}\exp(467.00/T)$	4.79×10^{-13}
259	R253	ETEP + MO2 → HO2 + 1.950*HCHO + 0.150*ALD + 0.250*MOH + 0.250*ETEG	$1.71\times10^{-13}\exp(708.00/T)$	1.84×10^{-12}
260	R254	OLTP + MO2 → HO2 + 1.500*HCHO + 0.705*ALD + 0.045*KET + 0.250*MOH + 0.250*ROH	$1.46\times10^{-13}\exp(708.00/T)$	1.57×10^{-12}
261	R255	OLIP + MO2 → HO2 + 0.750*HCHO + 1.280*ALD + 0.218*KET + 0.250*MOH + 0.250*ROH	$9.18\times10^{-14}\exp(708.00/T)$	9.87×10^{-13}
262	ROCARO35	BENP + MO2 → 0.680*HCHO + 1.370*HO2 + 0.320*MOH + 0.000*BALD + GLY + 0.500*FURANONE + 0.250*DCB2 + 0.250*DCB3	$3.56\times10^{-14}\exp(708.00/T)$	3.83×10^{-13}
263	ROCARO45	TOLP + MO2 → 0.680*HCHO + 1.285*HO2 + 0.320*MOH + 0.085*BALD + 0.549*GLY + 0.366*MGLY + 0.366*FURANONE + 0.549*DCB1	$3.56\times10^{-14}\exp(708.00/T)$	3.83×10^{-13}
264	ROCARO55	XYMP + MO2 → 0.680*HCHO + 1.322*HO2 + 0.320*MOH + 0.048*BALD + 0.704*GLY + 0.247*MGLY + 0.352*FURANONE + 0.600*DCB2	$3.56\times10^{-14}\exp(708.00/T)$	3.83×10^{-13}

N	CMAQ Label	Reaction	Rate Constant Formula[a,b,c]	k (molec cm^{-3} sec^{-1} or s^{-1})
265	ROCARO65	XYEP + MO2 → 0.680*HCHO + 1.285*HO2 + 0.320*MOH + 0.085*BALD + 0.549*GLY + 0.366*MGLY + 0.457*FURANONE + 0.457*DCB2	$3.56\times10^{-14}\exp(708.00/T)$	3.83×10^{-13}
266	R264	ISOP + MO2 → HO2 + 1.310*HCHO + 0.159*MACR + 0.250*MVK + 0.250*MOH + 0.250*ROH + 0.023*ALD + 0.018*GLY + 0.016*HKET	$3.40\times10^{-14}\exp(221.00/T)$	7.14×10^{-14}
267	R265	APIP1 + MO2 → HO2 + 0.680*HCHO + 0.600*PINAL + 0.070*KET + 0.320*MOH + 0.250*ROH	$3.56\times10^{-14}\exp(708.00/T)$	3.83×10^{-13}
268	TRP29	APIP2 + MO2 → HO2 + 0.750*HCHO + 0.250*MOH + HOM	1.00×10^{-10}	1.00×10^{-10}
269	TRP30	APINP1 + MO2 → 0.370*HO2 + 0.860*NO2 + 0.680*HCHO + 0.860*PINAL + 0.320*MOH + 0.140*TRPN	$3.56\times10^{-14}\exp(708.00/T)$	3.83×10^{-13}
270	TRP31	APINP2 + MO2 → 0.750*HO2 + 0.750*NO2 + 0.250*MOH + 0.750*HCHO + HOM	1.00×10^{-10}	1.00×10^{-10}
271	R266	LIMP1 + MO2 → HO2 + HCHO + 0.420*LIMAL + 0.300*KET + 0.320*MOH + 0.270*ROH	$3.56\times10^{-14}\exp(708.00/T)$	3.83×10^{-13}
272	TRP32	LIMP2 + MO2 → HO2 + 0.750*HCHO + 0.250*MOH + HOM	1.00×10^{-10}	1.00×10^{-10}
273	TRP33	LIMNP1 + MO2 → 0.370*HO2 + 0.680*HCHO + 0.700*LIMAL + 0.700*NO2 + 0.320*MOH + 0.300*TRPN	$3.56\times10^{-14}\exp(708.00/T)$	3.83×10^{-13}
274	TRP34	LIMNP2 + MO2 → 0.750*HO2 + 0.750*HCHO + 0.750*NO2 + 0.250*MOH + HOM	1.00×10^{-10}	1.00×10^{-10}
275	R267	ACO3 + MO2 → 0.900*HO2 + 0.900*MO2 + HCHO + 0.100*ORA2	$2.00\times10^{-11}\exp(500.00/T)$	1.07×10^{-10}
276	R268	RCO3 + MO2 → 0.900*HO2 + 0.900*MO2 + HCHO + 0.100*ORA2	$2.00\times10^{-11}\exp(500.00/T)$	1.07×10^{-10}
277	R269	ACTP + MO2 → 0.500*HO2 + 0.500*ACO3 + 1.500*HCHO + 0.250*MOH + 0.250*ROH + 0.125*ORA2	$7.50\times10^{-13}\exp(500.00/T)$	4.01×10^{-12}
278	R270	MEKP + MO2 → 0.834*HO2 + HCHO + 0.334*DCB1 + 0.250*MOH + 0.250*ROH	$6.91\times10^{-13}\exp(508.00/T)$	3.80×10^{-12}
279	R271	KETP + MO2 → HO2 + 0.750*HCHO + 0.500*DCB1 + 0.250*MOH + 0.250*ROH	$6.91\times10^{-13}\exp(508.00/T)$	3.80×10^{-12}
280	R272	MACP + MO2 → 0.500*HO2 + 0.269*ACO3 + 0.500*CO + 1.660*HCHO + 0.067*ORA2 + 0.250*MO2 + 0.250*MOH + 0.250*ROH	$3.40\times10^{-14}\exp(221.00/T)$	7.14×10^{-14}
281	R273	MCP + MO2 → NO2 + HO2 + 1.500*HCHO + 0.500*HKET + 0.250*MOH + 0.250*ROH	$3.40\times10^{-14}\exp(221.00/T)$	7.14×10^{-14}
282	R274	MVKP + MO2 → HO2 + 1.160*ACO3 + 1.160*XO2 + 1.500*HCHO + 1.750*ALD + 0.500*MGLY + 0.250*MOH + 0.250*ROH + 0.292*ORA2	8.37×10^{-14}	8.37×10^{-14}
283	R275	UALP + MO2 → HO2 + 0.305*CO + 0.773*HCHO + 0.203*ALD + 0.525*KET + 0.135*GLY + 0.105*MGLY + 0.250*MOH + 0.250*ROH	$3.40\times10^{-14}\exp(221.00/T)$	7.14×10^{-14}
284	R276	BALP + MO2 → HO2 + BAL1 + HCHO	$3.56\times10^{-14}\exp(708.00/T)$	3.83×10^{-13}
285	R277	BAL1 + MO2 → HO2 + BAL2 + HCHO	$3.56\times10^{-14}\exp(708.00/T)$	3.83×10^{-13}
286	R278	ADDC + MO2 → 2.000*HO2 + HCHO + 0.320*HKET + 0.680*GLY + 0.680*OP2	$3.56\times10^{-14}\exp(708.00/T)$	3.83×10^{-13}
287	R279	MCTP + MO2 → HO2 + MCTO + HCHO	$3.56\times10^{-14}\exp(708.00/T)$	3.83×10^{-13}
288	R280	ORAP + MO2 → HCHO + HO2 + GLY	$7.50\times10^{-13}\exp(500.00/T)$	4.01×10^{-12}
289	R281	OLNN + MO2 → 2.000*HO2 + HCHO + ONIT	$1.60\times10^{-13}\exp(708.00/T)$	1.72×10^{-12}
290	R282	OLND + MO2 → 0.500*HO2 + 0.500*NO2 + 0.965*HCHO + 0.930*ALD + 0.348*KET + 0.250*MOH + 0.250*ROH + 0.500*ONIT	$9.68\times10^{-14}\exp(708.00/T)$	1.04×10^{-12}
291	R283	ADCN + MO2 → HO2 + 0.700*NO2 + HCHO + 0.700*GLY + 0.700*OP2 + 0.300*ONIT	3.56×10^{-14}	3.56×10^{-14}

N	CMAQ Label	Reaction	Rate Constant Formula[a,b,c]	k (molec cm^{-3} sec^{-1} or s^{-1})
292	R284	XO2 + MO2 → HO2 + HCHO	$5.99\times10^{-15}\exp(1510.00/T)$	9.48×10^{-13}
293	R285	ETHP + ACO3 → 0.500*HO2 + 0.500*MO2 + ACD + 0.500*ORA2	$1.03\times10^{-12}\exp(211.00/T)$	2.09×10^{-12}
294	R286	HC3P + ACO3 → 0.394*HO2 + 0.580*MO2 + 0.026*ETHP + 0.026*XO2 + 0.130*HCHO + 0.273*ALD + 0.662*KET + 0.067*GLY + 0.500*ORA2	$6.90\times10^{-13}\exp(460.00/T)$	3.23×10^{-12}
295	R287	HC5P + ACO3 → 0.342*HO2 + 0.518*MO2 + 0.140*ETHP + 0.191*XO2 + 0.042*HCHO + 0.381*ALD + 0.824*KET + 0.500*ORA2	$5.59\times10^{-13}\exp(522.00/T)$	3.22×10^{-12}
296	R289	ETEP + ACO3 → 0.500*HO2 + 0.500*MO2 + 1.600*HCHO + 0.200*ALD + 0.500*ORA2	$9.48\times10^{-13}\exp(765.00/T)$	1.23×10^{-11}
297	R290	OLTP + ACO3 → 0.500*HO2 + 0.500*MO2 + HCHO + 0.940*ALD + 0.060*KET + 0.500*ORA2	$8.11\times10^{-13}\exp(765.00/T)$	1.06×10^{-11}
298	R291	OLIP + ACO3 → 0.500*HO2 + 0.500*MO2 + 1.710*ALD + 0.290*KET + 0.500*ORA2	$5.09\times10^{-13}\exp(765.00/T)$	6.62×10^{-12}
299	ROCARO36	BENP + ACO3 → 0.700*MO2 + HO2 + 0.300*ORA2 + 0.000*BALD + GLY + 0.500*FURANONE + 0.250*DCB2 + 0.250*DCB3	$7.40\times10^{-13}\exp(765.00/T)$	9.63×10^{-12}
300	ROCARO46	TOLP + ACO3 → 0.700*MO2 + 0.915*HO2 + 0.300*ORA2 + 0.085*BALD + 0.549*GLY + 0.366*MGLY + 0.366*FURANONE + 0.549*DCB1	$7.40\times10^{-13}\exp(765.00/T)$	9.63×10^{-12}
301	ROCARO56	XYMP + ACO3 → 0.700*MO2 + 0.952*HO2 + 0.300*ORA2 + 0.048*BALD + 0.704*GLY + 0.247*MGLY + 0.352*FURANONE + 0.600*DCB2	$7.40\times10^{-13}\exp(765.00/T)$	9.63×10^{-12}
302	ROCARO66	XYEP + ACO3 → 0.700*MO2 + 0.915*HO2 + 0.300*ORA2 + 0.085*BALD + 0.549*GLY + 0.366*MGLY + 0.457*FURANONE + 0.457*DCB2	$7.40\times10^{-13}\exp(765.00/T)$	9.63×10^{-12}
303	R300	ISOP + ACO3 → 0.500*HO2 + 0.500*MO2 + 1.048*HCHO + 0.219*MACR + 0.305*MVK + 0.500*ORA2	$8.40\times10^{-14}\exp(221.00/T)$	1.76×10^{-13}
304	R301	APIP1 + ACO3 → 0.630*HO2 + 0.700*MO2 + 0.600*PINAL + 0.300*ORA2 + 0.070*KET + 0.250*ROH	$7.40\times10^{-13}\exp(765.00/T)$	9.63×10^{-12}
305	TRP35	APIP2 + ACO3 → 0.500*HO + 0.500*MO2 + 0.500*ORA2 + HOM	1.00×10^{-10}	1.00×10^{-10}
306	TRP36	APINP1 + ACO3 → 0.860*NO2 + 0.140*TRPN + 0.860*PINAL + 0.700*MO2 + 0.300*ORA2	$7.40\times10^{-13}\exp(765.00/T)$	9.63×10^{-12}
307	TRP37	APINP2 + ACO3 → 0.500*NO2 + 0.500*MO2 + 0.500*ORA2 + HOM	1.00×10^{-10}	1.00×10^{-10}
308	R302	LIMP1 + ACO3 → 0.630*HO2 + 0.700*MO2 + 0.420*LIMAL + 0.300*KET + 0.300*ORA2 + 0.320*HCHO + 0.270*ROH	$7.40\times10^{-13}\exp(765.00/T)$	9.63×10^{-12}
309	TRP38	LIMP2 + ACO3 → 0.500*HO + 0.500*MO2 + 0.500*ORA2 + HOM	1.00×10^{-10}	1.00×10^{-10}
310	TRP39	LIMNP1 + ACO3 → 0.700*NO2 + 0.700*LIMAL + 0.300*TRPN + 0.700*MO2 + 0.300*ORA2	$7.40\times10^{-13}\exp(765.00/T)$	9.63×10^{-12}
311	TRP40	LIMNP2 + ACO3 → 0.500*MO2 + 0.500*NO2 + 0.500*ORA2 + HOM	1.00×10^{-10}	1.00×10^{-10}
312	R303	ACO3 + ACO3 → 2.000*MO2	$2.50\times10^{-12}\exp(500.00/T)$	1.34×10^{-11}
313	R304	RCO3 + ACO3 → MO2 + ETHP	$2.50\times10^{-12}\exp(500.00/T)$	1.34×10^{-11}
314	R305	ACTP + ACO3 → 0.500*MO2 + 0.500*ACO3 + HCHO + 0.750*ORA2	$7.51\times10^{-13}\exp(565.00/T)$	5.00×10^{-12}
315	R306	MEKP + ACO3 → 0.330*HO2 + 0.500*MO2 + 0.330*HCHO + 0.334*DCB1 + 0.500*ORA2	$7.51\times10^{-13}\exp(565.00/T)$	5.00×10^{-12}
316	R307	KETP + ACO3 → 0.500*HO2 + 0.500*MO2 + 0.500*DCB1 + 0.500*ORA2	$7.51\times10^{-13}\exp(565.00/T)$	5.00×10^{-12}

N	CMAQ Label	Reaction	Rate Constant Formula[a,b,c]	k (molec cm^{-3} sec^{-1} or s^{-1})
317	R308	MACP + ACO3 → 0.635*ORA2 + 0.500*MO2 + 0.269*ACO3 + 0.500*CO + HCHO	$8.40\times10^{-14}\exp(221.00/T)$	1.76×10^{-13}
318	R309	MCP + ACO3 → NO2 + 0.500*HO2 + HCHO + 0.500*HKET + 0.500*MO2 + 0.500*ORA2	$8.40\times10^{-14}\exp(221.00/T)$	1.76×10^{-13}
319	R310	MVKP + ACO3 → 0.500*HO2 + 0.500*MO2 + 1.160*ACO3 + 1.160*XO2 + HCHO + 2.300*ALD + 0.500*MGLY + 1.083*ORA2	$1.68\times10^{-12}\exp(500.00/T)$	8.99×10^{-12}
320	R311	UALP + ACO3 → 0.500*HO2 + 0.500*MO2 + 0.500*CO + 0.030*HCHO + 0.270*ALD + 0.700*KET + 0.180*GLY + 0.105*MGLY + 0.500*ORA2	$1.68\times10^{-12}\exp(500.00/T)$	8.99×10^{-12}
321	R312	BALP + ACO3 → MO2 + BAL1	$7.40\times10^{-13}\exp(765.00/T)$	9.63×10^{-12}
322	R313	BAL1 + ACO3 → MO2 + BAL2	$7.40\times10^{-13}\exp(765.00/T)$	9.63×10^{-12}
323	R314	ADDC + ACO3 → 2.000*HO2 + MO2 + 0.320*HKET + 0.680*GLY + 0.680*OP2	$7.40\times10^{-13}\exp(708.00/T)$	7.95×10^{-12}
324	R315	MCTP + ACO3 → HO2 + MO2 + MCTO	$7.40\times10^{-13}\exp(708.00/T)$	7.95×10^{-12}
325	R316	ORAP + ACO3 → MO2 + GLY	$7.51\times10^{-13}\exp(565.00/T)$	5.00×10^{-12}
326	R317	OLNN + ACO3 → HO2 + MO2 + ONIT	$8.85\times10^{-13}\exp(765.00/T)$	1.15×10^{-11}
327	R318	OLND + ACO3 → 0.500*MO2 + NO2 + 0.287*HCHO + 1.240*ALD + 0.464*KET + 0.500*ORA2	$5.37\times10^{-13}\exp(765.00/T)$	6.99×10^{-12}
328	R319	ADCN + ACO3 → HO2 + MO2 + 0.700*NO2 + 0.700*GLY + 0.700*OP2 + 0.300*ONIT	$7.40\times10^{-13}\exp(708.00/T)$	7.95×10^{-12}
329	R320	XO2 + ACO3 → MO2	$3.40\times10^{-14}\exp(1560.00/T)$	6.37×10^{-12}
330	R321	RCO3 + RCO3 → 2.000*ETHP	$2.50\times10^{-12}\exp(500.00/T)$	1.34×10^{-11}
331	R322	MO2 + NO3 → HO2 + HCHO + NO2	1.20×10^{-12}	1.20×10^{-12}
332	R323	ETHP + NO3 → HO2 + NO2 + ACD	1.20×10^{-12}	1.20×10^{-12}
333	R324	HC3P + NO3 → 0.254*HO2 + 0.140*MO2 + 0.092*XO2 + 0.503*ETHP + NO2 + 0.519*ACD + 0.147*ALD + 0.075*MEK + 0.095*ACT	1.20×10^{-12}	1.20×10^{-12}
334	R325	HC5P + NO3 → 0.488*HO2 + 0.055*MO2 + 0.280*ETHP + 0.485*XO2 + NO2 + 0.024*HCHO + 0.241*ALD + 0.060*KET + 0.063*MEK + 0.247*ACT + 0.048*ACD + 0.275*HKET	1.20×10^{-12}	1.20×10^{-12}
335	R327	ETEP + NO3 → HO2 + NO2 + 1.600*HCHO + 0.200*ALD	1.20×10^{-12}	1.20×10^{-12}
336	R328	OLTP + NO3 → 0.470*ALD + 0.790*HCHO + 0.790*HO2 + NO2 + 0.180*MEK + 0.020*ACD + 0.090*ACT	1.20×10^{-12}	1.20×10^{-12}
337	R329	OLIP + NO3 → 0.860*HO2 + 0.720*ALD + 0.110*KET + NO2 + 0.200*ACT + 0.850*ACD + 0.040*HKET	1.20×10^{-12}	1.20×10^{-12}
338	ROCARO34	BENP + NO3 → NO2 + HO2 + 0.000*BALD + GLY + 0.500*FURANONE + 0.250*DCB2 + 0.250*DCB3	2.30×10^{-12}	2.30×10^{-12}
339	ROCARO44	TOLP + NO3 → NO2 + 0.915*HO2 + 0.085*BALD + 0.549*GLY + 0.366*MGLY + 0.366*FURANONE + 0.549*DCB1	2.30×10^{-12}	2.30×10^{-12}
340	ROCARO54	XYMP + NO3 → NO2 + 0.952*HO2 + 0.048*BALD + 0.704*GLY + 0.247*MGLY + 0.352*FURANONE + 0.600*DCB2	2.30×10^{-12}	2.30×10^{-12}
341	ROCARO64	XYEP + NO3 → NO2 + 0.915*HO2 + 0.085*BALD + 0.549*GLY + 0.366*MGLY + 0.457*FURANONE + 0.457*DCB2	2.30×10^{-12}	2.30×10^{-12}
342	R338	ISOP + NO3 → HO2 + NO2 + 0.750*HCHO + 0.318*MACR + 0.500*MVK + 0.024*GLY + 0.033*HKET + 0.031*ALD	1.20×10^{-12}	1.20×10^{-12}
343	R339	APIP1 + NO3 → HO2 + NO2 + ALD + KET	1.20×10^{-12}	1.20×10^{-12}
344	R340	LIMP1 + NO3 → HO2 + NO2 + 0.385*OLI + 0.385*HCHO + 0.615*MACR	1.20×10^{-12}	1.20×10^{-12}
345	R341	ACO3 + NO3 → MO2 + NO2	4.00×10^{-12}	4.00×10^{-12}
346	R342	RCO3 + NO3 → ETHP + NO2	4.00×10^{-12}	4.00×10^{-12}
347	R343	ACTP + NO3 → ACO3 + NO2 + HCHO	1.20×10^{-12}	1.20×10^{-12}

N	CMAQ Label	Reaction	Rate Constant Formula[a,b,c]	k (molec cm^{-3} sec^{-1} or s^{-1})
348	R344	MEKP + NO3 → 0.670*HO2 + NO2 + 0.330*HCHO + 0.670*DCB1	1.20×10^{-12}	1.20×10^{-12}
349	R345	KETP + NO3 → HO2 + NO2 + DCB1	1.20×10^{-12}	1.20×10^{-12}
350	R346	MACP + NO3 → HCHO + 0.538*ACO3 + CO + NO2	1.20×10^{-12}	1.20×10^{-12}
351	R347	MCP + NO3 → NO2 + HO2 + HCHO + HKET	1.20×10^{-12}	1.20×10^{-12}
352	R348	MVKP + NO3 → 0.300*HO2 + 0.700*ACO3 + 0.700*XO2 + NO2 + 0.300*HCHO + 0.700*ALD + 0.300*MGLY	2.50×10^{-12}	2.50×10^{-12}
353	R349	UALP + NO3 → HO2 + NO2 + 0.610*CO + 0.030*HCHO + 0.270*ALD + 0.700*KET + 0.180*GLY + 0.210*MGLY	2.50×10^{-12}	2.50×10^{-12}
354	R350	BALP + NO3 → BAL1 + NO2	2.50×10^{-12}	2.50×10^{-12}
355	R351	BAL1 + NO3 → BAL2 + NO2	2.50×10^{-12}	2.50×10^{-12}
356	R352	ADDC + NO3 → HO2 + NO2 + 0.320*HKET + 0.680*GLY + 0.680*OP2	1.20×10^{-12}	1.20×10^{-12}
357	R353	MCTP + NO3 → NO2 + MCTO	1.20×10^{-12}	1.20×10^{-12}
358	R354	ORAP + NO3 → NO2 + GLY + HO2	1.20×10^{-12}	1.20×10^{-12}
359	R355	OLNN + NO3 → HO2 + NO2 + ONIT	1.20×10^{-12}	1.20×10^{-12}
360	R356	OLND + NO3 → 2.000*NO2 + 0.287*HCHO + 1.240*ALD + 0.464*KET	1.20×10^{-12}	1.20×10^{-12}
361	R357	ADCN + NO3 → 2.000*NO2 + GLY + OP2	1.20×10^{-12}	1.20×10^{-12}
362	R358	OLNN + OLNN → HO2 + 2.000*ONIT	$7.00\times10^{-14}\exp(1000.00/T)$	2.00×10^{-12}
363	R359	OLNN + OLND → 0.500*HO2 + 0.500*NO2 + 0.202*HCHO + 0.640*ALD + 0.149*KET + 1.500*ONIT	$4.25\times10^{-14}\exp(1000.00/T)$	1.22×10^{-12}
364	R360	OLND + OLND → NO2 + 0.504*HCHO + 1.210*ALD + 0.285*KET + ONIT	$2.96\times10^{-14}\exp(1000.00/T)$	8.47×10^{-13}
365	R361	XO2 + NO3 → NO2	1.20×10^{-12}	1.20×10^{-12}
366	R362	XO2 + RCO3 → ETHP	$2.50\times10^{-12}\exp(500.00/T)$	1.34×10^{-11}
367	R363	XO2 + XO2 →	$7.13\times10^{-17}\exp(2950.00/T)$	1.41×10^{-12}
368	TRP41	APIP2 + APIP1 → 0.960*HOM + 0.480*ROH + 0.480*PINAL + 0.480*HO + 0.480*HO2 + 0.040*ELHOM	1.00×10^{-10}	1.00×10^{-10}
369	TRP42	APIP2 + LIMP1 → 0.960*HOM + 0.480*ROH + 0.480*LIMAL + 0.480*HO + 0.480*HO2 + 0.040*ELHOM	1.00×10^{-10}	1.00×10^{-10}
370	TRP43	APIP2 + ISOP → 0.960*HOM + 0.480*ROH + 0.480*HCHO + 0.480*MVK + 0.480*HO + 0.480*HO2 + 0.040*ELHOM	1.00×10^{-10}	1.00×10^{-10}
371	TRP44	LIMP2 + APIP1 → 0.960*HOM + 0.480*ROH + 0.480*PINAL + 0.480*HO + 0.480*HO2 + 0.040*ELHOM	1.00×10^{-10}	1.00×10^{-10}
372	TRP45	LIMP2 + LIMP1 → 0.960*HOM + 0.480*ROH + 0.480*LIMAL + 0.480*HO + 0.480*HO2 + 0.040*ELHOM	1.00×10^{-10}	1.00×10^{-10}
373	TRP46	LIMP2 + ISOP → 0.960*HOM + 0.480*ROH + 0.480*HCHO + 0.480*MVK + 0.480*HO + 0.480*HO2 + 0.040*ELHOM	1.00×10^{-10}	1.00×10^{-10}
374	TRP47	APINP2 + APIP1 → 0.960*HOM + 0.480*ROH + 0.480*PINAL + 0.480*NO2 + 0.480*HO2 + 0.040*ELHOM	1.00×10^{-10}	1.00×10^{-10}
375	TRP48	APINP2 + LIMP1 → 0.960*HOM + 0.480*ROH + 0.480*LIMAL + 0.480*NO2 + 0.480*HO2 + 0.040*ELHOM	1.00×10^{-10}	1.00×10^{-10}
376	TRP49	APINP2 + ISOP → 0.960*HOM + 0.480*ROH + 0.480*HCHO + 0.480*MVK + 0.480*NO2 + 0.480*HO2 + 0.040*ELHOM	1.00×10^{-10}	1.00×10^{-10}
377	TRP50	LIMNP2 + APIP1 → 0.960*HOM + 0.480*ROH + 0.480*PINAL + 0.480*NO2 + 0.480*HO2 + 0.040*ELHOM	1.00×10^{-10}	1.00×10^{-10}
378	TRP51	LIMNP2 + LIMP1 → 0.960*HOM + 0.480*ROH + 0.480*LIMAL + 0.480*NO2 + 0.480*HO2 + 0.040*ELHOM	1.00×10^{-10}	1.00×10^{-10}
379	TRP52	LIMNP2 + ISOP → 0.960*HOM + 0.480*ROH + 0.480*HCHO + 0.480*MVK + 0.480*NO2 + 0.480*HO2 + 0.040*ELHOM	1.00×10^{-10}	1.00×10^{-10}
380	SA14	IEPOX + HO → HO	$5.78\times10^{-11}\exp(-400.00/T)$	1.51×10^{-11}

N	CMAQ Label	Reaction	Rate Constant Formula[a,b,c]	k (molec cm^{-3} sec^{-1} or s^{-1})
381	R001c	VROCIOXY + HO → 0.852*ETHP + 0.149*ASOATJ	6.89×10^{-12}	6.89×10^{-12}
382	R002c	SLOWROC + HO → ETHP + 0.001*ASOATJ	6.55×10^{-14}	6.55×10^{-14}
383	T17	ACRO + HO → 0.570*MACP + 0.430*MCP	$8.00\times10^{-12}\exp(380.00/T)$	2.86×10^{-11}
384	T18	ACRO + O3 → 0.840*CO + 0.560*HO2 + 0.280*HO + 0.720*HCHO + 0.620*GLY	2.90×10^{-19}	2.90E-19
385	T19	ACRO + NO3 → 0.680*HCHO + 0.320*MACP + 0.680*XO2 + 0.680*MGLY + 0.320*HNO3 + 0.680*NO2	3.40×10^{-15}	3.40×10^{-15}
386	T20	ACRO → CO + 0.477*HO2 + 0.250*ETE + 0.354*ACO3 + 0.204*HO + 0.150*HCHO + 0.027*MO2	φ from MVK (Atkinson et al., 2006; Gierczak et al., 1997), σ from Sander et al. (2006) as implemented by Hutzell et al. (2012)	Not Available
387	T10	BDE13 + HO → 0.667*BDE13P + 0.333*UALD + 0.333*HO2	$1.48\times10^{-11}\exp(448.00/T)$	6.65×10^{-11}
388	T10a	BDE13P + NO → 0.968*HO2 + 0.968*NO2 + 0.895*ACRO + 0.895*HCHO + 0.072*FURAN + 0.032*ONIT	9.05×10^{-12}	9.05×10^{-12}
389	T10b	BDE13P + NO3 → HO2 + NO2 + 0.925*ACRO + 0.925*HCHO + 0.075*FURAN	2.30×10^{-12}	2.30×10^{-12}
390	T10c	BDE13P + HO2 → OP2	1.61×10^{-11}	1.61×10^{-11}
391	T10d	BDE13P + MO2 → 0.320*MOH + 1.143*HCHO + 0.870*HO2 + 0.463*ACRO + 0.250*OLT + 0.231*MVK + 0.037*FURAN + 0.019*UALD	2.39×10^{-12}	2.39×10^{-12}
392	T10e	BDE13P + ACO3 → 0.700*MO2 + 0.300*ORA2 + 0.800*HO2 + 0.740*ACRO + 0.740*HCHO + 0.185*MVK + 0.060*FURAN + 0.015*UALD	1.37×10^{-11}	1.37×10^{-11}
393	T11	BDE13 + O3 → 0.620*ACRO + 0.630*CO + 0.420*HO2 + 0.080*HO + 0.830*HCHO + 0.170*ETE	$1.34\times10^{-14}\exp(-2283.00/T)$	6.33×10^{-18}
394	T12	BDE13 + NO3 → 0.900*OLNN + 0.100*OLND + 0.900*ACRO	1.00×10^{-13}	1.00×10^{-13}
395	R003c	FURAN + HO → 0.490*DCB1 + 0.490*HO2 + 0.510*FURANO2	5.01×10^{-11}	5.01×10^{-11}
396	R004c	FURANO2 + NO → 0.080*ONIT + 0.920*NO2 + 0.920*FURANONE + 0.750*HO2 + 0.170*MO2	$2.70\times10^{-12}\exp(360.00/T)$	9.03×10^{-12}
397	R005c	FURANO2 + HO2 → 0.600*OP2 + 0.400*FURANONE + 0.400*HO + 0.320*HO2 + 0.080*MO2	$3.75\times10^{-13}\exp(980.00/T)$	1.00×10^{-11}
398	R006c	FURANONE + HO → 0.650*KET + 0.310*GLY + 0.660*HO2 + 0.340*MO2 + 0.430*CO + 0.040*ASOATJ	4.40×10^{-11}	4.40×10^{-11}
399	R007c	FURAN + O3 → 0.020*HO + ALD	3.43×10^{-17}	3.43×10^{-17}
400	R008c	FURAN + NO3 → NO2 + 0.800*DCB1 + 0.200*DCB3	8.99×10^{-12}	8.99×10^{-12}
401	R010c	PROG + HO → 0.613*HKET + 0.387*ALD + HO2	1.20×10^{-11}	1.20×10^{-11}
402	R011c	SESQ + NO3 → SESQNRO2	1.90×10^{-11}	1.90×10^{-11}
403	R012c	SESQNRO2 + HO2 → VROCP0OXY4	$2.84\times10^{-13}\exp(1300.00/T)$	2.22×10^{-11}
404	R013c	SESQNRO2 + NO → VROCP3OXY2 + 2.000*NO2	$2.70\times10^{-12}\exp(360.00/T)$	9.03×10^{-12}
405	R014c	SESQNRO2 + NO3 → VROCP3OXY2 + 2.000*NO2	2.30×10^{-12}	2.30×10^{-12}
406	R015c	SESQ + O3 → 0.982*VROCP3OXY2 + 0.018*VROCN2OXY2	1.20×10^{-14}	1.20×10^{-14}
407	R016c	SESQ + HO → SESQRO2	1.97×10^{-10}	1.97×10^{-10}
408	R017c	SESQRO2 + HO2 → VROCP0OXY2	$2.84\times10^{-13}\exp(1300.00/T)$	2.22×10^{-11}
409	R019c	SESQRO2 + NO3 → VROCP3OXY2	2.30×10^{-12}	2.30×10^{-12}
410	R020c	SESQRO2 + NO → 0.247*VROCP1OXY3 + 0.753*VROCP3OXY2 + 0.753*NO2	$2.70\times10^{-12}\exp(360.00/T)$	9.03×10^{-12}
411	HET_GLY	GLY → AGLYJ	$\gamma=2.9\times10^{-3}$, based on Liggio et al. (2005) as implemented by Pye et al. (2015)	Not Available[b]

N	CMAQ Label	Reaction	Rate Constant Formula[a,b,c]	k (molec cm^{-3} sec^{-1} or s^{-1})
412	HET_MGLY	MGLY → AGLYJ	$\gamma=2.9\times10^{-3}$, based on Liggio et al. (2005) as implemented by Pye et al. (2015)	Not Available[b]
413	HET_N2O5	N2O5 → 2.000*HNO3	Davis et al. (2008) equation 15	Not Available[b]
414	HET_N02	NO2 → 0.500*HONO + 0.500*HNO3	$v\gamma= 4\times10^{-4}$ m s^{-1} (Vogel et al., 2003)	Not Available[b]
415	HAL_Ozone[e]	O3 →	min(6.701×10^{-11}exp($1.074\times10^{+1}$P)+ 3.415E-08exp(-6.713×10^{-1}P), 2.000×10^{-06})	2.00×10^{-6}
416	HET_IEPOX	IEPOX → IEPOXP	Uptake coefficient calculated based on particle composition following Pye et al. (2013) with parameter updates of Pye et al. (2017)	Not Applicable[b]
417	HET_ISO3TET	IEPOXP → AISO3NOSJ	Ratio of 2-methyltetrols+IEPOX-derived organonitrate formation rates to total condensed phase reaction rate	Not Applicable
418	HET_IEPOXOS	IEPOXP + ASO4J → AISO3OSJ	Ratio of Organosulfate formation rate to total IEPOX condensed phase reaction rate	Not Applicable
419	ROCALK1c	VROCP6ALK + HO → VROCP6ALKP	1.53×10^{-11}	1.53×10^{-11}
420	ROCALK2c	VROCP5ALK + HO → VROCP5ALKP	1.68×10^{-11}	1.68×10^{-11}
421	ROCALK3c	VROCP4ALK + HO → VROCP4ALKP	2.24×10^{-11}	2.24×10^{-11}
422	ROCALK4c	VROCP3ALK + HO → VROCP3ALKP	2.67×10^{-11}	2.67×10^{-11}
423	ROCALK5c	VROCP2ALK + HO → VROCP2ALKP	3.09×10^{-11}	3.09×10^{-11}
424	ROCALK6c	VROCP1ALK + HO → VROCP1ALKP	3.38×10^{-11}	3.38×10^{-11}
425	HC1001	HC10 + HO → HC10P	1.10×10^{-11}	1.10×10^{-11}
426	ROCALK7c	VROCP6ALKP + NO → 0.720*VROCP6ALKP2 + 0.280*VROCP4OXY2 + 0.720*NO2	2.70×10^{-12}exp(360.00/T)	9.03×10^{-12}
427	ROCALK8c	VROCP5ALKP + NO → 0.720*VROCP5ALKP2 + 0.280*VROCP3OXY2 + 0.720*NO2	2.70×10^{-12}exp(360.00/T)	9.03×10^{-12}
428	ROCALK9c	VROCP4ALKP + NO → 0.720*VROCP4ALKP2 + 0.280*VROCP2OXY2 + 0.720*NO2	2.70×10^{-12}exp(360.00/T)	9.03×10^{-12}
429	ROCALK10c	VROCP3ALKP + NO → 0.720*VROCP3ALKP2 + 0.280*VROCP1OXY1 + 0.720*NO2	2.70×10^{-12}exp(360.00/T)	9.03×10^{-12}
430	ROCALK11c	VROCP2ALKP + NO → 0.720*VROCP2ALKP2 + 0.280*VROCP0OXY2 + 0.720*NO2	2.70×10^{-12}exp(360.00/T)	9.03×10^{-12}
431	ROCALK12c	VROCP1ALKP + NO → 0.720*VROCP1ALKP2 + 0.280*VROCN1OXY1 + 0.720*NO2	2.70×10^{-12}exp(360.00/T)	9.03×10^{-12}
432	HC1002	HC10P + NO → 0.740*HC10P2 + 0.260*ONIT + 0.740*NO2	2.70×10^{-12}exp(360.00/T)	9.03×10^{-12}
433	ROCALK13c	VROCP6ALKP + NO3 → VROCP6ALKP2 + NO2	2.30×10^{-12}	2.30×10^{-12}
434	ROCALK14c	VROCP5ALKP + NO3 → VROCP5ALKP2 + NO2	2.30×10^{-12}	2.30×10^{-12}
435	ROCALK15c	VROCP4ALKP + NO3 → VROCP4ALKP2 + NO2	2.30×10^{-12}	2.30×10^{-12}
436	ROCALK16c	VROCP3ALKP + NO3 → VROCP3ALKP2 + NO2	2.30×10^{-12}	2.30×10^{-12}
437	ROCALK17c	VROCP2ALKP + NO3 → VROCP2ALKP2 + NO2	2.30×10^{-12}	2.30×10^{-12}
438	ROCALK18c	VROCP1ALKP + NO3 → VROCP1ALKP2 + NO2	2.30×10^{-12}	2.30×10^{-12}
439	HC1003	HC10P + NO3 → HC10P2 + NO2	2.30×10^{-12}	2.30×10^{-12}

N	CMAQ Label	Reaction	Rate Constant Formula[a,b,c]	k (molec cm^{-3} sec^{-1} or s^{-1})
440	ROCALK19c	VROCP6ALKP + HO2 → VROCP3OXY2	2.17×10^{-11}	2.17×10^{-11}
441	ROCALK20c	VROCP5ALKP + HO2 → VROCP2OXY2	2.20×10^{-11}	2.20×10^{-11}
442	ROCALK21c	VROCP4ALKP + HO2 → VROCP1OXY1	2.25×10^{-11}	2.25×10^{-11}
443	ROCALK22c	VROCP3ALKP + HO2 → VROCP0OXY2	2.26×10^{-11}	2.26×10^{-11}
444	ROCALK23c	VROCP2ALKP + HO2 → VROCN1OXY1	2.27×10^{-11}	2.27×10^{-11}
445	ROCALK24c	VROCP1ALKP + HO2 → VROCN2OXY2	2.27×10^{-11}	2.27×10^{-11}
446	HC1004	HC10P + HO2 → OP2	$2.66\times10^{-13}\exp(1300.00/T)$	2.08×10^{-11}
447	ROCALK25c	VROCP6ALKP2 → HO2 + VROCP3OXY2	1.88×10^{-1}	1.88E-01
448	ROCALK26c	VROCP5ALKP2 → HO2 + VROCP2OXY2	1.88×10^{-1}	1.88E-01
449	ROCALK27c	VROCP4ALKP2 → HO2 + VROCP1OXY1	1.88×10^{-1}	1.88E-01
450	ROCALK28c	VROCP3ALKP2 → HO2 + VROCP0OXY2	1.88×10^{-1}	1.88E-01
451	ROCALK29c	VROCP2ALKP2 → HO2 + VROCN1OXY1	1.88×10^{-1}	1.88E-01
452	ROCALK30c	VROCP1ALKP2 → HO2 + VROCN2OXY2	1.88×10^{-1}	1.88E-01
453	HC1005	HC10P2 → HO2 + VROCP4OXY2	1.88×10^{-1}	1.88E-01
454	ROCALK31c	VROCP6ALKP2 + NO → 0.140*VROCP2OXY2 + 0.860*NO2 + 0.860*VROCP3OXY2 + 0.860*HO2	$2.70\times10^{-12}\exp(360.00/T)$	9.03×10^{-12}
455	ROCALK32c	VROCP5ALKP2 + NO → 0.140*VROCP1OXY3 + 0.860*NO2 + 0.860*VROCP2OXY2 + 0.860*HO2	$2.70\times10^{-12}\exp(360.00/T)$	9.03×10^{-12}
456	ROCALK33c	VROCP4ALKP2 + NO → 0.140*VROCP0OXY2 + 0.860*NO2 + 0.860*VROCP1OXY1 + 0.860*HO2	$2.70\times10^{-12}\exp(360.00/T)$	9.03×10^{-12}
457	ROCALK34c	VROCP3ALKP2 + NO → 0.140*VROCN1OXY1 + 0.860*NO2 + 0.860*VROCP0OXY2 + 0.860*HO2	$2.70\times10^{-12}\exp(360.00/T)$	9.03×10^{-12}
458	ROCALK35c	VROCP2ALKP2 + NO → 0.140*VROCN2OXY2 + 0.860*NO2 + 0.860*VROCN1OXY1 + 0.860*HO2	$2.70\times10^{-12}\exp(360.00/T)$	9.03×10^{-12}
459	ROCALK36c	VROCP1ALKP2 + NO → VROCN2OXY2 + 0.860*NO2 + 0.860*HO2	$2.70\times10^{-12}\exp(360.00/T)$	9.03×10^{-12}
460	HC1006	HC10P2 + NO → 0.120*ONIT + 0.880*NO2 + 0.880*KET + 0.880*HO2	$2.70\times10^{-12}\exp(360.00/T)$	9.03×10^{-12}
461	ROCALK37c	VROCP6ALKP2 + NO3 → NO2 + VROCP3OXY2 + HO2	2.30×10^{-12}	2.30×10^{-12}
462	ROCALK38c	VROCP5ALKP2 + NO3 → NO2 + VROCP2OXY2 + HO2	2.30×10^{-12}	2.30×10^{-12}
463	ROCALK39c	VROCP4ALKP2 + NO3 → NO2 + VROCP1OXY1 + HO2	2.30×10^{-12}	2.30×10^{-12}
464	ROCALK40c	VROCP3ALKP2 + NO3 → NO2 + VROCP0OXY2 + HO2	2.30×10^{-12}	2.30×10^{-12}
465	ROCALK41c	VROCP2ALKP2 + NO3 → NO2 + VROCN1OXY1 + HO2	2.30×10^{-12}	2.30×10^{-12}
466	ROCALK42c	VROCP1ALKP2 + NO3 → NO2 + VROCN2OXY2 + HO2	2.30×10^{-12}	2.30×10^{-12}
467	HC1007	HC10P2 + NO3 → NO2 + KET + HO2	2.30×10^{-12}	2.30×10^{-12}
468	ROCALK43c	VROCP6ALKP2 + HO2 → VROCP1OXY3	2.17×10^{-11}	2.17×10^{-11}
469	ROCALK44c	VROCP5ALKP2 + HO2 → VROCP0OXY2	2.20×10^{-11}	2.20×10^{-11}
470	ROCALK45c	VROCP4ALKP2 + HO2 → VROCN1OXY1	2.25×10^{-11}	2.25×10^{-11}
471	ROCALK46c	VROCP3ALKP2 + HO2 → VROCN2OXY2	2.26×10^{-11}	2.26×10^{-11}
472	ROCALK47c	VROCP2ALKP2 + HO2 → VROCN2OXY2	2.27×10^{-11}	2.27×10^{-11}
473	ROCALK48c	VROCP1ALKP2 + HO2 → VROCN2OXY2	2.27×10^{-11}	2.27×10^{-11}
474	HC1008	HC10P2 + HO2 → VROCP2OXY2	$2.66\times10^{-13}\exp(1300.00/T)$	2.08×10^{-11}
475	ROCARO01	VROCP6ARO + HO → 0.840*VROCP6AROP + 0.160*HO2 + 0.160*VROCP4OXY2	1.81×10^{-11}	1.81×10^{-11}
476	ROCARO02	VROCP6AROP + HO2 → 0.059*VROCP4OXY2 + 0.905*VROCP1OXY3 + 0.036*VROCN2OXY4	$2.91\times10^{-13}\exp(1300.00/T)$	2.28×10^{-11}
477	ROCARO03	VROCP6AROP + NO → 0.000*VROCP4OXY2 + 0.002*VROCP2OXY2 + 0.000*VROCN1OXY3 + 0.998*NO2 + 0.998*HO2 + 0.059*BALD + 0.469*GLY + 0.469*MGLY + 0.469*FURANONE + 0.469*DCB2	$2.70\times10^{-12}\exp(360.00/T)$	9.03×10^{-12}
478	ROCARO04	VROCP6AROP + NO3 → NO2 + 0.941*HO2 + 0.059*BALD + 0.470*GLY + 0.470*MGLY + 0.470*FURANONE + 0.470*DCB2	2.30×10^{-12}	2.30×10^{-12}

N	CMAQ Label	Reaction	Rate Constant Formula[a,b,c]	k (molec cm^{-3} sec^{-1} or s^{-1})
479	ROCARO05	VROCP6AROP + MO2 → 0.680*HCHO + 1.310*HO2 + 0.320*MOH + 0.059*BALD + 0.470*GLY + 0.470*MGLY + 0.470*FURANONE + 0.470*DCB2	$3.56\times10^{-14}\exp(708.00/T)$	3.83×10^{-13}
480	ROCARO06	VROCP6AROP + ACO3 → 0.700*MO2 + 0.941*HO2 + 0.300*ORA2 + 0.059*BALD + 0.470*GLY + 0.470*MGLY + 0.470*FURANONE + 0.470*DCB2	$7.40\times10^{-13}\exp(765.00/T)$	9.63×10^{-12}
481	ROCARO11	VROCP5ARO + HO → 0.840*VROCP5AROP + 0.160*HO2 + 0.160*VROCP3OXY2	1.81×10^{-11}	1.81×10^{-11}
482	ROCARO12	VROCP5AROP + HO2 → 0.059*VROCP3OXY2 + 0.905*VROCP0OXY2 + 0.036*VROCN2OXY4	$2.91\times10^{-13}\exp(1300.00/T)$	2.28×10^{-11}
483	ROCARO13	VROCP5AROP + NO → 0.000*VROCP3OXY2 + 0.002*VROCP1OXY3 + 0.000*VROCN2OXY4 + 0.998*NO2 + 0.998*HO2 + 0.059*VROCP4OXY2 + 0.469*GLY + 0.469*MGLY + 0.469*FURANONE + 0.469*DCB2	$2.70\times10^{-12}\exp(360.00/T)$	9.03×10^{-12}
484	ROCARO14	VROCP5AROP + NO3 → NO2 + 0.941*HO2 + 0.059*VROCP4OXY2 + 0.470*GLY + 0.470*MGLY + 0.470*FURANONE + 0.470*DCB2	2.30×10^{-12}	2.30×10^{-12}
485	ROCARO15	VROCP5AROP + MO2 → 0.680*HCHO + 1.310*HO2 + 0.320*MOH + 0.059*VROCP4OXY2 + 0.470*GLY + 0.470*MGLY + 0.470*FURANONE + 0.470*DCB2	$3.56\times10^{-14}\exp(708.00/T)$	3.83×10^{-13}
486	ROCARO16	VROCP5AROP + ACO3 → 0.700*MO2 + 0.941*HO2 + 0.300*ORA2 + 0.059*VROCP4OXY2 + 0.470*GLY + 0.470*MGLY + 0.470*FURANONE + 0.470*DCB2	$7.40\times10^{-13}\exp(765.00/T)$	9.63×10^{-12}
487	ROCARO21	NAPH + HO → 0.840*NAPHP + 0.160*HO2 + 0.160*VROCP3OXY2	2.31×10^{-11}	2.31×10^{-11}
488	ROCARO22	NAPHP + HO2 → 0.059*VROCP3OXY2 + 0.905*VROCP1OXY3 + 0.036*VROCN2OXY8	$2.91\times10^{-13}\exp(1300.00/T)$	2.28×10^{-11}
489	ROCARO23	NAPHP + NO → 0.060*VROCP4OXY2 + 0.002*VROCP2OXY2 + 0.000*VROCN2OXY8 + 0.998*NO2 + 0.998*HO2 + 0.469*GLY + 0.469*MGLY + 0.469*FURANONE + 0.469*DCB2	$2.70\times10^{-12}\exp(360.00/T)$	9.03×10^{-12}
490	ROCARO24	NAPHP + NO3 → NO2 + 0.941*HO2 + 0.059*VROCP4OXY2 + 0.470*GLY + 0.470*MGLY + 0.470*FURANONE + 0.470*DCB2	2.30×10^{-12}	2.30×10^{-12}
491	ROCARO25	NAPHP + MO2 → 0.680*HCHO + 1.310*HO2 + 0.320*MOH + 0.059*VROCP4OXY2 + 0.470*GLY + 0.470*MGLY + 0.470*FURANONE + 0.470*DCB2	$3.56\times10^{-14}\exp(708.00/T)$	3.83×10^{-13}
492	ROCARO26	NAPHP + ACO3 → 0.700*MO2 + 0.941*HO2 + 0.300*ORA2 + 0.059*VROCP4OXY2 + 0.470*GLY + 0.470*MGLY + 0.470*FURANONE + 0.470*DCB2	$7.40\times10^{-13}\exp(765.00/T)$	9.63×10^{-12}
493	ROCOXY1c	VROCN2OXY8 + HO → HO + 0.085*VROCN2OXY8 + 0.258*DCB1 + 0.258*MEK + 0.258*ACD + 0.258*ALD + 0.258*MO2 + 0.258*ETHP + 0.258*HC3P + 0.258*MEKP	5.90×10^{-11}	5.90×10^{-11}
494	ROCOXY2c	VROCN2OXY4 + HO → HO + 0.464*VROCN2OXY8 + 0.198*VROCN2OXY4 + 0.012*VROCN1OXY6 + 0.015*VROCN1OXY3 + 0.062*VROCP0OXY4 + 0.039*VROCP1OXY3 + 0.049*VROCP2OXY2 + 0.040*VROCP3OXY2 + 0.018*VROCP4OXY2 + 0.031*OP3 + 0.004*OP2 + 0.079*DCB1 + 0.079*MEK + 0.079*KET + 0.079*ACD + 0.079*ALD + 0.079*MO2 + 0.079*ETHP + 0.079*HC3P + 0.079*MEKP + 0.079*HC5P + 0.079*KETP	6.07×10^{-11}	6.07×10^{-11}
495	ROCOXY3c	VROCN2OXY2 + HO → HO + 0.104*VROCN2OXY8 + 0.564*VROCN2OXY4 + 0.214*VROCN2OXY2 + 0.015*VROCN1OXY6 + 0.030*VROCN1OXY3 + 0.010*VROCN1OXY1 + 0.019*VROCP0OXY4 +	5.54×10^{-11}	5.54×10^{-11}

N	CMAQ Label	Reaction	Rate Constant Formula[a,b,c]	k (molec cm^{-3} sec^{-1} or s^{-1})
		0.046*VROCP0OXY2 + 0.031*VROCP1OXY3 + 0.020*VROCP1OXY1 + 0.046*VROCP2OXY2 + 0.045*VROCP3OXY2 + 0.045*VROCP4OXY2 + 0.033*VROCP5OXY1 + 0.037*VROCP6OXY1 + 0.003*OP3 + 0.039*DCB1 + 0.039*HKET + 0.039*MEK + 0.039*ACD + 0.039*ALD + 0.039*MO2 + 0.039*ETHP + 0.039*HC3P + 0.039*MEKP + 0.092*HC5P		
496	ROCOXY4c	VROCN1OXY6 + HO → HO + 0.204*VROCN2OXY8 + 0.007*VROCN2OXY4 + 0.184*DCB1 + 0.184*MEK + 0.184*KET + 0.184*ACD + 0.184*ALD + 0.184*MO2 + 0.184*ETHP + 0.184*HC3P + 0.184*MEKP + 0.184*HC5P	5.63×10^{-11}	5.63×10^{-11}
497	ROCOXY5c	VROCN1OXY3 + HO → HO + 0.279*VROCN2OXY8 + 0.403*VROCN2OXY4 + 0.009*VROCN2OXY2 + 0.032*VROCN1OXY6 + 0.008*VROCN1OXY3 + 0.019*VROCP0OXY4 + 0.010*VROCP0OXY2 + 0.051*VROCP1OXY3 + 0.007*VROCP1OXY1 + 0.051*VROCP2OXY2 + 0.046*VROCP3OXY2 + 0.051*VROCP4OXY2 + 0.014*VROCP5OXY1 + 0.013*OP2 + 0.065*DCB1 + 0.065*HKET + 0.065*MEK + 0.065*ACD + 0.065*ALD + 0.065*MO2 + 0.065*ETHP + 0.065*HC3P + 0.065*MEKP + 0.175*HC5P	5.46×10^{-11}	5.46×10^{-11}
498	ROCOXY6c	VROCN1OXY1 + HO → HO + 0.007*VROCN2OXY8 + 0.119*VROCN2OXY4 + 0.726*VROCN2OXY2 + 0.012*VROCN1OXY6 + 0.030*VROCN1OXY3 + 0.007*VROCN1OXY1 + 0.029*VROCP0OXY4 + 0.045*VROCP0OXY2 + 0.023*VROCP1OXY3 + 0.035*VROCP1OXY1 + 0.062*VROCP2OXY2 + 0.052*VROCP3OXY2 + 0.051*VROCP4OXY2 + 0.035*VROCP5OXY1 + 0.075*VROCP6OXY1 + 0.016*OP3 + 0.006*OP2 + 0.024*DCB1 + 0.024*HKET + 0.024*MEK + 0.024*ACD + 0.024*ALD + 0.024*MO2 + 0.024*ETHP + 0.024*HC3P + 0.024*MEKP + 0.054*HC5P	4.50×10^{-11}	4.50×10^{-11}
499	ROCOXY7c	VROCP0OXY4 + HO → HO + 0.282*VROCN2OXY8 + 0.117*VROCN2OXY4 + 0.032*VROCN1OXY6 + 0.018*VROCN1OXY3 + 0.001*VROCP0OXY4 + 0.066*VROCP2OXY2 + 0.053*VROCP3OXY2 + 0.025*VROCP4OXY2 + 0.005*OP2 + 0.107*DCB1 + 0.107*MEK + 0.107*KET + 0.107*ACD + 0.107*ALD + 0.107*MO2 + 0.107*ETHP + 0.107*HC3P + 0.107*MEKP + 0.107*HC5P + 0.107*KETP	5.17×10^{-11}	5.17×10^{-11}
500	ROCOXY8c	VROCP0OXY2 + HO → HO + 0.066*VROCN2OXY8 + 0.458*VROCN2OXY4 + 0.116*VROCN2OXY2 + 0.033*VROCN1OXY6 + 0.066*VROCN1OXY3 + 0.005*VROCN1OXY1 + 0.031*VROCP0OXY4 + 0.002*VROCP0OXY2 + 0.040*VROCP1OXY3 + 0.021*VROCP1OXY1 + 0.054*VROCP2OXY2 + 0.052*VROCP3OXY2 + 0.052*VROCP4OXY2 + 0.037*VROCP5OXY1 + 0.042*VROCP6OXY1 + 0.011*OP3 + 0.044*DCB1 + 0.044*HKET + 0.044*MEK + 0.044*ACD + 0.044*ALD + 0.044*MO2 + 0.044*ETHP + 0.044*HC3P + 0.044*MEKP + 0.105*HC5P	4.73×10^{-11}	4.73×10^{-11}
501	ROCOXY9c	VROCP1OXY3 + HO → HO + 0.178*VROCN2OXY8 + 0.192*VROCN2OXY4 + 0.000*VROCN2OXY2 + 0.074*VROCN1OXY6 + 0.045*VROCN1OXY3 +	4.60×10^{-11}	4.60×10^{-11}

N	CMAQ Label	Reaction	Rate Constant Formula[a,b,c]	k (molec cm^{-3} sec^{-1} or s^{-1})
		0.063*VROCP0OXY4 + 0.001*VROCP0OXY2 + 0.001*VROCP1OXY3 + 0.023*VROCP2OXY2 + 0.059*VROCP3OXY2 + 0.065*VROCP4OXY2 + 0.017*VROCP5OXY1 + 0.015*OP3 + 0.017*OP2 + 0.082*DCB1 + 0.082*HKET + 0.082*MEK + 0.082*ACD + 0.082*ALD + 0.082*MO2 + 0.082*ETHP + 0.082*HC3P + 0.082*MEKP + 0.222*HC5P		
502	ROCOXY10c	VROCP1OXY1 + HO → HO + 0.002*VROCN2OXY8 + 0.134*VROCN2OXY4 + 0.335*VROCN2OXY2 + 0.008*VROCN1OXY6 + 0.119*VROCN1OXY3 + 0.076*VROCN1OXY1 + 0.029*VROCP0OXY4 + 0.077*VROCP0OXY2 + 0.028*VROCP1OXY3 + 0.012*VROCP1OXY1 + 0.065*VROCP2OXY2 + 0.071*VROCP3OXY2 + 0.067*VROCP4OXY2 + 0.042*VROCP5OXY1 + 0.091*VROCP6OXY1 + 0.007*OP3 + 0.003*OP2 + 0.030*DCB1 + 0.030*HKET + 0.030*MEK + 0.030*ACD + 0.030*ALD + 0.030*MO2 + 0.030*ETHP + 0.030*HC3P + 0.030*MEKP + 0.065*HC5P	3.80×10^{-11}	3.80×10^{-11}
503	ROCOXY11c	VROCP2OXY2 + HO → HO + 0.044*VROCN2OXY8 + 0.173*VROCN2OXY4 + 0.010*VROCN2OXY2 + 0.051*VROCN1OXY6 + 0.112*VROCN1OXY3 + 0.001*VROCN1OXY1 + 0.134*VROCP0OXY4 + 0.040*VROCP0OXY2 + 0.051*VROCP1OXY3 + 0.007*VROCP1OXY1 + 0.024*VROCP2OXY2 + 0.029*VROCP3OXY2 + 0.073*VROCP4OXY2 + 0.052*VROCP5OXY1 + 0.059*VROCP6OXY1 + 0.004*OP3 + 0.002*OP2 + 0.063*DCB1 + 0.063*HKET + 0.063*MEK + 0.063*ACD + 0.063*ALD + 0.063*MO2 + 0.063*ETHP + 0.063*HC3P + 0.063*MEKP + 0.149*HC5P	3.93×10^{-11}	3.93×10^{-11}
504	ROCOXY12c	VROCP3OXY2 + HO → HO + 0.032*VROCN2OXY8 + 0.076*VROCN2OXY4 + 0.001*VROCN2OXY2 + 0.053*VROCN1OXY6 + 0.049*VROCN1OXY3 + 0.155*VROCP0OXY4 + 0.015*VROCP0OXY2 + 0.105*VROCP1OXY3 + 0.001*VROCP1OXY1 + 0.053*VROCP2OXY2 + 0.009*VROCP3OXY2 + 0.043*VROCP4OXY2 + 0.058*VROCP5OXY1 + 0.066*VROCP6OXY1 + 0.051*OP3 + 0.011*OP2 + 0.070*DCB1 + 0.070*HKET + 0.070*MEK + 0.070*ACD + 0.070*ALD + 0.070*MO2 + 0.070*ETHP + 0.070*HC3P + 0.070*MEKP + 0.166*HC5P	3.52×10^{-11}	3.52×10^{-11}
505	ROCOXY13c	VROCP4OXY2 + HO → HO + 0.012*VROCN2OXY8 + 0.017*VROCN2OXY4 + 0.048*VROCN1OXY6 + 0.025*VROCN1OXY3 + 0.088*VROCP0OXY4 + 0.092*VROCP1OXY3 + 0.007*VROCP1OXY1 + 0.097*VROCP2OXY2 + 0.046*VROCP3OXY2 + 0.002*VROCP4OXY2 + 0.048*VROCP5OXY1 + 0.074*VROCP6OXY1 + 0.061*OP3 + 0.015*OP2 + 0.079*DCB1 + 0.079*HKET + 0.079*MEK + 0.079*ACD + 0.079*ALD + 0.079*MO2 + 0.079*ETHP + 0.079*HC3P + 0.079*MEKP + 0.173*HC5P	3.12×10^{-11}	3.12×10^{-11}
506	ROCOXY14c	VROCP5OXY1 + HO → HO + 0.010*VROCN2OXY4 + 0.001*VROCN2OXY2 + 0.009*VROCN1OXY6 + 0.015*VROCN1OXY3 + 0.070*VROCP0OXY4 + 0.015*VROCP0OXY2 + 0.104*VROCP1OXY3 +	2.40×10^{-11}	2.40×10^{-11}

N	CMAQ Label	Reaction	Rate Constant Formula[a,b,c]	k (molec cm^{-3} sec^{-1} or s^{-1})
		0.003*VROCP1OXY1 + 0.165*VROCP2OXY2 + 0.157*VROCP3OXY2 + 0.072*VROCP4OXY2 + 0.006*VROCP5OXY1 + 0.140*VROCP6OXY1 + 0.022*OP3 + 0.038*OP2 + 0.053*DCB1 + 0.053*HKET + 0.053*MEK + 0.053*ACD + 0.053*ALD + 0.053*MO2 + 0.053*ETHP + 0.053*HC3P + 0.053*MEKP + 0.128*HC5P		
507	ROCOXY15c	VROCP6OXY1 + HO → HO + 0.006*VROCN1OXY6 + 0.005*VROCN1OXY3 + 0.022*VROCP0OXY4 + 0.050*VROCP1OXY3 + 0.002*VROCP1OXY1 + 0.088*VROCP2OXY2 + 0.138*VROCP3OXY2 + 0.146*VROCP4OXY2 + 0.043*VROCP5OXY1 + 0.096*VROCP6OXY1 + 0.032*OP3 + 0.059*OP2 + 0.057*DCB1 + 0.057*HKET + 0.057*MEK + 0.057*ACD + 0.057*ALD + 0.057*MO2 + 0.057*ETHP + 0.057*HC3P + 0.057*MEKP + 0.154*HC5P	2.05×10^{-11}	2.05×10^{-11}
508	ROCOXY16c	OP3 + HO → HO + 0.119*VROCN2OXY8 + 0.001*VROCN2OXY4 + 0.039*VROCN1OXY6 + 0.011*VROCP0OXY4 + 0.227*DCB1 + 0.227*MEK + 0.227*ACD + 0.227*ALD + 0.227*MO2 + 0.227*ETHP + 0.227*HC3P + 0.227*MEKP	4.69×10^{-11}	4.69×10^{-11}

[a]Reaction rate constants following Arrhenius behavior are specified as $k = Ae^{-Ea/RT}$. Fall-off or pressure dependent reaction rate constants are specified as follows (M equals air number density):

for rate constants with k_o, k_i, n, F values: $k = [\, k_oM/(1+k_oM/k_i)]F^G$, where $G=(1+(\log_{10}(k_oM/k_i)/n)^2))^{-1}$;

for rate constants with k_1, k_2: $k = k_1 + k_2M$;

for rate constants with k_0, k_2, k_3: $k = k_0 + k_3M/(1+k_3M/k_2)$;

for rate constants with k_1, k_2, k_3: $k = k_1 + k_2M + k_3$.

[b]Heterogeneous rates are specified as, $k_{HET} = \frac{S_A}{r_{p/D_g}+4/v\gamma}$, where S_A is the fine aerosol surface area, r_p is the effective particle radius, D_g is the gas-phase diffusivity, v is the mean molecular speed, and γ is the uptake coefficient. In the case of heterogeneous NO_2 reaction, the gas-phase diffusivity term in the denominator is neglected.

[c]CMAQ calculates photolysis rate coefficients (J-values) as follows:

$$J_i = \int_{\lambda 1}^{\lambda 2} F(\lambda)\sigma_i(\lambda)\phi_i(\lambda)d\lambda$$

where $F(\lambda)$ is the actinic flux (photons cm^{-2} min^{-1} nm^{-1}), $\sigma_i(\lambda)$ is the absorption cross section for the molecule undergoing photolytic reaction (cm^2 molecule^{-1}), $\varphi_i(\lambda)$ is the quantum yield of the photolysis reaction (molecules photon^{-1}), and λ is the wavelength (nm). CMAQ uses 7-binned absorption cross-section and quantum yield data for calculating J-values. Sources of absorption cross-section and quantum yield data are provided in the table.

[d]The rate constant for R067 is scaled to the reverse equilibrium of R066.

[e]The HAL_Ozone reaction represents loss of ozone over ocean surfaces due to halogen chemistry. The rate is set to zero if the sun is below the horizon and if the surface does not include sea or surf zones (P = air pressure in atmospheres) (Sarwar et al., 2015).

1255

References

Achten, C., and Andersson, J. T.: Overview of polycyclic aromatic compounds (PAC), Polycyclic Aromat. Compd., 35, 177-186, https://doi.org/10.1080/10406638.2014.994071, 2015.

Agency for Toxic Substances and Disease Registry: Toxicological profile for 1,3-butadiene: https://www.atsdr.cdc.gov/ToxProfiles/tp28.pdf, access: 17 May 2022, 2012.

Ahmadov, R., McKeen, S. A., Robinson, A. L., Bahreini, R., Middlebrook, A. M., de Gouw, J. A., Meagher, J., Hsie, E.-Y., Edgerton, E., Shaw, S., and Trainer, M.: A volatility basis set model for summertime secondary organic aerosols over the eastern United States in 2006, J. Geophys. Res.-Atmos., 117, https://doi.org/10.1029/2011JD016831, 2012.

Appel, K. W., Chemel, C., Roselle, S. J., Francis, X. V., Hu, R.-M., Sokhi, R. S., Rao, S. T., and Galmarini, S.: Examination of the Community Multiscale Air Quality (CMAQ) model performance over the North American and European domains, Atmos. Environ., 53, 142-155, https://doi.org/10.1016/j.atmosenv.2011.11.016, 2012.

Appel, K. W., Bash, J. O., Fahey, K. M., Foley, K. M., Gilliam, R. C., Hogrefe, C., Hutzell, W. T., Kang, D., Mathur, R., Murphy, B. N., Napelenok, S. L., Nolte, C. G., Pleim, J. E., Pouliot, G. A., Pye, H. O. T., Ran, L., Roselle, S. J., Sarwar, G., Schwede, D. B., Sidi, F. I., Spero, T. L., and Wong, D. C.: The Community Multiscale Air Quality (CMAQ) model versions 5.3 and 5.3.1: system updates and evaluation, Geosci. Model Dev., 14, 2867-2897, https://doi.org/10.5194/gmd-14-2867-2021, 2021.

Atkinson, R., Baulch, D. L., Cox, R. A., Crowley, J. N., Hampson, R. F., Hynes, R. G., Jenkin, M. E., Rossi, M. J., and Troe, J.: Evaluated kinetic and photochemical data for atmospheric chemistry: Volume I - gas phase reactions of O_X, HO_X, NO_X and SO_X species, Atmos. Chem. Phys., 4, 1461-1738, https://doi.org/10.5194/acp-4-1461-2004, 2004.

Atkinson, R., Baulch, D. L., Cox, R. A., Crowley, J. N., Hampson, R. F., Hynes, R. G., Jenkin, M. E., Rossi, M. J., Troe, J., and Subcommittee, I.: Evaluated kinetic and photochemical data for atmospheric chemistry: Volume II - gas phase reactions of organic species, Atmos. Chem. Phys., 6, 3625-4055, https:/doi.org/10.5194/acp-6-3625-2006, 2006.

Aumont, B., Szopa, S., and Madronich, S.: Modelling the evolution of organic carbon during its gas-phase tropospheric oxidation: development of an explicit model based on a self generating approach, Atmos. Chem. Phys., 5, 2497-2517, https://doi.org/10.5194/acp-5-2497-2005, 2005.

Baboomian, V. J., Gu, Y., and Nizkorodov, S. A.: Photodegradation of Secondary Organic Aerosols by Long-Term Exposure to Solar Actinic Radiation, ACS Earth Space Chem., 4, 1078-1089, https://doi.org/10.1021/acsearthspacechem.0c00088, 2020.

Bates, K. H., Jacob, D. J., Li, K., Ivatt, P. D., Evans, M. J., Yan, Y., and Lin, J.: Development and evaluation of a new compact mechanism for aromatic oxidation in atmospheric models, Atmos. Chem. Phys., 21, 18351-18374, https://doi.org/10.5194/acp-21-18351-2021, 2021.

Berndt, T., Richters, S., Jokinen, T., Hyttinen, N., Kurtén, T., Otkjær, R. V., Kjaergaard, H. G., Stratmann, F., Herrmann, H., Sipilä, M., Kulmala, M., and Ehn, M.: Hydroxyl radical-induced formation of highly oxidized organic compounds, Nat. Commun., 7, 13677, https://doi.org/10.1038/ncomms13677, 2016.

Berndt, T., Chen, J., Kjærgaard, E. R., Møller, K. H., Tilgner, A., Hoffmann, E. H., Herrmann, H., Crounse, J. D., Wennberg, P. O., and Kjaergaard, H. G.: Hydrotrioxide (ROOOH) formation in the atmosphere, Science, 376, 979-982, https://doi.org/10.1126/science.abn6012, 2022.

Bianchi, F., Kurtén, T., Riva, M., Mohr, C., Rissanen, M. P., Roldin, P., Berndt, T., Crounse, J. D., Wennberg, P. O., Mentel, T. F., Wildt, J., Junninen, H., Jokinen, T., Kulmala, M., Worsnop, D. R., Thornton, J. A., Donahue, N., Kjaergaard, H. G., and Ehn, M.: Highly Oxygenated Organic Molecules (HOM) from gas-phase autoxidation involving peroxy radicals: A key contributor to atmospheric aerosol, Chem. Rev., 119, 3472-3509, https://doi.org/10.1021/acs.chemrev.8b00395, 2019.

Birdsall, A. W., and Elrod, M. J.: Comprehensive NO-dependent study of the products of the oxidation of atmospherically relevant aromatic compounds, J. Phys. Chem. A, 115, 5397-5407, https://doi.org/10.1021/jp2010327, 2011.

Blitz, M. A., Heard, D. E., Pilling, M. J., Arnold, S. R., and Chipperfield, M. P.: Pressure and temperature-dependent quantum yields for the photodissociation of acetone between 279 and 327.5 nm, Geophys. Res. Lett., 31, https://doi.org/10.1029/2003GL018793, 2004.

Bloss, C., Wagner, V., Jenkin, M. E., Volkamer, R., Bloss, W. J., Lee, J. D., Heard, D. E., Wirtz, K., Martin-Reviejo, M., Rea, G., Wenger, J. C., and Pilling, M. J.: Development of a detailed chemical mechanism (MCMv3.1) for the atmospheric oxidation of aromatic hydrocarbons, Atmos. Chem. Phys., 5, 641-664, https://doi.org/10.5194/acp-5-641-2005, 2005.

Brewer, J. F., Papanastasiou, D. K., Burkholder, J. B., Fischer, E. V., Ren, Y., Mellouki, A., and Ravishankara, A. R.: Atmospheric photolysis of methyl ethyl, diethyl, and propyl ethyl ketones: Temperature-dependent UV absorption cross sections, J. Geophys. Res.-Atmos., 124, 5906-5918, https://doi.org/10.1029/2019JD030391, 2019.

Browne, E. C., Wooldridge, P. J., Min, K. E., and Cohen, R. C.: On the role of monoterpene chemistry in the remote continental boundary layer, Atmos. Chem. Phys., 14, 1225-1238, https://doi.org/10.5194/acp-14-1225-2014, 2014.

Bruns, E. A., El Haddad, I., Slowik, J. G., Kilic, D., Klein, F., Baltensperger, U., and Prévôt, A. S. H.: Identification of significant precursor gases of secondary organic aerosols from residential wood combustion, Sci. Rep., 6, 27881, https://doi.org/10.1038/srep27881, 2016.

Burkholder, J. B., Sander, S. P., Abbatt, J., Barker, J. R., Cappa, C., Crounse, J. D., Dibble, T. S., Huie, R. E., Kolb, C. E., Kurylo, M. J., Orkin, V. L., Percival, C. J., Wilmouth, D. M., and Wine, P. H.: Chemical Kinetics and Photochemical Data for Use in Atmospheric Studies, Evaluation No. 19 JPL Publication 19-5: https://jpldataeval.jpl.nasa.gov/pdf/NASA-JPL%20Evaluation%2019-5.pdf, access: 16 May 2022, 2019.

Canagaratna, M. R., Jimenez, J. L., Kroll, J. H., Chen, Q., Kessler, S. H., Massoli, P., Hildebrandt Ruiz, L., Fortner, E., Williams, L. R., Wilson, K. R., Surratt, J. D., Donahue, N. M., Jayne, J. T., and Worsnop, D. R.: Elemental ratio measurements of organic compounds using aerosol mass spectrometry: characterization, improved calibration, and implications, Atmos. Chem. Phys., 15, 253-272, https://doi.org/10.5194/acp-15-253-2015, 2015.

Carlton, A. G., Turpin, B. J., Altieri, K. E., Seitzinger, S. P., Mathur, R., Roselle, S. J., and Weber, R. J.: CMAQ Model Performance Enhanced When In-Cloud Secondary Organic Aerosol is Included: Comparisons of Organic Carbon Predictions with Measurements, Environ. Sci. Technol., 42, 8798-8802, https://doi.org/10.1021/es801192n, 2008.

Carlton, A. G., Bhave, P. V., Napelenok, S. L., Edney, E. O., Sarwar, G., Pinder, R. W., Pouliot, G. A., and Houyoux, M.: Model representation of secondary organic aerosol in CMAQv4.7, Environ. Sci. Technol., 44, 8553-8560, https://doi.org/10.1021/es100636q, 2010.

Carter, W. P. L.: Development of the SAPRC-07 chemical mechanism, Atmos. Environ., 44, 5324-5335, https://doi.org/10.1016/j.atmosenv.2010.01.026, 2010.

Carter, W. P. L.: Updated maximum incremental reactivity scale and hydrocarbon bin reactivities for regulatory applications and Reactivity values in an Excel File: https://intra.engr.ucr.edu/~carter/SAPRC/, access: 10 May 2022, 2019.

Carter, W. P. L.: Development of an Improved Chemical Speciation Database for Processing Emissions of Volatile Organic Compounds for Air Quality Models: https://intra.engr.ucr.edu/~carter/emitdb/, access: 11 March 2021, 2020a.

Carter, W. P. L.: Documentation of the SAPRC-18 mechanism: https://intra.engr.ucr.edu/~carter/SAPRC/18/S18doc.pdf, access: 13 June 2022, 2020b.

Chan, E. A. W., Gantt, B., and McDow, S.: The reduction of summer sulfate and switch from summertime to wintertime $PM_{2.5}$ concentration maxima in the United States, Atmos. Environ., 175, 25-32, https://doi.org/10.1016/j.atmosenv.2017.11.055, 2018.

Chen, J., Møller, K. H., Wennberg, P. O., and Kjaergaard, H. G.: Unimolecular reactions following indoor and outdoor limonene ozonolysis, J. Phys. Chem. A, 125, 669-680, https://doi.org/10.1021/acs.jpca.0c09882, 2021a.

Chen, Q., Heald, C. L., Jimenez, J. L., Canagaratna, M. R., Zhang, Q., He, L.-Y., Huang, X.-F., Campuzano-Jost, P., Palm, B. B., Poulain, L., Kuwata, M., Martin, S. T., Abbatt, J. P. D., Lee, A. K. Y., and Liggio, J.: Elemental composition of organic aerosol: The gap between ambient and laboratory measurements, Geophys. Res. Lett., 42, 4182-4189, https://doi.org/10.1002/2015GL063693, 2015.

Chen, Y., Guo, H., Nah, T., Tanner, D. J., Sullivan, A. P., Takeuchi, M., Gao, Z., Vasilakos, P., Russell, A. G., Baumann, K., Huey, L. G., Weber, R. J., and Ng, N. L.: Low-molecular-weight carboxylic acids in the Southeastern U.S.: Formation, partitioning, and implications for organic aerosol aging, Environ. Sci. Technol., 55, 6688-6699, https://doi.org/10.1021/acs.est.1c01413, 2021b.

Choi, H., Schmidbauer, N., Sundell, J., Hasselgren, M., Spengler, J., and Bornehag, C.-G.: Common household chemicals and the allergy risks in pre-school age children, PLoS One, 5, e13423, https://doi.org/10.1371/journal.pone.0013423, 2010.

Code of Federal Regulations: Volatile organic compounds (VOC): https://ecfr.federalregister.gov/current/title-40/chapter-I/subchapter-C/part-51, access: 17 June 2022, 1986.

Coggon, M. M., Lim, C. Y., Koss, A. R., Sekimoto, K., Yuan, B., Gilman, J. B., Hagan, D. H., Selimovic, V., Zarzana, K. J., Brown, S. S., Roberts, J. M., Müller, M., Yokelson, R., Wisthaler, A., Krechmer, J. E., Jimenez, J. L., Cappa, C., Kroll, J. H., de Gouw, J., and Warneke, C.: OH chemistry of non-methane organic gases (NMOGs) emitted from laboratory and ambient biomass burning smoke: evaluating the influence of furans and oxygenated aromatics on ozone and secondary NMOG formation, Atmos. Chem. Phys., 19, 14875-14899, https://doi.org/10.5194/acp-19-14875-2019, 2019.

Coggon, M. M., Gkatzelis, G. I., McDonald, B. C., Gilman, J. B., Schwantes, R. H., Abuhassan, N., Aikin, K. C., Arend, M. F., Berkoff, T. A., Brown, S. S., Campos, T. L., Dickerson, R. R., Gronoff, G., Hurley, J. F., Isaacman-VanWertz, G., Koss, A. R., Li, M., McKeen, S. A., Moshary, F., Peischl, J., Pospisilova, V., Ren, X., Wilson, A., Wu, Y., Trainer, M., and Warneke, C.: Volatile chemical product emissions enhance ozone and modulate urban chemistry, P. Natl. Acad. Sci. USA, 118, e2026653118, https://doi.org/10.1073/pnas.2026653118, 2021.

Crounse, J. D., Nielsen, L. B., Jørgensen, S., Kjaergaard, H. G., and Wennberg, P. O.: Autoxidation of Organic Compounds in the Atmosphere, J. Phys. Chem. Lett., 4, 3513-3520, https://doi.org/10.1021/jz4019207, 2013.

D'Ambro, E. L., Schobesberger, S., Gaston, C. J., Lopez-Hilfiker, F. D., Lee, B. H., Liu, J., Zelenyuk, A., Bell, D., Cappa, C. D., Helgestad, T., Li, Z., Guenther, A., Wang, J., Wise, M., Caylor, R., Surratt, J. D., Riedel, T., Hyttinen, N., Salo, V. T., Hasan, G., Kurtén, T., Shilling, J. E., and Thornton, J. A.: Chamber-based insights into the factors controlling epoxydiol (IEPOX) secondary organic aerosol (SOA) yield, composition, and volatility, Atmos. Chem. Phys., 19, 11253-11265, https://doi.org/10.5194/acp-19-11253-2019, 2019.

D'Ambro, E. L., Pye, H. O. T., Bash, J. O., Bowyer, J., Allen, C., Efstathiou, C., Gilliam, R. C., Reynolds, L., Talgo, K., and Murphy, B. N.: Characterizing the air emissions, fransport, and deposition of per- and polyfluoroalkyl substances from a fluoropolymer manufacturing facility, Environ. Sci. Technol., 55, 862-870, https://doi.org/10.1021/acs.est.0c06580, 2021.

Davis, J. M., Bhave, P. V., and Foley, K. M.: Parameterization of N_2O_5 reaction probabilities on the surface of particles containing ammonium, sulfate, and nitrate, Atmos. Chem. Phys., 8, 5295-5311, https://doi.org/10.5194/acp-8-5295-2008, 2008.

Dlugokencky, E.: Trends in Atmospheric Methane: https://gml.noaa.gov/ccgg/trends_ch4/, access: 29 June 2022, 2022.

Donahue, N. M., Robinson, A. L., Stanier, C. O., and Pandis, S. N.: Coupled partitioning, dilution, and chemical aging of semivolatile organics, Environ. Sci. Technol., 40, 2635-2643, https:/doi.org/10.1021/es052297c, 2006.

Donahue, N. M., Kroll, J. H., Pandis, S. N., and Robinson, A. L.: A two-dimensional volatility basis set – Part 2: Diagnostics of organic-aerosol evolution, Atmos. Chem. Phys., 12, 615-634, https://doi.org/10.5194/acp-12-615-2012, 2012.

Donahue, N. M., Chuang, W., Epstein, S. A., Kroll, J. H., Worsnop, D. R., Robinson, A. L., Adams, P. J., and Pandis, S. N.: Why do organic aerosols exist? Understanding aerosol lifetimes using the two-dimensional volatility basis set, Environ. Chem., 10, 151-157, https://doi.org/10.1071/EN13022, 2013.

Dunne, J. P., Horowitz, L. W., Adcroft, A. J., Ginoux, P., Held, I. M., John, J. G., Krasting, J. P., Malyshev, S., Naik, V., Paulot, F., Shevliakova, E., Stock, C. A., Zadeh, N., Balaji, V., Blanton, C., Dunne, K. A., Dupuis, C., Durachta, J., Dussin, R., Gauthier, P. P. G., Griffies, S. M., Guo, H., Hallberg, R. W., Harrison, M., He, J., Hurlin, W., McHugh, C., Menzel, R., Milly, P. C. D., Nikonov, S., Paynter, D. J., Ploshay, J., Radhakrishnan, A., Rand, K., Reichl, B. G., Robinson, T., Schwarzkopf, D. M., Sentman, L. T., Underwood, S., Vahlenkamp, H., Winton, M., Wittenberg, A. T., Wyman, B., Zeng, Y., and Zhao, M.: The GFDL Earth System Model Version 4.1 (GFDL-ESM 4.1): Overall coupled model description and simulation characteristics, J. Adv. Model. Earth Syst., 12, e2019MS002015, https://doi.org/10.1029/2019MS002015, 2020.

Edwards, P. M., Brown, S. S., Roberts, J. M., Ahmadov, R., Banta, R. M., deGouw, J. A., Dubé, W. P., Field, R. A., Flynn, J. H., Gilman, J. B., Graus, M., Helmig, D., Koss, A., Langford, A. O., Lefer, B. L., Lerner, B. M., Li, R., Li, S.-M., McKeen, S. A., Murphy, S. M., Parrish, D. D., Senff, C. J., Soltis, J., Stutz, J., Sweeney, C., Thompson, C. R., Trainer, M. K., Tsai, C., Veres, P. R., Washenfelder, R. A., Warneke, C., Wild, R. J., Young, C. J., Yuan, B., and Zamora, R.: High winter ozone pollution from carbonyl photolysis in an oil and gas basin, Nature, 514, 351-354, https://doi.org/10.1038/nature13767, 2014.

Ehn, M., Thornton, J. A., Kleist, E., Sipilä, M., Junninen, H., Pullinen, I., Springer, M., Rubach, F., Tillmann, R., Lee, B., Lopez-Hilfiker, F., Andres, S., Acir, I.-H., Rissanen, M., Jokinen, T., Schobesberger, S., Kangasluoma, J., Kontkanen, J., Nieminen, T., Kurtén, T., Nielsen, L. B., Jørgensen, S., Kjaergaard, H. G., Canagaratna, M., Maso, M. D., Berndt, T., Petäjä, T., Wahner, A., Kerminen, V.-M., Kulmala, M., Worsnop, D. R., Wildt, J., and Mentel, T. F.: A large source of low-volatility secondary organic aerosol, Nature, 506, 476-479, https://doi.org/10.1038/nature13032, 2014.

Foley, K. M., Pouliot, G., Eyth, A., Aldridge, M., Allen, C., Appel, K. W., Bash, J. O., Beardsley, M., Beidler, J., Choi, D., Farkas, C., Gilliam, R., Godfrey, J., Henderson, B. H., Hogrefe, C., Koplitz, S., Mason, R., Mathur, R., Misenis, C., Possiel, N., Pye, H. O. T., Reynolds, L., Roark, M., Roberts, S., Schwede, D. B., Seltzer, K. M., Sonntag, D., Talgo, K., Toro, C., Vukovich, J., and Xing, J.: 2002-2017 Anthropogenic emissions data for air quality modeling over the United States, submitted to Data in Brief, 2022.

Fountoukis, C., and Nenes, A.: ISORROPIA II: a computationally efficient thermodynamic equilibrium model for K^+–Ca^{2+}–Mg^{2+}–NH_4^+–Na^+–SO_4^{2-}–NO_3^-–Cl^-–H_2O aerosols, Atmos. Chem. Phys., 7, 4639-4659, https://doi.org/10.5194/acp-7-4639-2007, 2007.

Gierczak, T., Burkholder, J. B., Talukdar, R. K., Mellouki, A., Barone, S. B., and Ravishankara, A. R.: Atmospheric fate of methyl vinyl ketone and methacrolein, J. Photchem. Photobiol. A, 110, 1-10, https://doi.org/10.1016/S1010-6030(97)00159-7, 1997.

Goliff, W. S., Stockwell, W. R., and Lawson, C. V.: The regional atmospheric chemistry mechanism, version 2, Atmos. Environ., 68, 174-185, https://doi.org/10.1016/j.atmosenv.2012.11.038, 2013.

Gómez Alvarez, E., Borrás, E., Viidanoja, J., and Hjorth, J.: Unsaturated dicarbonyl products from the OH-initiated photo-oxidation of furan, 2-methylfuran and 3-methylfuran, Atmos. Environ., 43, 1603-1612, https://doi.org/10.1016/j.atmosenv.2008.12.019, 2009.

Gordon, H., Sengupta, K., Rap, A., Duplissy, J., Frege, C., Williamson, C., Heinritzi, M., Simon, M., Yan, C., Almeida, J., Tröstl, J., Nieminen, T., Ortega, I. K., Wagner, R., Dunne, E. M., Adamov, A., Amorim, A., Bernhammer, A.-K., Bianchi, F., Breitenlechner, M., Brilke, S., Chen, X., Craven, J. S., Dias, A., Ehrhart, S., Fischer, L., Flagan, R. C., Franchin, A., Fuchs, C., Guida, R., Hakala, J., Hoyle, C. R., Jokinen, T., Junninen, H., Kangasluoma, J., Kim, J., Kirkby, J., Krapf, M., Kürten, A., Laaksonen, A., Lehtipalo, K., Makhmutov, V., Mathot, S., Molteni, U., Monks, S. A., Onnela, A., Peräkylä, O., Piel, F., Petäjä, T., Praplan, A. P., Pringle, K. J., Richards, N. A. D., Rissanen, M. P., Rondo, L., Sarnela, N., Schobesberger, S., Scott, C. E., Seinfeld, J. H., Sharma, S., Sipilä, M., Steiner, G., Stozhkov, Y., Stratmann, F., Tomé, A., Virtanen, A., Vogel, A. L., Wagner, A. C., Wagner, P. E., Weingartner, E., Wimmer, D., Winkler, P. M., Ye, P., Zhang, X., Hansel, A., Dommen, J., Donahue, N. M., Worsnop, D. R., Baltensperger, U., Kulmala, M., Curtius, J., and Carslaw, K. S.: Reduced anthropogenic aerosol radiative forcing caused by biogenic new particle formation, P. Natl. Acad. Sci. USA, 113, 12053-12058, https://doi.org/10.1073/pnas.1602360113, 2016.

Griffin, R. J., Cocker III, D. R., Flagan, R. C., and Seinfeld, J. H.: Organic aerosol formation from the oxidation of biogenic hydrocarbons, J. Geophys. Res.-Atmos., 104, 3555-3567, https://doi.org/10.1029/1998JD100049, 1999.

Grulke, C. M., Williams, A. J., Thillanadarajah, I., and Richard, A. M.: EPA's DSSTox database: History of development of a curated chemistry resource supporting computational toxicology research, Comput. Toxicol., 12, 100096, https://doi.org/10.1016/j.comtox.2019.100096, 2019.

Haywood, J., and Boucher, O.: Estimates of the direct and indirect radiative forcing due to tropospheric aerosols: A review, Rev. Geophys., 38, 513-543, https://doi.org/10.1029/1999RG000078, 2000.

He, Y., Lambe, A. T., Seinfeld, J. H., Cappa, C. D., Pierce, J. R., and Jathar, S. H.: Process-level modeling can simultaneously explain secondary organic aerosol evolution in chambers and flow reactors, Environ. Sci. Technol., 56, 6262-6273, https://doi.org/10.1021/acs.est.1c08520, 2022.

Heald, C. L., Kroll, J. H., Jimenez, J. L., Docherty, K. S., DeCarlo, P. F., Aiken, A. C., Chen, Q., Martin, S. T., Farmer, D. K., and Artaxo, P.: A simplified description of the evolution of organic aerosol composition in the atmosphere, Geophys. Res. Lett., 37, https://doi.org/10.1029/2010GL042737, 2010.

Heald, C. L., Gouw, J. d., Goldstein, A. H., Guenther, A. B., Hayes, P. L., Hu, W., Isaacman-VanWertz, G., Jimenez, J. L., Keutsch, F. N., Koss, A. R., Misztal, P. K., Rappenglück, B., Roberts, J. M., Stevens, P. S., Washenfelder, R. A., Warneke, C., and Young, C. J.: Contrasting reactive organic carbon observations in the Southeast United States (SOAS) and Southern California (CalNex), Environ. Sci. Technol., 54, 14923-14935, https://doi.org/10.1021/acs.est.0c05027, 2020.

Heald, C. L., and Kroll, J. H.: The fuel of atmospheric chemistry: Toward a complete description of reactive organic carbon, Sci. Adv., 6, eaay8967, https://doi.org/10.1126/sciadv.aay8967, 2020.

Heicklen, J., Desai, J., Bahta, A., Harper, C., and Simonaitis, R.: The temperature and wavelength dependence of the photo-oxidation of propionaldehyde, J. Photochem., 34, 117-135, https://doi.org/10.1016/0047-2670(86)85014-6, 1986.

Hodzic, A., and Jimenez, J. L.: Modeling anthropogenically controlled secondary organic aerosols in a megacity: a simplified framework for global and climate models, Geosci. Model Dev., 4, 901-917, https://doi.org/10.5194/gmd-4-901-2011, 2011.

Hoffmann, T., Odum, J. R., Bowman, F., Collins, D., Klockow, D., Flagan, R. C., and Seinfeld, J. H.: Formation of organic aerosols from the oxidation of biogenic hydrocarbons, J. Atmos. Chem., 26, 189-222, https://doi.org/10.1023/A:1005734301837, 1997.

Hutzell, W. T., Luecken, D. J., Appel, K. W., and Carter, W. P. L.: Interpreting predictions from the SAPRC07 mechanism based on regional and continental simulations, Atmos. Environ., 46, 417-429, https://doi.org/10.1016/j.atmosenv.2011.09.030, 2012.

IUPAC: IUPAC subcommittee for gas kinetic data evaluation: http://www.iupac-kinetic.ch.cam.ac.uk/, access: 13 May 2022, 2010.

Ivatt, P. D., Evans, M. J., and Lewis, A. C.: Suppression of surface ozone by an aerosol-inhibited photochemical ozone regime, Nature Geoscience, 15, 536-540, https://doi.org/10.1038/s41561-022-00972-9, 2022.

Jaffe, D. A., and Wigder, N. L.: Ozone production from wildfires: A critical review, Atmos. Environ., 51, 1-10, https://doi.org/10.1016/j.atmosenv.2011.11.063, 2012.

Jaoui, M., Kleindienst, T. E., Docherty, K. S., Lewandowski, M., and Offenberg, J. H.: Secondary organic aerosol formation from the oxidation of a series of sesquiterpenes: α-cedrene, β-caryophyllene, α-humulene and α-farnesene with O_3, OH and NO_3 radicals, Environ. Chem., 10, 178-193, https://doi.org/10.1071/EN13025, 2013.

Jathar, S. H., Gordon, T. D., Hennigan, C. J., Pye, H. O. T., Pouliot, G., Adams, P. J., Donahue, N. M., and Robinson, A. L.: Unspeciated organic emissions from combustion sources and their influence on the secondary organic aerosol budget in the United States, P. Natl. Acad. Sci. USA, 111, 10473, https://doi.org/10.1073/pnas.1323740111, 2014.

Jenkin, M. E., Saunders, S. M., and Pilling, M. J.: The tropospheric degradation of volatile organic compounds: a protocol for mechanism development, Atmos. Environ., 31, 81-104, https://doi.org/10.1016/S1352-2310(96)00105-7, 1997.

Jenkin, M. E., Saunders, S. M., Wagner, V., and Pilling, M. J.: Protocol for the development of the Master Chemical Mechanism, MCM v3 (Part B): tropospheric degradation of aromatic volatile organic compounds, Atmos. Chem. Phys., 3, 181-193, https://doi.org/10.5194/acp-3-181-2003, 2003.

Jenkin, M. E., Wyche, K. P., Evans, C. J., Carr, T., Monks, P. S., Alfarra, M. R., Barley, M. H., McFiggans, G. B., Young, J. C., and Rickard, A. R.: Development and chamber evaluation of the MCM v3.2 degradation scheme for β-caryophyllene, Atmos. Chem. Phys., 12, 5275-5308, https://doi.org/10.5194/acp-12-5275-2012, 2012.

Jiang, X., Tsona, N. T., Jia, L., Liu, S., Zhang, H., Xu, Y., and Du, L.: Secondary organic aerosol formation from photooxidation of furan: effects of NO_X and humidity, Atmos. Chem. Phys., 19, 13591-13609, https://doi.org/10.5194/acp-19-13591-2019, 2019.

Jokinen, T., Berndt, T., Makkonen, R., Kerminen, V.-M., Junninen, H., Paasonen, P., Stratmann, F., Herrmann, H., Guenther, A. B., Worsnop, D. R., Kulmala, M., Ehn, M., and Sipilä, M.: Production of extremely low volatile organic compounds from biogenic emissions: Measured yields and atmospheric implications, P. Natl. Acad. Sci. USA, 112, 7123-7128, https://doi.org/10.1073/pnas.1423977112, 2015.

Kaduwela, A., Luecken, D., Carter, W., and Derwent, R.: New directions: Atmospheric chemical mechanisms for the future, Atmos. Environ., 122, 609-610, https://doi.org/10.1016/j.atmosenv.2015.10.031, 2015.

Karl, T., Striednig, M., Graus, M., Hammerle, A., and Wohlfahrt, G.: Urban flux measurements reveal a large pool of oxygenated volatile organic compound emissions, P. Natl. Acad. Sci. USA, 115, 1186-1191, https://doi.org/10.1073/pnas.1714715115, 2018.

Kim, P. S., Jacob, D. J., Fisher, J. A., Travis, K., Yu, K., Zhu, L., Yantosca, R. M., Sulprizio, M. P., Jimenez, J. L., Campuzano-Jost, P., Froyd, K. D., Liao, J., Hair, J. W., Fenn, M. A., Butler, C. F., Wagner, N. L., Gordon, T. D., Welti, A., Wennberg, P. O., Crounse, J. D., St. Clair, J. M., Teng, A. P., Millet, D. B., Schwarz, J. P., Markovic, M. Z., and Perring, A. E.: Sources, seasonality, and trends of southeast US aerosol: an integrated analysis of surface, aircraft, and satellite observations with the GEOS-Chem chemical transport model, Atmos. Chem. Phys., 15, 10411-10433, https://doi.org/10.5194/acp-15-10411-2015, 2015.

Knote, C., Tuccella, P., Curci, G., Emmons, L., Orlando, J. J., Madronich, S., Baró, R., Jiménez-Guerrero, P., Luecken, D., Hogrefe, C., Forkel, R., Werhahn, J., Hirtl, M., Pérez, J. L., San José, R., Giordano, L., Brunner, D., Yahya, K., and Zhang, Y.: Influence of the choice of gas-phase mechanism on predictions of key gaseous pollutants during the AQMEII phase-2 intercomparison, Atmos. Environ., 115, 553-568, https://doi.org/10.1016/j.atmosenv.2014.11.066, 2015.

Koo, B., Knipping, E., and Yarwood, G.: 1.5-Dimensional volatility basis set approach for modeling organic aerosol in CAMx and CMAQ, Atmos. Environ., 95, 158-164, https://doi.org/10.1016/j.atmosenv.2014.06.031, 2014.

Koss, A. R., Sekimoto, K., Gilman, J. B., Selimovic, V., Coggon, M. M., Zarzana, K. J., Yuan, B., Lerner, B. M., Brown, S. S., Jimenez, J. L., Krechmer, J., Roberts, J. M., Warneke, C., Yokelson, R. J., and de Gouw, J.: Non-methane organic gas emissions from biomass burning: identification, quantification, and emission factors from PTR-ToF during the FIREX 2016 laboratory experiment, Atmos. Chem. Phys., 18, 3299-3319, https://doi.org/10.5194/acp-18-3299-2018, 2018.

Kroll, J. H., Smith, J. D., Che, D. L., Kessler, S. H., Worsnop, D. R., and Wilson, K. R.: Measurement of fragmentation and functionalization pathways in the heterogeneous oxidation of oxidized organic aerosol, Phys. Chem. Chem. Phys., 11, 8005-8014, https://doi.org/10.1039/B905289E, 2009.

Kroll, J. H., Donahue, N. M., Jimenez, J. L., Kessler, S. H., Canagaratna, M. R., Wilson, K. R., Altieri, K. E., Mazzoleni, L. R., Wozniak, A. S., Bluhm, H., Mysak, E. R., Smith, J. D., Kolb, C. E., and Worsnop, D. R.: Carbon oxidation state as a metric for describing the chemistry of atmospheric organic aerosol, Nat. Chem., 3, 133-139, https://doi.org/10.1038/nchem.948, 2011.

Kurtén, T., Møller, K. H., Nguyen, T. B., Schwantes, R. H., Misztal, P. K., Su, L., Wennberg, P. O., Fry, J. L., and Kjaergaard, H. G.: Alkoxy radical bond scissions explain the anomalously low secondary organic serosol and organonitrate yields from α-pinene + NO_3, The Journal of Physical Chemistry Letters, 8, 2826-2834, https://doi.org/10.1021/acs.jpclett.7b01038, 2017.

Lannuque, V., Camredon, M., Couvidat, F., Hodzic, A., Valorso, R., Madronich, S., Bessagnet, B., and Aumont, B.: Exploration of the influence of environmental conditions on secondary organic aerosol formation and organic species properties using explicit simulations: development of the VBS-GECKO parameterization, Atmos. Chem. Phys., 18, 13411-13428, https://doi.org/10.5194/acp-18-13411-2018, 2018.

Lawrence, C. E., Casson, P., Brandt, R., Schwab, J. J., Dukett, J. E., Snyder, P., Yerger, E., Kelting, D., VandenBoer, T. C., and Lance, S.: Long-term monitoring of cloud water chemistry at Whiteface Mountain: The emergence of a new chemical regime, Atmos. Chem. Phys. Discuss., 2022, 1-31, https://doi.org/10.5194/acp-2022-313, 2022.

Lee, B. H., D'Ambro, E. L., Lopez-Hilfiker, F. D., Schobesberger, S., Mohr, C., Zawadowicz, M. A., Liu, J., Shilling, J. E., Hu, W., Palm, B. B., Jimenez, J. L., Hao, L., Virtanen, A., Zhang, H., Goldstein, A. H., Pye, H. O. T., and Thornton, J. A.:

Resolving ambient organic aerosol formation and aging pathways with simultaneous molecular composition and volatility observations, ACS Earth Space Chem., 4, 391-402, https://doi.org/10.1021/acsearthspacechem.9b00302, 2020.

Li, Y., Schichtel Bret, A., Walker John, T., Schwede Donna, B., Chen, X., Lehmann Christopher, M. B., Puchalski Melissa, A., Gay David, A., and Collett Jeffrey, L.: Increasing importance of deposition of reduced nitrogen in the United States, P. Natl. Acad. Sci. USA, 113, 5874-5879, https://doi.org/10.1073/pnas.1525736113, 2016.

Liggio, J., Li, S.-M., and McLaren, R.: Reactive uptake of glyoxal by particulate matter, J. Geophys. Res.-Atmos., 110, https://doi.org/10.1029/2004JD005113, 2005.

Loeffler, K. W., Koehler, C. A., Paul, N. M., and De Haan, D. O.: Oligomer formation in evaporating aqueous glyoxal and methyl glyoxal solutions, Environ. Sci. Technol., 40, 6318-6323, https://doi.org/10.1021/es060810w, 2006.

Lowe, C. N., and Williams, A. J.: Enabling high-throughput searches for multiple chemical data using the U.S.-EPA CompTox Chemicals Dashboard, J. Chem. Inf. Model, 61, 565-570, https://doi.org/10.1021/acs.jcim.0c01273, 2021.

Lu, Q., Zhao, Y., and Robinson, A. L.: Comprehensive organic emission profiles for gasoline, diesel, and gas-turbine engines including intermediate and semi-volatile organic compound emissions, Atmos. Chem. Phys., 18, 17637-17654, https://doi.org/10.5194/acp-18-17637-2018, 2018.

Lu, Q., Murphy, B. N., Qin, M., Adams, P. J., Zhao, Y., Pye, H. O. T., Efstathiou, C., Allen, C., and Robinson, A. L.: Simulation of organic aerosol formation during the CalNex study: updated mobile emissions and secondary organic aerosol parameterization for intermediate-volatility organic compounds, Atmos. Chem. Phys., 20, 4313-4332, https://doi.org/10.5194/acp-20-4313-2020, 2020.

Magneron, I., Thévenet, R., Mellouki, A., Le Bras, G., Moortgat, G. K., and Wirtz, K.: A study of the photolysis and OH-initiated oxidation of acrolein and trans-crotonaldehyde, J. Phys. Chem. A, 106, 2526-2537, https://doi.org/10.1021/jp013413a, 2002.

Makar, M., Antonelli, J., Di, Q., Cutler, D., Schwartz, J., and Dominici, F.: Estimating the causal effect of low levels of fine particulate matter on hospitalization, Epidemiol., 28, https://doi.org/10.1097/ede.0000000000000690, 2017.

Mansouri, K., Grulke, C. M., Judson, R. S., and Williams, A. J.: OPERA models for predicting physicochemical properties and environmental fate endpoints, J. Cheminformatics, 10, 10, https://doi.org/10.1186/s13321-018-0263-1, 2018.

McClure, C. D., and Jaffe, D. A.: US particulate matter air quality improves except in wildfire-prone areas, P. Natl. Acad. Sci. USA, 115, 7901-7906, https://doi.org/10.1073/pnas.1804353115, 2018.

McDonald, B. C., de Gouw, J. A., Gilman, J. B., Jathar, S. H., Akherati, A., Cappa, C. D., Jimenez, J. L., Lee-Taylor, J., Hayes, P. L., McKeen, S. A., Cui, Y. Y., Kim, S.-W., Gentner, D. R., Isaacman-VanWertz, G., Goldstein, A. H., Harley, R. A., Frost, G. J., Roberts, J. M., Ryerson, T. B., and Trainer, M.: Volatile chemical products emerging as largest petrochemical source of urban organic emissions, Science, 359, 760, https://doi.org/10.1126/science.aaq0524, 2018.

McFiggans, G., Mentel, T. F., Wildt, J., Pullinen, I., Kang, S., Kleist, E., Schmitt, S., Springer, M., Tillmann, R., Wu, C., Zhao, D., Hallquist, M., Faxon, C., Le Breton, M., Hallquist, Å. M., Simpson, D., Bergström, R., Jenkin, M. E., Ehn, M., Thornton, J. A., Alfarra, M. R., Bannan, T. J., Percival, C. J., Priestley, M., Topping, D., and Kiendler-Scharr, A.: Secondary organic aerosol reduced by mixture of atmospheric vapours, Nature, 565, 587-593, https://doi.org/10.1038/s41586-018-0871-y, 2019.

Moch, J. M., Dovrou, E., Mickley, L. J., Keutsch, F. N., Cheng, Y., Jacob, D. J., Jiang, J., Li, M., Munger, J. W., Qiao, X., and Zhang, Q.: Contribution of hydroxymethane sulfonate to ambient particulate matter: A potential explanation for high

particulate sulfur during severe winter haze in Beijing, Geophys. Res. Lett., 45, 11,969-911,979, https://doi.org/10.1029/2018GL079309, 2018.

Møller, K. H., Otkjær, R. V., Chen, J., and Kjaergaard, H. G.: Double bonds are key to fast unimolecular reactivity in first-generation monoterpene hydroxy peroxy radicals, J. Phys. Chem. A, 124, 2885-2896, https://doi.org/10.1021/acs.jpca.0c01079, 2020.

Molteni, U., Bianchi, F., Klein, F., El Haddad, I., Frege, C., Rossi, M. J., Dommen, J., and Baltensperger, U.: Formation of highly oxygenated organic molecules from aromatic compounds, Atmos. Chem. Phys., 18, 1909-1921, https://doi.org/10.5194/acp-18-1909-2018, 2018.

Molteni, U., Simon, M., Heinritzi, M., Hoyle, C. R., Bernhammer, A.-K., Bianchi, F., Breitenlechner, M., Brilke, S., Dias, A., Duplissy, J., Frege, C., Gordon, H., Heyn, C., Jokinen, T., Kürten, A., Lehtipalo, K., Makhmutov, V., Petäjä, T., Pieber, S. M., Praplan, A. P., Schobesberger, S., Steiner, G., Stozhkov, Y., Tomé, A., Tröstl, J., Wagner, A. C., Wagner, R., Williamson, C., Yan, C., Baltensperger, U., Curtius, J., Donahue, N. M., Hansel, A., Kirkby, J., Kulmala, M., Worsnop, D. R., and Dommen, J.: Formation of highly oxygenated organic molecules from α-pinene ozonolysis: Chemical characteristics, mechanism, and kinetic model development, ACS Earth Space Chem., 3, 873-883, https://doi.org/10.1021/acsearthspacechem.9b00035, 2019.

Murphy, B. N., Woody, M. C., Jimenez, J. L., Carlton, A. M. G., Hayes, P. L., Liu, S., Ng, N. L., Russell, L. M., Setyan, A., Xu, L., Young, J., Zaveri, R. A., Zhang, Q., and Pye, H. O. T.: Semivolatile POA and parameterized total combustion SOA in CMAQv5.2: impacts on source strength and partitioning, Atmos. Chem. Phys., 17, 11107-11133, https://doi.org/10.5194/acp-17-11107-2017, 2017.

Nakao, S., Clark, C., Tang, P., Sato, K., and Cocker Iii, D.: Secondary organic aerosol formation from phenolic compounds in the absence of NO_X, Atmos. Chem. Phys., 11, 10649-10660, https://doi.org/10.5194/acp-11-10649-2011, 2011.

Nannoolal, Y., Rarey, J., Ramjugernath, D., and Cordes, W.: Estimation of pure component properties: Part 1. Estimation of the normal boiling point of non-electrolyte organic compounds via group contributions and group interactions, Fluid Phase Equilib., 226, 45-63, https://doi.org/10.1016/j.fluid.2004.09.001, 2004.

Nannoolal, Y., Rarey, J., and Ramjugernath, D.: Estimation of pure component properties: Part 3. Estimation of the vapor pressure of non-electrolyte organic compounds via group contributions and group interactions, Fluid Phase Equilib., 269, 117-133, https://doi.org/10.1016/j.fluid.2008.04.020, 2008.

Nault, B. A., Campuzano-Jost, P., Day, D. A., Schroder, J. C., Anderson, B., Beyersdorf, A. J., Blake, D. R., Brune, W. H., Choi, Y., Corr, C. A., de Gouw, J. A., Dibb, J., DiGangi, J. P., Diskin, G. S., Fried, A., Huey, L. G., Kim, M. J., Knote, C. J., Lamb, K. D., Lee, T., Park, T., Pusede, S. E., Scheuer, E., Thornhill, K. L., Woo, J. H., and Jimenez, J. L.: Secondary organic aerosol production from local emissions dominates the organic aerosol budget over Seoul, South Korea, during KORUS-AQ, Atmos. Chem. Phys., 18, 17769-17800, https://doi.org/10.5194/acp-18-17769-2018, 2018.

Ng, N. L., Kroll, J. H., Chan, A. W. H., Chhabra, P. S., Flagan, R. C., and Seinfeld, J. H.: Secondary organic aerosol formation from *m*-xylene, toluene, and benzene, Atmos. Chem. Phys., 7, 3909-3922, https://doi.org/10.5194/acp-7-3909-2007, 2007.

Ng, N. L., Canagaratna, M. R., Jimenez, J. L., Chhabra, P. S., Seinfeld, J. H., and Worsnop, D. R.: Changes in organic aerosol composition with aging inferred from aerosol mass spectra, Atmos. Chem. Phys., 11, 6465-6474, https://doi.org/10.5194/acp-11-6465-2011, 2011.

Nozière, B., Barnes, I., and Becker, K.-H.: Product study and mechanisms of the reactions of α-pinene and of pinonaldehyde with OH radicals, J. Geophys. Res.-Atmos., 104, 23645-23656, https://doi.org/10.1029/1999JD900778, 1999.

Paciga, A. L., Riipinen, I., and Pandis, S. N.: Effect of Ammonia on the Volatility of Organic Diacids, Environ. Sci. Technol., 48, 13769-13775, 10.1021/es5037805, 2014.

Pai, S. J., Carter, T. S., Heald, C. L., and Kroll, J. H.: Updated World Health Organization Air Quality Guidelines highlight the importance of non-anthropogenic $PM_{2.5}$, Environ. Sci. Tech. Lett., 9, 501-506, https://doi.org/10.1021/acs.estlett.2c00203, 2022.

Pankow, J. F.: An absorption model of the gas/aerosol partitioning involved in the formation of secondary organic aerosol, Atmos. Environ., 28, 189-193, https://doi.org/10.1016/1352-2310(94)90094-9, 1994.

Pankow, J. F., and Asher, W. E.: SIMPOL.1: a simple group contribution method for predicting vapor pressures and enthalpies of vaporization of multifunctional organic compounds, Atmos. Chem. Phys., 8, 2773-2796, https://doi.org/10.5194/acp-8-2773-2008, 2008.

Pennington, E. A., Seltzer, K. M., Murphy, B. N., Qin, M., Seinfeld, J. H., and Pye, H. O. T.: Modeling secondary organic aerosol formation from volatile chemical products, Atmos. Chem. Phys., 21, 18247-18261, https://doi.org/10.5194/acp-21-18247-2021, 2021.

Piletic, I. R., and Kleindienst, T. E.: Rates and yields of unimolecular reactions producing highly oxidized peroxy radicals in the OH-induced autoxidation of α-pinene, β-pinene, and limonene, J. Phys. Chem. A, 126, 88-100, https://doi.org/10.1021/acs.jpca.1c07961, 2022.

Place, B. K., Hutzell, W. T., Appel, K. W., Farrell, S., Valin, L., Murphy, B. N., Seltzer, K. M., Sarwar, G., Allen, C., Piletic, I. R., D'Ambro, E. L., Saunders, E., Simon, H., Torres-Vasquez, A., Pleim, J., Schwantes, R. H., Coggon, M. M., Xu, L., Stockwell, W. R., and Pye, H. O. T.: Sensitivity of Northeast U.S. surface ozone predictions to the representation of atmospheric chemistry in CRACMMv1.0, in prep.

Pond, Z. A., Hernandez, C. S., Adams, P. J., Pandis, S. N., Garcia, G. R., Robinson, A. L., Marshall, J. D., Burnett, R., Skyllakou, K., Garcia Rivera, P., Karnezi, E., Coleman, C. J., and Pope, C. A.: Cardiopulmonary mortality and fine particulate air pollution by species and source in a national U.S. cohort, Environ. Sci. Technol., 56, 7214-7223, https://doi.org/10.1021/acs.est.1c04176, 2022.

Porter, W. C., Jimenez, J. L., and Barsanti, K. C.: Quantifying atmospheric parameter ranges for ambient secondary organic aerosol formation, ACS Earth Space Chem., 5, 2380-2397, https://doi.org/10.1021/acsearthspacechem.1c00090, 2021.

Praske, E., Otkjær, R. V., Crounse, J. D., Hethcox, J. C., Stoltz, B. M., Kjaergaard, H. G., and Wennberg, P. O.: Atmospheric autoxidation is increasingly important in urban and suburban North America, P. Natl. Acad. Sci. USA, 115, 64-69, https://doi.org/10.1073/pnas.1715540115, 2018.

Pye, H. O. T., Chan, A. W. H., Barkley, M. P., and Seinfeld, J. H.: Global modeling of organic aerosol: the importance of reactive nitrogen (NO_X and NO_3), Atmos. Chem. Phys., 10, 11261-11276, https://doi.org/10.5194/acp-10-11261-2010, 2010.

Pye, H. O. T., and Pouliot, G. A.: Modeling the role of alkanes, polycyclic aromatic hydrocarbons, and their oligomers in secondary organic aerosol formation, Environ. Sci. Technol., 46, 6041-6047, https://doi.org/10.1021/es300409w, 2012.

Pye, H. O. T., Pinder, R. W., Piletic, I. R., Xie, Y., Capps, S. L., Lin, Y.-H., Surratt, J. D., Zhang, Z., Gold, A., Luecken, D. J., Hutzell, W. T., Jaoui, M., Offenberg, J. H., Kleindienst, T. E., Lewandowski, M., and Edney, E. O.: Epoxide pathways improve model predictions of isoprene markers and reveal key role of acidity in aerosol formation, Environ. Sci. Technol., 47, 11056-11064, https://doi.org/10.1021/es402106h, 2013.

Pye, H. O. T., Luecken, D. J., Xu, L., Boyd, C. M., Ng, N. L., Baker, K. R., Ayres, B. R., Bash, J. O., Baumann, K., Carter, W. P. L., Edgerton, E., Fry, J. L., Hutzell, W. T., Schwede, D. B., and Shepson, P. B.: Modeling the current and future roles of particulate organic nitrates in the southeastern United States, Environ. Sci. Technol., 49, 14195-14203, https://doi.org/10.1021/acs.est.5b03738, 2015.

Pye, H. O. T., Murphy, B. N., Xu, L., Ng, N. L., Carlton, A. G., Guo, H., Weber, R., Vasilakos, P., Appel, K. W., Budisulistiorini, S. H., Surratt, J. D., Nenes, A., Hu, W., Jimenez, J. L., Isaacman-VanWertz, G., Misztal, P. K., and Goldstein, A. H.: On the implications of aerosol liquid water and phase separation for organic aerosol mass, Atmos. Chem. Phys., 17, 343-369, https://doi.org/10.5194/acp-17-343-2017, 2017.

Pye, H. O. T., Ward-Caviness, C. K., Murphy, B. N., Appel, K. W., and Seltzer, K. M.: Secondary organic aerosol association with cardiorespiratory disease mortality in the United States, Nat. Commun., 12, 7215, https://doi.org/10.1038/s41467-021-27484-1, 2021.

Pye, H. O. T., Appel, K. W., Seltzer, K. M., Ward-Caviness, C. K., and Murphy, B. N.: Human-health impacts of controlling secondary air pollution precursors, Environ. Sci. Tech. Lett., 9, 96-101, https://doi.org/10.1021/acs.estlett.1c00798, 2022.

Qin, M., Murphy, B. N., Isaacs, K. K., McDonald, B. C., Lu, Q., McKeen, S. A., Koval, L., Robinson, A. L., Efstathiou, C., Allen, C., and Pye, H. O. T.: Criteria pollutant impacts of volatile chemical products informed by near-field modelling, Nat. Sustain., 4, 129-137, https://doi.org/10.1038/s41893-020-00614-1, 2021.

Raber, W. H., and Moortgat, G. K.: Progress and Problems in Atmospheric Chemistry, World Scientific, edited by: Baker, J., Singapore, 1996.

RDKit: rdkit/rdkit: 2020_09_1 (Q3 2020) Release: https://doi.org/10.5281/zenodo.4107869, access: 2 September 2022, 2020.

RDKit: Open-source cheminformatics: https://www.rdkit.org, access: 2 September 2022, 2022.

Richters, S., Herrmann, H., and Berndt, T.: Highly oxidized RO_2 radicals and consecutive products from the ozonolysis of three sesquiterpenes, Environ. Sci. Technol., 50, 2354-2362, https://doi.org/10.1021/acs.est.5b05321, 2016.

Riedel, T. P., Lin, Y.-H., Budisulistiorini, S. H., Gaston, C. J., Thornton, J. A., Zhang, Z., Vizuete, W., Gold, A., and Surratt, J. D.: Heterogeneous reactions of isoprene-derived epoxides: Reaction probabilities and molar secondary organic aerosol yield estimates, Environ. Sci. Tech. Lett., 2, 38-42, https://doi.org/10.1021/ez500406f, 2015.

Riva, M., Chen, Y., Zhang, Y., Lei, Z., Olson, N. E., Boyer, H. C., Narayan, S., Yee, L. D., Green, H. S., Cui, T., Zhang, Z., Baumann, K., Fort, M., Edgerton, E., Budisulistiorini, S. H., Rose, C. A., Ribeiro, I. O., e Oliveira, R. L., dos Santos, E. O., Machado, C. M. D., Szopa, S., Zhao, Y., Alves, E. G., de Sá, S. S., Hu, W., Knipping, E. M., Shaw, S. L., Duvoisin Junior, S., de Souza, R. A. F., Palm, B. B., Jimenez, J.-L., Glasius, M., Goldstein, A. H., Pye, H. O. T., Gold, A., Turpin, B. J., Vizuete, W., Martin, S. T., Thornton, J. A., Dutcher, C. S., Ault, A. P., and Surratt, J. D.: Increasing isoprene epoxydiol-to-inorganic sulfate aerosol ratio results in extensive conversion of inorganic sulfate to organosulfur forms: Implications for aerosol physicochemical properties, Environ. Sci. Technol., 53, 8682-8694, https://doi.org/10.1021/acs.est.9b01019, 2019.

Robinson, A. L., Donahue, N. M., Shrivastava, M. K., Weitkamp, E. A., Sage, A. M., Grieshop, A. P., Lane, T. E., Pierce, J. R., and Pandis, S. N.: Rethinking organic aerosols: Semivolatile emissions and photochemical aging, Science, 315, 1259, https://doi.org/10.1126/science.1133061, 2007.

Roldin, P., Ehn, M., Kurtén, T., Olenius, T., Rissanen, M. P., Sarnela, N., Elm, J., Rantala, P., Hao, L., Hyttinen, N., Heikkinen, L., Worsnop, D. R., Pichelstorfer, L., Xavier, C., Clusius, P., Öström, E., Petäjä, T., Kulmala, M., Vehkamäki, H., Virtanen,

A., Riipinen, I., and Boy, M.: The role of highly oxygenated organic molecules in the Boreal aerosol-cloud-climate system, Nat. Commun., 10, 4370, https://doi.org/10.1038/s41467-019-12338-8, 2019.

Rolletter, M., Blocquet, M., Kaminski, M., Bohn, B., Dorn, H. P., Hofzumahaus, A., Holland, F., Li, X., Rohrer, F., Tillmann, R., Wegener, R., Kiendler-Scharr, A., Wahner, A., and Fuchs, H.: Photooxidation of pinonaldehyde at ambient conditions investigated in the atmospheric simulation chamber SAPHIR, Atmos. Chem. Phys., 20, 13701-13719, https://doi.org/10.5194/acp-20-13701-2020, 2020.

Safieddine, S. A., Heald, C. L., and Henderson, B. H.: The global nonmethane reactive organic carbon budget: A modeling perspective, Geophys. Res. Lett., 44, 3897-3906, https://doi.org/10.1002/2017GL072602, 2017.

Sander, S. P., Golden, D. M., Kurylo, M. J., Moortgat, G. K., Wine, P. H., Ravishankara, A. R., Kolb, C. E., Molina, M. J., Finlayson-Pitts, B. J., Huie, R. E., and Orkin, V. L.: Chemical kinetics and photochemical data for use in Atmospheric Studies Evaluation Number 15: http://hdl.handle.net/2014/41648, 2006.

Sander, S. P., Abbatt, J. P. D., Barker, J. R., Burkholder, J. B., Friedl, R. R., Golden, D. M., Huie, R. E., Kolb, C. E., Kurylo, M. J., Moortgat, G. K., Orkin, V. L., and Wine, P. H.: Chemical Kinetics and Photochemical Data for Use in Atmospheric Studies, Evaluation No. 17, access: 16 May 2022, 2011.

Sarwar, G., Godowitch, J., Henderson, B. H., Fahey, K., Pouliot, G., Hutzell, W. T., Mathur, R., Kang, D., Goliff, W. S., and Stockwell, W. R.: A comparison of atmospheric composition using the Carbon Bond and Regional Atmospheric Chemistry Mechanisms, Atmos. Chem. Phys., 13, 9695-9712, https://doi.org/10.5194/acp-13-9695-2013, 2013.

Sarwar, G., Gantt, B., Schwede, D., Foley, K., Mathur, R., and Saiz-Lopez, A.: Impact of enhanced ozone deposition and halogen chemistry on tropospheric ozone over the Northern Hemisphere, Environ. Sci. Technol., 49, 9203-9211, https://doi.org/10.1021/acs.est.5b01657, 2015.

Saunders, S. M., Jenkin, M. E., Derwent, R. G., and Pilling, M. J.: Protocol for the development of the Master Chemical Mechanism, MCM v3 (Part A): tropospheric degradation of non-aromatic volatile organic compounds, Atmos. Chem. Phys., 3, 161-180, https://doi.org/10.5194/acp-3-161-2003, 2003.

Scheffe, R. D., Strum, M., Phillips, S. B., Thurman, J., Eyth, A., Fudge, S., Morris, M., Palma, T., and Cook, R.: Hybrid modeling approach to estimate exposures of Hazardous Air Pollutants (HAPs) for the National Air Toxics Assessment (NATA), Environ. Sci. Technol., 50, 12356-12364, https://doi.org/10.1021/acs.est.6b04752, 2016.

Schervish, M., and Donahue, N. M.: Peroxy radical chemistry and the volatility basis set, Atmos. Chem. Phys., 20, 1183-1199, https://doi.org/10.5194/acp-20-1183-2020, 2020.

Schwantes, R. H., Schilling, K. A., McVay, R. C., Lignell, H., Coggon, M. M., Zhang, X., Wennberg, P. O., and Seinfeld, J. H.: Formation of highly oxygenated low-volatility products from cresol oxidation, Atmos. Chem. Phys., 17, 3453-3474, https://doi.org/10.5194/acp-17-3453-2017, 2017.

Seltzer, K. M., Pennington, E., Rao, V., Murphy, B. N., Strum, M., Isaacs, K. K., and Pye, H. O. T.: Reactive organic carbon emissions from volatile chemical products, Atmos. Chem. Phys., 21, 5079-5100, https://doi.org/10.5194/acp-21-5079-2021, 2021.

Seltzer, K. M., Murphy, B. N., Pennington, E. A., Allen, C., Talgo, K., and Pye, H. O. T.: Volatile Chemical Product Enhancements to Criteria Pollutants in the United States, Environ. Sci. Technol., 56, 6905-6913, https://doi.org/10.1021/acs.est.1c04298, 2022.

Shah, T., Shi, Y., Beardsley, R., and Yarwood, G.: Speciation Tool User's Guide Version 5.0: https://www.cmascenter.org/speciation_tool/documentation/5.0/Ramboll_sptool_users_guide_V5.pdf, access: 2 August 2022, 2020.

Shah, V., Jacob, D. J., Dang, R., Lamsal, L. N., Strode, S. A., Steenrod, S. D., Boersma, K. F., Eastham, S. D., Fritz, T. M., Thompson, C., Peischl, J., Bourgeois, I., Pollack, I. B., Nault, B. A., Cohen, R. C., Campuzano-Jost, P., Jimenez, J. L., Andersen, S. T., Carpenter, L. J., Sherwen, T., and Evans, M. J.: Nitrogen oxides in the free troposphere: implications for tropospheric oxidants and the interpretation of satellite NO_2 measurements, Atmos. Chem. Phys., 23, 1227-1257, https://doi.org/10.5194/acp-23-1227-2023, 2023.

Simon, H., Beck, L., Bhave, P. V., Divita, F., Hsu, Y., Luecken, D., Mobley, J. D., Pouliot, G. A., Reff, A., Sarwar, G., and Strum, M.: The development and uses of EPA's SPECIATE database, Atmos. Pollut. Res., 1, 196-206, https://doi.org/10.5094/APR.2010.026, 2010.

Simon, H., Baker, K. R., and Phillips, S.: Compilation and interpretation of photochemical model performance statistics published between 2006 and 2012, Atmos. Environ., 61, 124-139, https://doi.org/10.1016/j.atmosenv.2012.07.012, 2012.

Solazzo, E., Bianconi, R., Hogrefe, C., Curci, G., Tuccella, P., Alyuz, U., Balzarini, A., Baró, R., Bellasio, R., Bieser, J., Brandt, J., Christensen, J. H., Colette, A., Francis, X., Fraser, A., Vivanco, M. G., Jiménez-Guerrero, P., Im, U., Manders, A., Nopmongcol, U., Kitwiroon, N., Pirovano, G., Pozzoli, L., Prank, M., Sokhi, R. S., Unal, A., Yarwood, G., and Galmarini, S.: Evaluation and error apportionment of an ensemble of atmospheric chemistry transport modeling systems: multivariable temporal and spatial breakdown, Atmos. Chem. Phys., 17, 3001-3054, https://doi.org/10.5194/acp-17-3001-2017, 2017.

Srivastava, D., Vu, T. V., Tong, S., Shi, Z., and Harrison, R. M.: Formation of secondary organic aerosols from anthropogenic precursors in laboratory studies, NPJ Clim. Atmos., 5, 22, https://doi.org/10.1038/s41612-022-00238-6, 2022.

Stanfield, Z., Addington, C. K., Dionisio, K. L., Lyons, D., Tornero-Velez, R., Phillips, K. A., Buckley, T. J., and Isaacs, K. K.: Mining of Consumer Product Ingredient and Purchasing Data to Identify Potential Chemical Coexposures, Environ. Health Perspect., 129, 067006, https://doi.org/10.1289/EHP8610, 2021.

Stockwell, W. R., Middleton, P., Chang, J. S., and Tang, X.: The second generation regional acid deposition model chemical mechanism for regional air quality modeling, J. Geophys. Res.-Atmos., 95, 16343-16367, https://doi.org/10.1029/JD095iD10p16343, 1990.

Stockwell, W. R., Kirchner, F., Kuhn, M., and Seefeld, S.: A new mechanism for regional atmospheric chemistry modeling, J. Geophys. Res.-Atmos., 102, 25847-25879, https://doi.org/10.1029/97JD00849, 1997.

Surratt, J., D., Chan, A., W. H., Eddingsaas, N., C., Chan, M., Loza, C., L., Kwan, A., J., Hersey, S., P., Flagan, R., C., Wennberg, P., O., and Seinfeld, J., H.: Reactive intermediates revealed in secondary organic aerosol formation from isoprene, P. Natl. Acad. Sci. USA, 107, 6640-6645, https://doi.org/10.1073/pnas.0911114107, 2010.

Talukdar, R. K., Burkholder, J. B., Hunter, M., Gilles, M. K., Roberts, J. M., and Ravishankara, A. R.: Atmospheric fate of several alkyl nitrates Part 2UV absorption cross-sections and photodissociation quantum yields, J. Chem. Soc., Faraday Trans., 93, 2797-2805, https://doi.org/10.1039/A701781B, 1997.

Tilmes, S., Lamarque, J. F., Emmons, L. K., Kinnison, D. E., Ma, P. L., Liu, X., Ghan, S., Bardeen, C., Arnold, S., Deeter, M., Vitt, F., Ryerson, T., Elkins, J. W., Moore, F., Spackman, J. R., and Val Martin, M.: Description and evaluation of tropospheric chemistry and aerosols in the Community Earth System Model (CESM1.2), Geosci. Model Dev., 8, 1395-1426, https://doi.org/10.5194/gmd-8-1395-2015, 2015.

Tsigaridis, K., Daskalakis, N., Kanakidou, M., Adams, P. J., Artaxo, P., Bahadur, R., Balkanski, Y., Bauer, S. E., Bellouin, N., Benedetti, A., Bergman, T., Berntsen, T. K., Beukes, J. P., Bian, H., Carslaw, K. S., Chin, M., Curci, G., Diehl, T., Easter, R. C., Ghan, S. J., Gong, S. L., Hodzic, A., Hoyle, C. R., Iversen, T., Jathar, S., Jimenez, J. L., Kaiser, J. W., Kirkevåg, A., Koch, D., Kokkola, H., Lee, Y. H., Lin, G., Liu, X., Luo, G., Ma, X., Mann, G. W., Mihalopoulos, N., Morcrette, J. J., Müller, J. F., Myhre, G., Myriokefalitakis, S., Ng, N. L., O'Donnell, D., Penner, J. E., Pozzoli, L., Pringle, K. J., Russell, L. M., Schulz, M., Sciare, J., Seland, Ø., Shindell, D. T., Sillman, S., Skeie, R. B., Spracklen, D., Stavrakou, T., Steenrod, S. D., Takemura, T., Tiitta, P., Tilmes, S., Tost, H., van Noije, T., van Zyl, P. G., von Salzen, K., Yu, F., Wang, Z., Wang, Z., Zaveri, R. A., Zhang, H., Zhang, K., Zhang, Q., and Zhang, X.: The AeroCom evaluation and intercomparison of organic aerosol in global models, Atmos. Chem. Phys., 14, 10845-10895, https://doi.org/10.5194/acp-14-10845-2014, 2014.

Tuazon, E. C., Alvarado, A., Aschmann, S. M., Atkinson, R., and Arey, J.: Products of the gas-phase reactions of 1,3-Butadiene with OH and NO_3 Radicals, Environ. Sci. Technol., 33, 3586-3595, https://doi.org/10.1021/es990193u, 1999.

U.S. Environmental Protection Agency: Motor Vehicle EMission Simulator: MOVES3.0.0: https://www.epa.gov/moves, access: 1 July 2022, 2020.

U.S. Environmental Protection Agency: Human Exposure Model: https://www.epa.gov/fera/download-human-exposure-model-hem, access: 19 April 2022, 2021a.

U.S. Environmental Protection Agency: Dose-Response Assessment for Assessing Health Risks Associated With Exposure to Hazardous Air Pollutants: https://www.epa.gov/fera/dose-response-assessment-assessing-health-risks-associated-exposure-hazardous-air-pollutants, access: 29 September 2021, 2021b.

U.S. Environmental Protection Agency: Community Regional Atmospheric Chemistry Multiphase Mechanism (CRACMM) for Improving Air Quality Modeling: https://www.epa.gov/system/files/documents/2021-11/cracmm-factsheet-october-2021-v2.pdf, access: 21 October 2022, 2021c.

U.S. Environmental Protection Agency: CompTox Chemicals Dashboard: https://comptox.epa.gov/dashboard/, access: 19 August 2021, 2021d.

U.S. Environmental Protection Agency: Federal Register, 40 CFR Part 63, [EPA–HQ–OAR–2014–0471; FRL–5562–08–OAR], RIN 2060–AS26, Clean Air Act Section 112 List of Hazardous Air Pollutant: Amendments to the List of Hazardous Air Pollutants (HAP) https://www.govinfo.gov/content/pkg/FR-2022-01-05/pdf/2021-28315.pdf, access: 13 July 2022, 2022a.

U.S. Environmental Protection Agency: CRACMM: https://github.com/USEPA/CRACMM, access: 21 November 2022, 2022b.

U.S. Environmental Protection Agency: List of chemicals within the certain glycol ethers category: https://ordspub.epa.gov/ords/guideme_ext/f?p=GUIDEME:GD::::RP:gd:glycol_ethers, access: 19 April 2022, 2022c.

U.S. Environmental Protection Agency: Nonattainment Areas for Criteria Pollutants (Green Book): https://www.epa.gov/green-book, access: 13 May 2022, 2022d.

U.S. Environmental Protection Agency: SPECIATE Version 5.2 Database Development Documentation, https://www.epa.gov/system/files/documents/2022-09/SPECIATE%205.2%20Addendum.pdf, 2022e.

U.S. Environmental Protection Agency: CTS: Chemical Transformation Simulator: https://qed.epa.gov/cts/, access: 5 August 2022, 2022f.

U.S. Environmental Protection Agency Office of Research and Development: CMAQ (Version 5.3.3): http://doi.org/10.5281/zenodo.3585898, 2019.

U.S. EPA Office of Research and Development: CMAQ Version 5.4: https://doi.org/10.5281/zenodo.7218076, access: 14 October 2022, 2022.

Vannucci, P. F., and Cohen, R. C.: Decadal trends in the temperature dependence of summertime urban $PM_{2.5}$ in the Northeast United States, ACS Earth Space Chem., https://doi.org/10.1021/acsearthspacechem.2c00077, 2022.

Vasquez, K. T., Crounse, J. D., Schulze, B. C., Bates, K. H., Teng, A. P., Xu, L., Allen, H. M., and Wennberg, P. O.: Rapid hydrolysis of tertiary isoprene nitrate efficiently removes NO_X from the atmosphere, P. Natl. Acad. Sci. USA, 117, 33011-33016, https://doi.org/10.1073/pnas.2017442117, 2020.

Venecek, M. A., Carter, W. P. L., and Kleeman, M. J.: Updating the SAPRC Maximum Incremental Reactivity (MIR) scale for the United States from 1988 to 2010, J. Air Waste Manage. Assoc., 68, 1301-1316, https://doi.org/10.1080/10962247.2018.1498410, 2018.

Vereecken, L., and Nozière, B.: H migration in peroxy radicals under atmospheric conditions, Atmos. Chem. Phys., 20, 7429-7458, https://doi.org/10.5194/acp-20-7429-2020, 2020.

Vogel, B., Vogel, H., Kleffmann, J., and Kurtenbach, R.: Measured and simulated vertical profiles of nitrous acid—Part II. Model simulations and indications for a photolytic source, Atmos. Environ., 37, 2957-2966, https://doi.org/10.1016/S1352-2310(03)00243-7, 2003.

Wang, S., Wu, R., Berndt, T., Ehn, M., and Wang, L.: Formation of highly oxidized radicals and multifunctional products from the atmospheric oxidation of alkylbenzenes, Environ. Sci. Technol., 51, 8442-8449, https://doi.org/10.1021/acs.est.7b02374, 2017.

Wang, S., Coggon, M. M., Gkatzelis, G. I., Warneke, C., Bourgeois, I., Ryerson, T., Peischl, J., Veres, P. R., Neuman, J. A., Hair, J., Shingler, T., Fenn, M., Diskin, G., Huey, L. G., Lee, Y. R., Apel, E. C., Hornbrook, R. S., Hills, A. J., Hall, S. R., Ullmann, K., Bela, M. M., Trainer, M. K., Kumar, R., Orlando, J. J., Flocke, F. M., and Emmons, L. K.: Chemical tomography in a fresh wildland fire plume: A Large Eddy Simulation (LES) Study, J. Geophys. Res.-Atmos., 126, e2021JD035203, https://doi.org/10.1029/2021JD035203, 2021.

Weber, J., Archer-Nicholls, S., Griffiths, P., Berndt, T., Jenkin, M., Gordon, H., Knote, C., and Archibald, A. T.: CRI-HOM: A novel chemical mechanism for simulating highly oxygenated organic molecules (HOMs) in global chemistry–aerosol–climate models, Atmos. Chem. Phys., 20, 10889-10910, https://doi.org/10.5194/acp-20-10889-2020, 2020.

Wennberg, P. O., Bates, K. H., Crounse, J. D., Dodson, L. G., McVay, R. C., Mertens, L. A., Nguyen, T. B., Praske, E., Schwantes, R. H., Smarte, M. D., St Clair, J. M., Teng, A. P., Zhang, X., and Seinfeld, J. H.: Gas-Phase reactions of isoprene and its major oxidation products, Chem. Rev., 118, 3337-3390, https://doi.org/10.1021/acs.chemrev.7b00439, 2018.

Williams, A. J., Grulke, C. M., Edwards, J., McEachran, A. D., Mansouri, K., Baker, N. C., Patlewicz, G., Shah, I., Wambaugh, J. F., Judson, R. S., and Richard, A. M.: The CompTox Chemistry Dashboard: a community data resource for environmental chemistry, J. Cheminformatics, 9, 61, https://doi.org/10.1186/s13321-017-0247-6, 2017.

Wiser, F. W., Place, B. K., Siddhartha, S., Pye, H. O. T., Westervelt, D. M., Henze, D. K., Fiore, A. M., and McNeill, V. F.: AMORE-Isoprene v1.0: A new reduced mechanism for gas-phase isoprene oxidation, in prep.

Womack, C. C., McDuffie, E. E., Edwards, P. M., Bares, R., de Gouw, J. A., Docherty, K. S., Dubé, W. P., Fibiger, D. L., Franchin, A., Gilman, J. B., Goldberger, L., Lee, B. H., Lin, J. C., Long, R., Middlebrook, A. M., Millet, D. B., Moravek, A., Murphy, J. G., Quinn, P. K., Riedel, T. P., Roberts, J. M., Thornton, J. A., Valin, L. C., Veres, P. R., Whitehill, A. R., Wild, R. J., Warneke, C., Yuan, B., Baasandorj, M., and Brown, S. S.: An Odd Oxygen Framework for Wintertime Ammonium Nitrate Aerosol Pollution in Urban Areas: NOx and VOC Control as Mitigation Strategies, Geophys. Res. Lett., 46, 4971-4979, https://doi.org/10.1029/2019GL082028, 2019.

Woody, M. C., Baker, K. R., Hayes, P. L., Jimenez, J. L., Koo, B., and Pye, H. O. T.: Understanding sources of organic aerosol during CalNex-2010 using the CMAQ-VBS, Atmos. Chem. Phys., 16, 4081-4100, https://doi.org/10.5194/acp-16-4081-2016, 2016.

Xing, J., Mathur, R., Pleim, J., Hogrefe, C., Gan, C. M., Wong, D. C., Wei, C., Gilliam, R., and Pouliot, G.: Observations and modeling of air quality trends over 1990–2010 across the Northern Hemisphere: China, the United States and Europe, Atmos. Chem. Phys., 15, 2723-2747, https://10.5194/acp-15-2723-2015, 2015.

Xu, L., Pye, H. O. T., He, J., Chen, Y., Murphy, B. N., and Ng, N. L.: Experimental and model estimates of the contributions from biogenic monoterpenes and sesquiterpenes to secondary organic aerosol in the southeastern United States, Atmos. Chem. Phys., 18, 12613-12637, https://doi.org/10.5194/acp-18-12613-2018, 2018.

Xu, L., Møller, K. H., Crounse, J. D., Otkjær, R. V., Kjaergaard, H. G., and Wennberg, P. O.: Unimolecular Reactions of Peroxy Radicals Formed in the Oxidation of α-Pinene and β-Pinene by Hydroxyl Radicals, J. Phys. Chem. A, 123, 1661-1674, https://doi.org/10.1021/acs.jpca.8b11726, 2019.

Xu, L., Møller, K. H., Crounse, J. D., Kjaergaard, H. G., and Wennberg, P. O.: New Insights into the Radical Chemistry and Product Distribution in the OH-Initiated Oxidation of Benzene, Environ. Sci. Technol., 54, 13467-13477, https://doi.org/10.1021/acs.est.0c04780, 2020.

Xu, W., Han, T., Du, W., Wang, Q., Chen, C., Zhao, J., Zhang, Y., Li, J., Fu, P., Wang, Z., Worsnop, D. R., and Sun, Y.: Effects of aqueous-phase and photochemical processing on secondary organic aerosol formation and evolution in Beijing, China, Environ. Sci. Technol., 51, 762-770, https://doi.org/10.1021/acs.est.6b04498, 2017.

Yee, L. D., Isaacman-VanWertz, G., Wernis, R. A., Meng, M., Rivera, V., Kreisberg, N. M., Hering, S. V., Bering, M. S., Glasius, M., Upshur, M. A., Gray Bé, A., Thomson, R. J., Geiger, F. M., Offenberg, J. H., Lewandowski, M., Kourtchev, I., Kalberer, M., de Sá, S., Martin, S. T., Alexander, M. L., Palm, B. B., Hu, W., Campuzano-Jost, P., Day, D. A., Jimenez, J. L., Liu, Y., McKinney, K. A., Artaxo, P., Viegas, J., Manzi, A., Oliveira, M. B., de Souza, R., Machado, L. A. T., Longo, K., and Goldstein, A. H.: Observations of sesquiterpenes and their oxidation products in central Amazonia during the wet and dry seasons, Atmos. Chem. Phys., 18, 10433-10457, https://doi.org/10.5194/acp-18-10433-2018, 2018.

Yeh, G. K., and Ziemann, P. J.: Alkyl nitrate formation from the reactions of C8–C14 n-alkanes with OH radicals in the presence of NO_x: Measured yields with essential corrections for gas–wall partitioning, J. Phys. Chem. A, 118, 8147-8157, https://doi.org/10.1021/jp500631v, 2014.

Young, P. J., Naik, V., Fiore, A. M., Gaudel, A., Guo, J., Lin, M. Y., Neu, J. L., Parrish, D. D., Rieder, H. E., Schnell, J. L., Tilmes, S., Wild, O., Zhang, L., Ziemke, J., Brandt, J., Delcloo, A., Doherty, R. M., Geels, C., Hegglin, M. I., Hu, L., Im, U., Kumar, R., Luhar, A., Murray, L., Plummer, D., Rodriguez, J., Saiz-Lopez, A., Schultz, M. G., Woodhouse, M. T., and Zeng, G.: Tropospheric Ozone Assessment Report: Assessment of global-scale model performance for global and regional ozone distributions, variability, and trends, Elementa: Science of the Anthropocene, 6, https://doi.org/10.1525/elementa.265, 2018.

Yujing, M., and Mellouki, A.: The near-UV absorption cross sections for several ketones, J. Photchem. Photobiol. A, 134, 31-36, https://doi.org/10.1016/S1010-6030(00)00243-4, 2000.

Zare, A., Fahey, K. M., Sarwar, G., Cohen, R. C., and Pye, H. O. T.: Vapor-Pressure pathways initiate but hydrolysis products dominate the aerosol estimated from organic nitrates, ACS Earth Space Chem., 3, 1426-1437, https://doi.org/10.1021/acsearthspacechem.9b00067, 2019.

Zhang, Q., Jimenez, J. L., Canagaratna, M. R., Ulbrich, I. M., Ng, N. L., Worsnop, D. R., and Sun, Y.: Understanding atmospheric organic aerosols via factor analysis of aerosol mass spectrometry: a review, Anal. Bioanal. Chem., 401, 3045-3067, https://doi.org/10.1007/s00216-011-5355-y, 2011.

Zhang, X., Cappa, C. D., Jathar, S. H., McVay, R. C., Ensberg, J. J., Kleeman, M. J., and Seinfeld, J. H.: Influence of vapor wall loss in laboratory chambers on yields of secondary organic aerosol, P. Natl. Acad. Sci. USA, 111, 5802, https://doi.org/10.1073/pnas.1404727111, 2014.

Zhao, B., Wang, S., Donahue, N. M., Jathar, S. H., Huang, X., Wu, W., Hao, J., and Robinson, A. L.: Quantifying the effect of organic aerosol aging and intermediate-volatility emissions on regional-scale aerosol pollution in China, Sci. Rep., 6, 28815-28815, https://doi.org/10.1038/srep28815, 2016.

Zhao, Y., Thornton Joel, A., and Pye Havala, O. T.: Quantitative constraints on autoxidation and dimer formation from direct probing of monoterpene-derived peroxy radical chemistry, P. Natl. Acad. Sci. USA, 115, 12142-12147, https://doi.org/10.1073/pnas.1812147115, 2018.

Zheng, B., Tong, D., Li, M., Liu, F., Hong, C., Geng, G., Li, H., Li, X., Peng, L., Qi, J., Yan, L., Zhang, Y., Zhao, H., Zheng, Y., He, K., and Zhang, Q.: Trends in China's anthropogenic emissions since 2010 as the consequence of clean air actions, Atmos. Chem. Phys., 18, 14095-14111, https://doi.org/10.5194/acp-18-14095-2018, 2018.

Zhu, S., Kinnon, M. M., Shaffer, B. P., Samuelsen, G. S., Brouwer, J., and Dabdub, D.: An uncertainty for clean air: Air quality modeling implications of underestimating VOC emissions in urban inventories, Atmos. Environ., 211, 256-267, https://doi.org/10.1016/j.atmosenv.2019.05.019, 2019.